

Wayne State University Dissertations

January 2020

Investigation Of Physiochemical Properties And Biocompatibility Of Amorphous Calcium Polyphosphate Hydrogel Doped With Antibiotics And Injectable Polymeric Dicalcium Phosphate Dihydrate Bone Cement

Yasaman Chehrehganzabi
Wayne State University

Follow this and additional works at: https://digitalcommons.wayne.edu/oa_dissertations

 Part of the [Biomedical Engineering and Bioengineering Commons](#), [Materials Science and Engineering Commons](#), and the [Medicine and Health Sciences Commons](#)

Recommended Citation

Chehrehganzabi, Yasaman, "Investigation Of Physiochemical Properties And Biocompatibility Of Amorphous Calcium Polyphosphate Hydrogel Doped With Antibiotics And Injectable Polymeric Dicalcium Phosphate Dihydrate Bone Cement" (2020). *Wayne State University Dissertations*. 2348.
https://digitalcommons.wayne.edu/oa_dissertations/2348

This Open Access Dissertation is brought to you for free and open access by DigitalCommons@WayneState. It has been accepted for inclusion in Wayne State University Dissertations by an authorized administrator of DigitalCommons@WayneState.

**INVESTIGATION OF PHYSIOCHEMICAL PROPERTIES AND BIOCOMPATIBILITY
OF AMORPHOUS CALCIUM POLYPHOSPHATE HYDROGEL DOPED WITH
ANTIBIOTICS AND INJECTABLE POLYMERIC DICALCIUM
PHOSPHATE DIHYDRATE BONE CEMENT**

by

YASAMAN CHEHREGHANIANZABI

DISSERTATION

Submitted to the Graduate School

of Wayne State University,

Detroit, Michigan

in partial fulfillment of the requirements

for the degree of

DOCTOR OF PHILOSOPHY

2020

BIOMEDICAL ENGINEERING

Approved By:

DEDICATION

**This Dissertation Is
Dedicated
To**

My Beloved Parents.

For their endless love, support, and encouragement

ACKNOWLEDGMENTS

First of all, I would like to thank God for granting me health and effort that I needed to successfully complete my dissertation.

I would also like to take this opportunity to acknowledge many people without whom this work would not have been possible. First, I would like to express my sincere gratitude to my advisor, Prof. Weiping Ren, for his technical/financial support and valuable guidance. He taught me to be an independent thinker and gave me the freedom to choose problems that I found interesting. I have been very fortunate to work in his research group. This, coupled with his continued encouragement, patience and invaluable suggestions, made this work successful.

I would also like to extend special thanks to other members of my committee, Prof. Juri Gelovani, Prof. Gregory Auner, and Prof. Yawen Li. I learned a lot from each of my committee members, whether this was through direct one-on-one discussions, research collaborations, or even through their graduate students.

In particular, I am extremely grateful to Prof. Auner for the opportunity to acquire valuable techniques in his SSIM lab. I would also like to thank research associates; Kiran Koya and Sally Yurgelevic from Dr. Auner's lab to share their great experiences on Raman Spectroscopy data acquisition and analysis with me.

I would also like to thank Prof. Gelovani for his useful comments and suggestions during my prospectus defense that helped me out to improve the shortcomings of my work for the final defense.

Also, I would like to thank Prof. Li for her useful comments and suggestions about using a scanning electron microscopy (SEM) to capture the most precise pictures from the material surface.

I would especially like to thank each and every one of my labmates for all their help with my research, iv Thank you Mrs. Tong Shi and Dr. Liang Chen for your help with experiment setups and cell culture works, and thank you Dr. Wei Song and Joe Seta for all your training with material fabrication,

quality control, hydrogel preparation, etc. I would also like to thank Dr. Rajib Barua, post-doc in our lab for his helpful insights in Raman Spectroscopy and X-ray diffraction analysis.

I would like to thank the Department of Bioengineering at Wayne State University that provided support during my graduate study. I would like to thank our collaborators at the orthopedic research group of the Providence Hospital, especially Dr. Therese Bou-akl for all the help and guidance they have given me during my Ph.D. study.

Coming to my family, words cannot express how grateful I am to my mother and father. Your prayer for me was what sustained me thus far. I am so grateful for your love, support, and encouragement throughout my life.

Yasaman Chehrehghanianzabi

Wayne State University

January 2020

TABLE OF CONTENTS

LIST OF TABLES	xii
LIST OF FIGURES	xiii
LIST OF ABBREVIATIONS AND SYMBOLS USED	xvi
CHAPTER 1.....	1
Introduction	1
1.1 Basic Bone Physiology & Regeneration.....	1
1.1.1 Bone Structure.....	1
1.1.2 Bone Modeling & Remodeling.....	2
1.1.3 Current Bone Regeneration Strategies	3
1.2. Problem Statement: Osteomyelitis	4
1.2.1 Pathophysiology	4
1.2.2 Treatment Options (Localized)	4
1.2.3 Antibiotics Studied for Localized Osteomyelitis Treatment.....	5
1.3 Currently Studied Carrier Materials for Localized Osteomyelitis Therapy	8
1.4 Calcium Polyphosphate (CPP) Hydrogel.....	10
1.4.1. CPP Structure	10
1.4.2. CPP <i>In Vitro</i> Properties	11
1.4.3. CPP Synthesis	12
1.5 Matrix Fabrication Strategy for Localized Osteomyelitis Therapy	13
1.5.1 Current Status in the Literature	13
1.5.2 Novel P-DCPD Bone Cement.....	14
1.6 Summary of Dissertation & Specific Aims	17

1.6.1 Specific Aim 1: Develop a Strategy to Study Antibiotics Effect on Structural and Physiochemical Properties of Calcium Polyphosphate.....	18
1.6.2 Specific Aim 2: Antibacterial Activity of Polymeric Dicalcium Phosphate Dihydrate (P-DCPD) Loaded with Antibiotics.....	18
1.6.3 Specific Aim 3: Physiochemical Comparison of DCPD and P-DCPD.....	19
1.6.4 Specific Aim 4: Biocompatibility comparison studies of P-DCPD and DCPD in Vitro and in Vivo.....	20
CHAPTER 2	22
Comparing the Release of Erythromycin and Vancomycin from Calcium Polyphosphate Hydrogel Using Different Drug Loading Methods.....	22
2.1 Purpose and Hypothesis.....	22
2.2 Introduction.....	23
2.3 2.3 Materials and Methods.....	25
2.3.1 Synthesis of CPP powder and CPP hydrogel.....	25
2.3.2 Antibiotic loading.....	25
2.3.3 Antibiotic release measurements.....	26
2.3.4 Raman spectroscopy.....	27
2.3.5 Rheological evaluation	28
2.4 Statistical analysis.....	28
2.5 Results.....	29
2.5.1 Antibiotic assay.....	29
2.5.2 Raman Spectroscopy.....	31
2.5.3 Viscoelastic properties.....	35
2.6 Discussion.....	39
2.7 Conclusion and Future Work.....	41

CHAPTER 3	43
Impacts of Compaction Methods on the Delivery Capabilities of Erythromycin and Vancomycin from Calcium Polyphosphate Hydrogel Matrices.....	43
3.1 Purpose and Hypothesis.....	43
3.2 Introduction.....	43
3.3 Materials and Methods.....	46
3.3.1 Synthesis of CPP powder and CPP hydrogel.....	46
3.3.2 Drug loading.....	47
3.3.3 Disc compaction methods.....	47
3.3.4 Structural evaluation of discs' pre-elution	48
3.3.5 Antibiotics release and bactericidal activity assay.....	49
3.3.6 Structural analysis of remnants post-elution.....	50
3.3.7 Eluent pH.....	51
3.4 Statistical analysis.....	51
3.5 Results	52
3.5.1 Structural evaluation of discs' pre-elution.....	52
3.5.2 Antibiotic release and bactericidal activity assay.....	54
3.5.3 Structural analysis of remnants post-elution.....	56
3.5.4 Eluent pH.....	58
3.6 Discussion.....	59
3.7 Conclusion and Future Work.....	62
CHAPTER 4.....	63
Antibacterial Activity of Polymeric Dicalcium Phosphate Dihydrate (P-DCPD) Loaded with Antibiotics.....	63

4.1 Purpose and Hypothesis.....	63
4.2 Introduction.....	64
4.3 Materials and Methods.....	65
4.3.1 Discs Materials, Manufacturing, and Antibiotics Loading.....	65
4.3.2 Antibacterial Activity of P-DCPD Disc-Agar Diffusion Method.....	66
4.4 Data Analysis.....	67
4.5 Results.....	68
4.5.1 Bactericidal Activity.....	68
4.6 Discussion.....	69
4.7 Conclusion and Future Work.....	70
CHAPTER 5.....	71
Physiochemical Comparison of DCPD and P-DCPD.....	71
5.1 Purpose and Hypothesis.....	71
5.2 Introduction.....	72
5.3 Materials and Methods.....	73
5.3.1 P-DCPD and DCPD particle preparation.....	73
5.3.2 Phase determination of DCPD and P-DCPD using X-Ray Diffraction (XRD).....	74
5.3.3 Setting reaction mechanism study of DCPD and P-DCPD using Raman spectroscopy.....	75
5.3.4 Identification of particle morphology and content using scanning electron microscopy(SEM)	76
5.3.5 Stability and adhesion of DCPD and P-DCPD particles using Zeta Potential.....	78
5.3.6 Contact angle measurements.....	80
5.4 Data Analysis.....	82

5.5 Discussion.....	83
5.6 Conclusion and Future Work.....	86
CHAPTER 6.....	88
Biocompatibility Comparison of the P-DCPD and DCPD Particles in Vitro and in Vivo....	88
6.1 Purpose and Hypothesis.....	88
6.2 Introduction.....	88
6.3 Materials and Methods.....	94
6.3.1 Particle preparation.....	94
6.3.2 Particle sterilization.....	95
6.3.3 Cell culture	95
6.3.4 Cell Proliferation.....	96
6.3.5 Cell differentiation.....	97
6.3.6 Cell toxicity.....	98
6.3.7 In Vivo implantation of injectable particles using animal air pouch model.....	98
6.3.8 Histological Analysis of Air Pouch Tissue.....	100
6.4 Data analysis.....	101
6.5 Results.....	101
6.5.1 Cell Proliferation.....	101
6.5.2 Cell Differentiation.....	103
6.5.3 Cell Toxicity.....	103
6.5.4 Quantitative Analysis of Histological Slides.....	104
6.6 Discussion.....	106
6.7 Conclusion and Future Work.....	108

APPENDIX.....	110
BIBLIOGRAPHY.....	116
ABSTRACT	132
VITA AUCTORIS.....	134

LIST OF TABLES

Table 1.1. Chemical properties of EM and VCM.....	7
Table 3.1. Physical properties of compressed and manual samples used in elution study.....	51
Table 3.2. Structural Properties of Discs by μ -CT.....	52
Table 3.3. Post-elution weight loss of discs.....	57
Table 5.1. Zeta potential values for P-DCPD and DCPD in water.....	77
Table 5.2. Water contact angle values for P-DCPD and DCPD	78
Table 5.3. The water absorption rate for P-DCPD and DCPD.....	79
Table 6.1. MC3T3-E1 cells were treated by P-DCPD and DCPD particles undergone 3 cell-based assays to determine proliferation, differentiation, and toxicity.....	89
Table 6.2. Study Design and Mice Group.....	93

LIST OF FIGURES

Figure 1.1. Bone Composition.....	4
Figure 1.2. Molecular schematic of a) EM: $C_{37}H_{67}NO_{13}$ and b) VCM: $C_{66}H_{75}Cl_2N_9O_{24}$ (adapted from PubChem)	7
Figure 1.3. Q^i phosphate tetrahedral species.....	11
Figure 2.1. ACPP Particle size analysis.	27
Figure 2.2. Erythromycin (EM) and vancomycin (VCM) release (10 wt.%) from CPP hydrogel prepared with both “Gel_Mixture” and “Powder_Mixture” methods for 2, 24, 48 hrs.....	30
Figure 2.3. Raman spectra of antibiotics isolation and combination with CPP hydrogel. CPP hydrogel loaded with EM (10 wt.%) in both “Gel_Mixture” and “Powder_Mixture” methods.	32
Figure 2.4. Viscoelastic properties of EM loaded CPP hydrogel with “Gel_Mixture” method.....	35
Figure 2.5. Viscoelastic properties of VCM loaded CPP hydrogel with “Gel_Mixture” method.....	37
Figure 3.1. Schematic of molding methods used in this study; compressed and manual.....	47
Figure 3.2. Surface morphology of antibiotic release samples prior to release for M (A) and C (B) discs. Magnification is 100x.....	52
Figure 3.3. The release pattern of vancomycin and erythromycin	54
Figure 3.4. Bacterial growth inhibition percentage.....	55
Figure 3.5. Raman spectra of VCM, VCM-C discs	56
Figure 3.6. Monitored pH of elution within 2 weeks.....	58
Figure 4.1. pH values for P-DCPD and ACPP elution medium	63
Figure 4.2. Disc-agar diffusion method.....	66
Figure 4.3. Growth of <i>S. aureus</i> on the agar plate.....	67

Figure 4.4. Quantitative analysis of the inhibition zone diameter for each disc.	68
Figure 5.1. XRD peaks of DCPD and P-DCPD powders	73
Figure 5.2. Raman Spectra of DCPD and P-DCPD powders for 1, 14 days of incubation.....	74
Figure 5.3. Morphologies of DCPD and P-DCPD with EDS data over time	75
Figure 5.4. Average Ca/P ratio progression over time. (a) DCPD, (b) P-DCPD.....	76
Figure 5.5. Average zeta potential values for P-DCPD and DCPD, indicating.....	78
Figure 5.6. The water contact angle of P-DCPD vs. DCPD, indicating super hydrophilicity nature of DCPD.....	79
Figure 5.7. Water absorption behavior for DCPD and P-DCPD in 1 day, 4 days, 7 days, and 14 days after incubation.....	80
Figure 6.1. MC3T3-E ₁ cells treated with particles. (a) DCPD and (b) P-DCPD particles.....	90
Figure 6.2. Mice were sacrificed and the pouch tissue were collected for histological analysis.....	93
Figure 6.3. Schematic outline of the air pouch model.....	94
Figure 6.4. MTT assay results of MC3T3-E ₁ cells cultured by P-DCPD and DCPD particles with concentrations of 1, 5, 10, and 1000 µg/ml for 3 and 7 days.....	96
Figure 6.5. Normalized ALP activities of MC3T3 cells cultured with DCPD and P-DCPD particles	97
Figure 6.6. LDH activity of MC3T3-E ₁ cells in presence of 1, 5, 10, and 1000 µg/ml DCPD and P-DCPD particles for culturing duration of 3 and 7 days.....	98
Figure 6.7. Quantitative image analysis of mouse air-pouch tissue treated by P-DCPD and DCPD particles for 1 week and 1 month. Membrane thickness analysis	100
Figure 6.8. Representative pouch tissues histology of microscopic appearance.....	101

LIST OF ABBREVIATIONS AND SYMBOLS USED

CPC's	Calcium Phosphate Cements
ACPP	Amourphous Calcium Polyphosphat
CPP	Calcium Polyphosphat
DCPD	Dicalcium Phosphate Dihydrate
P-DCPD	Polymeric Dicalcium Phosphate Dihydrate
PMMA	Poly(methyle methacrylate)
VCM	Vancomycin
EM	Erythromycin
XRD	X-ray Diffraction
SEM	Scaning Electron Microscopy
EDS	Energy Dispersive Spectroscopy
MIC	Minimum Inhibitory Concentration
Micro-CT	Micro Computed Tomography
PBS	Phospahte Buffer Saline

CHAPTER 1

INTRODUCTION

1.1 Basic Bone Physiology

Bone is a highly mineralized supporting frame of the body which is characterized by its mechanical stability, ability to regenerate and repair. In addition to protecting the role of vital organs, it provides an environment for marrow regarding blood formation and fat storage. One of the most critical roles of bone is to act as a mineral reservoir for calcium homeostasis and a reservoir of growth factors and cytokines, and also to maintain acid-base balance [1]. Bone continuously undergoes modeling and remodeling during our life span. This process is essential in order to change biomechanical forces, remodel or remove old bone and replace it with new, stronger bone tissue to help preserve its strength.

1.1.1 Bone Structure

Generally, bone is made up of: I. Inorganic (~69 %) component, mostly consisting of hydroxyapatite (~99 %) II. Organic (~22 %), constituted by collagen (~90 %) and non-collagen structural proteins. The functional component of the bone includes growth factors and cytokines. The hardness and rigidity of bone are due to the presence of mineral salt in the osteoid matrix, which is a crystalline complex of calcium and phosphate (hydroxyapatite). Calcified bone contains ~25 % organic matrix, 5 % water, and 70 % inorganic mineral (hydroxyapatite). Collagen I constitute 90–95 % of the organic matrix of bone (**Figure 1.1**). Osteoblasts synthesize and lay down precursors of collagen I [2]. They also produce osteocalcin, which is the most abundant non-

collagenous protein of bone matrix, and the proteoglycans of ground substance. The collagen I formed by osteoblasts is deposited in parallel or concentric layers to produce mature (lamellar) bone. When the bone is rapidly formed, as in the fetus or certain pathological conditions (e.g., fracture callus, fibrous dysplasia, hyperparathyroidism), the collagen is not deposited in a parallel array but in a basket-like weave resulting in woven, immature, or primitive bone. Osteoblasts also synthesize and secrete non-collagenous protein, such as proteoglycans, glycosylated proteins, glycosylated proteins with potential cell-attachment activities, and g-carboxylated (gla) proteins. The main glycosylated protein present in bone is alkaline phosphatase, which plays an as-yet-undefined role in mineralization of bone [3].

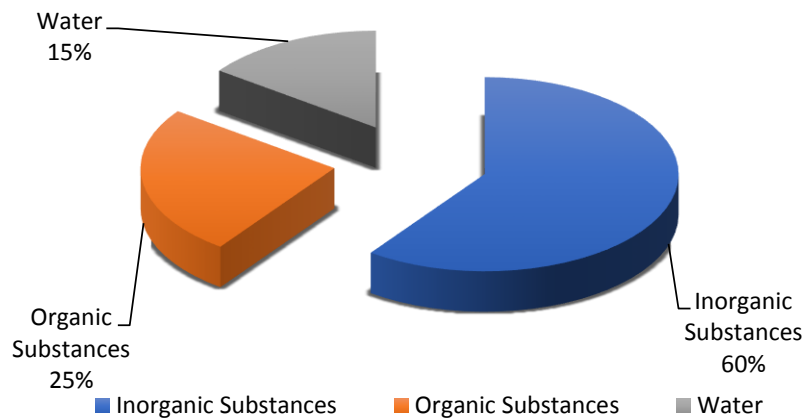


Figure 1.1. Bone composition

1.1.2 Bone Modeling & Remodeling

Bone consists of support cells; osteoblasts and osteocytes, remodeling cells; osteoclasts, and non-mineral matrix of collagen and non-collagenous proteins called osteoid, with inorganic mineral salts deposited within the matrix. During life, the bones undergo processes of the longitudinal and radial growth, modeling, and remodeling [4]. Longitudinal growth occurs at the

growth plates, where cartilage proliferates in the epiphyseal and metaphyseal areas of long bones, before subsequently undergoing mineralization to form primary new bone.

1.1.3 Current Bone Regeneration Strategies

Based on the type of bone loss, many options are possible. Currently, the standard bone fillers are autografts, allografts, and synthetic bone fillers. Due to limitation on autogenous bone availability in a patient, especially in pediatric patients and the elderly, and allografts fatal infection, the autografts and allografts use are limited [5-7].

From a synthetic bone substitute point of view, biodegradable calcium phosphates offer superior biocompatibility (resembling the mineral phase of bone) and, in many instances, a more readily controlled antibiotic release [8]. Therefore, for the purposes of subsequent recovery of bone, there is strong interest in calcium phosphate-based carrier development. Calcium phosphate cement (CPC) has been widely used as synthetic bone graft by injecting it into the bone defect area.

Owing biocompatible, osteoconductive and biodegradable nature; [9] calcium polyphosphate (CPP) has been studied for use in cartilage and bone repair, as well as for angiogenesis [9-13]. In addition, some of the studies have been done to develop low-temperature fabrication protocols for the inclusion of thermal-labile biological agents in CPP. Further the potential of this material for local drug delivery has been investigated [14-16]. This chapter intended to highlight the problem statement, possible solutions and some of the structural and in vitro properties of CPP that may impact its potential to serve as a carrier in a local delivery system.

1.2 Problem Statement: Osteomyelitis

1.2.1 Pathophysiology

Chronic osteomyelitis is an infection of the bone that does not result from acute hematogenous seeding or penetrating injury and usually occurs by contiguous spread and has been present for several weeks. In osteomyelitis cases, *staphylococcus aureus* is the most pathogenic; it typically causes skin infections and sometimes pneumonia, endocarditis, and osteomyelitis. It commonly leads to abscess formation. However, healthy bone is highly resistant to infection, upon implantation or surgical procedures, bacterial can reach the bone and cause inflammation. Advancement of infection to the rigid limitations of the marrow space causes reduction of blood flow provides an ideal site for bacteria to settle, and will eventually lead to local vascular occlusion and thrombosis as the inflammatory response grows.

Consequently, bone necrosis and the development of local sequestra are leading a complicated anatomical site to treat by systemic antibiotic delivery [5-8].

1.2.2 Treatment Options

Effective treatment of osteomyelitis can be achieved by addressing three interacting components: 1) anatomic stability, 2) microbiological virulence, and 3) host physiology [9]. A combination of antibiotic delivery and surgical approaches may be considered for addressing all osteomyelitis cases [10-12].

The standard method to overcome osteomyelitis consists of debridement, dead space management, and a prolonged antibiotics administration. Surgical debridement is an essential first step in treating this disease. It reduces bacterial load, removes necrotic tissue and visible sequestra, and potentially allows for the apposition of healthy bone, though not without temporarily causing

some destabilization of the site [9]. Additional to surgical debridement and dead space management, antibiotics are traditionally administered systemically for at least six weeks [11-13]. However, as 6 weeks of systemic antibiotic administration is insufficient in many cases of chronic osteomyelitis [14, 15] and there is a growing concern over antimicrobial resistance development with prolonged antibiotic presence [10], therefore introducing a carrier for localized delivery of antibiotics come to play a critical role. This strategy may achieve elevated antibiotic concentrations at the site of infection and limit the side effects and risk of overdose otherwise seen with systemically administered therapeutics, as well as offer additional therapeutic value by supporting bone restoration. Although CPC materials are biocompatible and set isothermally, they have some drawbacks regarding mechanical stability and drug burst release. The initial reason for these limitations refers to weak binding mechanism of hydroxyapatite with drug [16]. As previously discussed more complexity of material prolongs drug release. A unique class of calcium phosphate, calcium polyphosphate (CPP) may offer an advantage in this regard as it resembles a polymeric compound and can make complex with drugs. The partial objective of this research is to examine CPP capacity to act as a local delivery system for treatment of osteomyelitis, and subsequently effect of CPP on DCPD formation and drug delivery capacity of newly developed P-DCPD.

1.2.3 Antibiotics Studied for Localized Osteomyelitis Treatment

Vancomycin (VCM) and erythromycin (EM), with minimum inhibitory concentration (MIC); 2 mg/L, are two antibiotics of choice in this study.

VCM is water-soluble and stable in body temperature. As a tricyclic glycopeptide antibiotic, VCM reportedly inhibits cell wall peptidoglycan synthesis in gram-positive bacteria [17]; by preventing DNA, RNA, and protein synthesis it will in time lead to the death of the

bacterial cell. Furthermore, VCM has shown fewer negative effects on osteoblasts *in vitro* and should be less likely to impede bone growth than other commonly used antibiotics [18-20].

EM is an antibiotic from macrolide family which suppressing bacterial growth by inhibiting crucial proteins for bacterial function. EM is stable in body temperature but it belongs to the hydrophobic category of antibiotics agents. EM is broadly used to treat infections caused by various bacteria, including *S. aureus*[21]. The first use of EM in clinical setting dated back to the early 1950s. In addition to direct targeting against bacteria, EM also helps with bacterial infection symptoms by suppressing inflammation [22, 23]. EM has been shown to reduce the production of pro-inflammatory cytokines in various scenarios [24, 25]. While *S. Aureus* frequently evolves to acquire resistance to antibiotic treatment, the combination of EM with other antibiotics or herbal medicines seems to be able to overcome this difficulty and results in a synergistic effect in suppressing bacterial growth [26]. Interestingly, although the efficacy of EM has been reported in various scenarios, its role in treating Methicillin-resistant *Staphylococcus aureus* (**MRSA**) induced osteomyelitis is not well documented.

This dissertation, including both hydrophilic and hydrophobic antibiotics leads to a better understanding of interaction between fully hydrated polyphosphate chains of ACPP with these therapeutics.

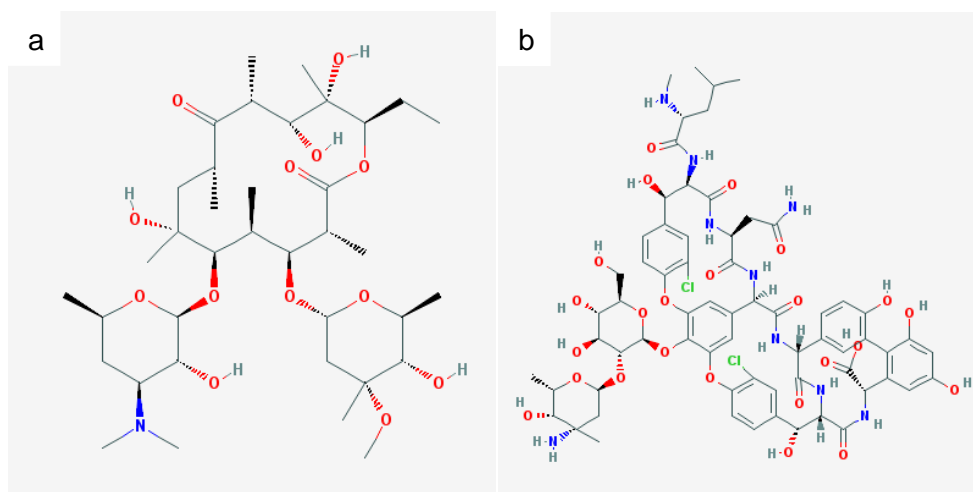


Figure 1.2. Molecular schematic of a) EM: $C_{37}H_{67}NO_{13}$ and b) VCM: $C_{66}H_{75}Cl_2N_9O_{24}$ (adapted from PubChem)

Table 1.1. Chemical properties of EM and VCM

Erythromycin (EM)		Vancomycin (VCM)	
Molecular Weight (g/mol)	pKa	Molecular Weight (g/mol)	pKa
733.93	8.6 - 8.8[27, 28]	1449.265	2.6, 7.7, 8.6, 9.6, 10.5, 11.7

The molecular structure of VCM (**Figure 2.2**) consists of 18 chiral centers surrounding three “cavities” that are bridged by five aromatic rings [29]. This antibiotic is able to have strong polar interactions with solutes likely as a result of the strong polar groups proximate to the ring structures.

These groups include a carboxyl group (pKa of 2.18), a primary amino group (pKa of 7.75), a secondary amino group (pKa at 8.89) and three phenol groups (pKa of 9.59, 10.40, 12.00) [29]. The two amino groups have basic properties, while the carboxyl and phenol groups are more

acidic. The net positive charge of VCM across a 0 to 13 pH range is varied: it is +2.1 at pH of 2, +0.7 at a pH of 3-7.4, and +4.0 at a pH of 13[29]. The unique size and structure of VCM may impact how this antibiotic is loaded and released from the CPP-based local delivery system. For example, owing to VCM being a large molecule and potentially having some chemical steric hindrance, strong evidence has been presented that any chemical interaction between this antibiotic and calcium phosphate materials is limited [30-33]. Instead, the loaded VCM interacts with calcium phosphate materials via physical adsorption and, as a result, the manner in which VCM is incorporated into a calcium phosphate material is of particular importance [34, 35]. VCM is a hydrophilic molecule with a molecular size of around 1.8 nm [36].

The molecular structure of EM consists of 14 lactone ring. EM is an antibiotic that belongs to the group of macrolide antibiotics. The structural characteristic of macrolides, to which EM affiliates, is a macrocyclic lactone ring of fourteen, fifteen or sixteen members. Substituents on the main chain are cladinose on C-3 and desosamine on C-5. EM is not a single compound but represents an alloy of structural very similar components. EM is hydrophobic molecule with a size of 1.6 nm [37].

1.3 Currently Studied Biodegradable Carrier Materials for Localized Osteomyelitis Therapy

Biodegradable delivery vehicles have been the focus of recent local therapy research and are of interest in the doctoral research presented here largely as they eliminate the need for reoperation and removal following treatment [38-44]. Also owing to its eventual degradation, a biodegradable carrier is not as limited by the size or type of antibiotic that may be loaded and offers greater antibiotic availability than that possible with PMMA. Biodegradable carrier materials of interest include natural polymers such as collagen (e.g. CollatrapG® and

Septocol®E), and bone graft substitutes including calcium sulphate (e.g. Herafill®, Osteoset®T), bioactive glass (e.g. Bioglass®, BonAlive®), and calcium phosphate (e.g. Vitoss®, Bonesource®). Disadvantages of collagenous and calcium sulfate carriers include the high risk of seroma formation (i.e. an accumulation of serum) and burst release owing to a ready absorption of large amounts of water into these materials [45-48]. For synthetic aliphatic polyester polymers, the most significant disadvantage is the potential for bone resorption during carrier degradation [47]. With bioactive glass matrices the processing control is more complex and has, to date, limited their application for drug delivery [47, 49]. For example, conventional organic compounds used to create porosity within the Bioglass® matrices cannot be readily removed upon heat treatment [50]. Furthermore, despite the relative interest in many of the aforementioned carriers, there is a lack of knowledge to evaluate their relative value in treating chronic osteomyelitis [48]. As a result, there are still many carriers awaiting FDA approval for use as an antibiotic delivery vehicle. Commercially available applications in osteomyelitis treatment remain sparse and much research is still required in this field.

Based on studied carriers, biodegradable calcium phosphates offer superior biocompatibility (owing to chemistry resembling the mineral phase of bone) and, in many instances, a more readily controlled antibiotic release [48]. Therefore, for the purposes of osteomyelitis therapy and subsequent recovery of bone, there is strong interest in calcium phosphate-based carrier development. A unique class of calcium phosphate, calcium polyphosphate (CPP) may offer an advantage in this regard as it possesses some potentially unique drug delivery-relevant attributes of its own.

Owing to its biocompatible, osteoconductive and biodegradable nature [51-53], CPP has been studied for use in cartilage and bone repair, as well as for angiogenesis [51, 54-57]. In

addition, recent progress in the development of low-temperature fabrication protocols for the inclusion of thermal-labile biological agents in CPP has further supported the potential of this material for local drug delivery[43, 58, 59]. The next section highlights some of the structural and in vitro properties of CPP that may impact its potential to serve as a local drug delivery system.

1.4 Calcium Polyphosphate (CPP) Hydrogel

1.4.1 CPP Structure

Structural properties of polyphosphate glasses are more dependent on the P-O-cation interchain bonding than the nature of the P-O-P bonds that form the phosphate chain [60]

The phosphate structure consists of phosphorus atom surrounded by four oxygen atoms arranged at corners of a tetrahedron; this satisfies Zachariasen's criteria [60, 61]; Interconnected PO_4 tetrahedra are then produced when these oxygen atoms are shared via covalent bonds [61]. These basic building blocks of phosphate are classified following Q^i terminology, where "i" indicates the number of bridging oxygen per tetrahedral.

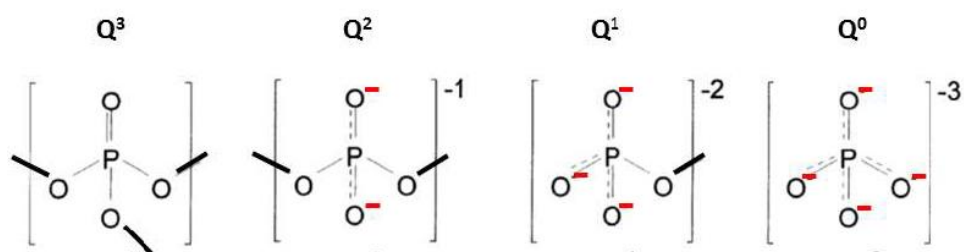


Figure 1.3. Q^i phosphate tetrahedral species [60]

The phosphate species include Q^0 as an orthophosphate ion, Q^1 as a pyrophosphate or chain end group, Q^2 as an internal phosphate group, and Q^3 as a branched phosphate group. By combining the end groups, middle groups, and branching points a number of different phosphate networks

can be formed. Of interest in this thesis is a linear long-chain phosphate structure that consists mainly of the Q^2 species. As a result of the high charge associated with the tetrahedral anions, phosphates tend to associate strongly with cations under most conditions [61]. CPP itself consists of long polymeric chains of phosphate connected via covalent bonds and “chelated” calcium (Ca) ions as network modifiers/connectors between chains [62, 63].

1.4.2 CPP *In Vitro* Properties

The sharing of available oxygen atoms alters the environment around the calcium ions in a way that, upon contact with water, there is a competition between the oxygen from terminal phosphate groups and water to bond with calcium ions. Continued exposure to aqueous media encourages the gradual degradation of CPP by two interdependent steps: (1) the exchange of calcium ions in CPP with hydrogen ions from the media, resulting in the formation of a hydrated layer at the interface between CPP and media, and (2) the network breakage of P-O-P bonds under the attack of hydrogen ions and water molecules [44, 63-67]. Fully hydrated phosphate chains disentangle from partially hydrated chains still attached to the surface and leach into the solution [66]. Hydrolytic degradation in the presence of calcium occurs significantly at the inner P-O-P linkages and continues to produce shorter and shorter polyphosphate chains [68, 69]. However, alternative degradation paths include splitting of end PO_4 groups and, to a lesser degree, ring formation (e.g. tri- and tetra-metaphosphate) [69, 70]. Depending on the solution pH, as CPP degradation continues beyond several days precipitates such as $Ca_3(HP_2O_7)_2 \cdot 4H_2O$ and $Ca(H_2PO_4)_2$ start to form [70]. Overall, longer chains do not release the orthophosphate as quickly as shorter chains, pH will not drop as quickly, and there will be fewer preferable sites for chain scission with a reduced degradation rate compared to short molecular chains [67]. Increasing the

chain length of CPP, then, maybe one useful approach to further control the degradation of the carrier and release of the loaded antibiotic in vitro.

1.4.3 CPP Synthesis

CPP can be fabricated to give phosphate glass or crystalline material by manipulating the processing parameters and starting compounds used. In the proposed studies, the CPP glass is the material of interest. According to the literature, the most common method for fabricating amorphous CPP is directly from phosphate melts following prior condensation of a starting calcium phosphate hydrate [71]. The heat ramp rates, temperatures, and dwell times of calcination are important parameters to consider when synthesizing CPP from a calcium phosphate monobasic monohydrate (CPMM) (i.e. $\text{Ca}(\text{H}_2\text{PO}_4)_2 \cdot \text{H}_2\text{O}$). These parameters need to be of sufficient magnitude in order to drive off the crystalline water and initiate condensation and to, subsequently, further polymerize the phosphates [67, 71]. In this proposal we always synthesize ACP using aforementioned protocol [72], briefly; Calcium phosphate monobasic monohydrate, ($\text{Ca}[\text{H}_2\text{PO}_4]_2 \cdot \text{H}_2\text{O}$; Sigma-Aldrich, St. Louis, MO) were calcined for 10 hours at 500°C followed by melting for 1 hour at 1200°C to produce an amorphous glass and quenching at room temperature for cooling. The resulting material was hammered to make small particles prior to grind in a planetary ball mill (Across International, Berkeley, NJ). The resulting particles were sieved (Laboratory Test Sieves, Fisher Scientific, Pittsburg, PA) continuously to segregate particles less than 75 μm . Prior to usage, ACP powders were stored in a vacuum desiccator to avoid moisture absorption.

1.5 Matrix Fabrication Strategy for Localized Osteomyelitis Therapy

1.5.1 Current Status in the Literature

One of the greatest challenges in designing drug delivery systems is how to load the drug in a way that retains its activity as well as maintaining all necessary scaffold characteristics for optimal elution. As traditional ceramics processing involves the consolidation of powders by molding and sintering, the high temperatures involved prevent the loading of the drug until the shaping of the final implant has been completed [73]. Various techniques have been used to incorporate a therapeutic agent with a pre-made calcium phosphate biomaterial [34]. These techniques include powder-powder mixing [74-76], adsorption of agent on the biomaterial following some degree of solution soaking, and centrifugation of solution into porous construct. These methods face some limitations due to relatively fast therapeutic release common to many of these approaches. The matrix design presented in this research takes advantage of fully hydrated and moldable amorphous CPP to create a delivery device with sustained release.

For several years our research group has sought to exploit the unique protocol of making hydrogel from CPP glass to achieve more robust therapeutic loading with the more controllable and sustained antibiotic release [72]. Due to the chelation of calcium ions to the phosphate chains of CPP, any exposure to water molecules is believed to cause a preferential bonding of hydrogens to the protons already connected to the non-bridging-oxygen atoms [62, 63]. One early theory proposed by Dion et. al., based on this behavior of CPP in high humidity, suggested that the solvation or hydrolysis, then condensation, and, lastly, drying steps involved in gelling of CPP could create an altered polyphosphate structure [43]. In this method, they were able to reduce the burst release of VCM from the gelled amorphous CPP disks and extend the therapeutically-relevant release period compared to un-gelled disks to six days. However, despite greater sample densities observed in the internal regions of the gelled samples compared to non-gelled samples, the disk tensile strength decreased with increased gelling time until a minimum of 0.411MPa was

reached following 48 hours of gelling [43, 58]. This was believed to be due to the congruent creation of larger pores at the surface of the disks with longer exposure to humidity, and the changing distribution of pores and pore sizes throughout the bulk of the disk. The uneven distribution of pores also likely contributed to the still present, though reduced, burst release.

Currently, in our research group, a new method to prepare CPP hydrogel was introduced. In this method, polyphosphate chains become fully hydrated by exposing to water. As it has been noted in previous studies on this hydrogel, because of the numerous advantages of CPP hydrogel, it can take place of monomeric calcium phosphate in forming calcium phosphate cement (CPC). The resulting cement is called “polymeric dicalcium phosphate dihydrate” (P-DCPD).

1.5.2 Novel P-DCPD Bone Cement

Calcium phosphate cement (CPC) is promising for clinical applications due to their advantageous properties including bioactivity, osteoconductivity, injectability, and moldability. The discovery of the first CPC occurred via the observation of calcium phosphate solubility behavior [77]. The self-setting reaction is usually based on the freshly prepared mixtures of monomeric calcium phosphate powders, such as acidic monocalcium phosphate monohydrate (MCPM) and basic calcium phosphates (e.g., tetracalcium phosphate, TTCP) with an aqueous solution, which undergo setting in a continuous dissolution–precipitation reaction [77, 78]. Various mixtures of calcium and phosphate, basically produce two cement types [79]: hydroxyapatite (HA), and dicalcium phosphate dihydrate. CPC is biodegradable in vivo and replaced by new bone tissue [80, 81]. DCPD forming cement degrade much faster than HA forming cement. Many studies have demonstrated the bone remodeling capacity of such cement in various animal models within a time period of 8–52 weeks [82-84]. CPCs are commonly used

to repair bone defects due to their good biocompatibility and isothermally setting reaction. However, the clinical application of CPCs has been greatly limited because of their inherent low mechanical strength [78, 85] and poor cohesion [78, 86]. Many efforts have been applied to CPC granules modification [87, 88]. Some actions have been taken to increase CPC mechanical strength to modify the cement liquid with some polymeric materials such as collagen [89, 90], the use of dual-setting cement in which a dissolved monomer is simultaneously cross-linked during cement setting [85, 91]. The other kind of modification refers to dual-setting system applying polymeric compounds, in a way that can be cross-linked by binding calcium ions in the polymer chain, e.g., polyacrylic acid. In these methods, polymers bind through dissolution–precipitation mechanism as well as deprotonating the organic acid following the formation of intra- or inter-chained bonding Ca^{2+} –Acid chelates. One of the most important concerns regarding this organic polymer-based dual-setting system is the toxicity of non-degradable additives (fibers, polymers). In addition after 40 years, there are still limitations in generating effective methods to overcome weak mechanical strength and poor cohesion of CPCs [78]. Basically, Polyphosphates are polyelectrolytes that play major roles in biological and material science [92, 93]. Calcium polyphosphate (CPP) is composed of linear polyphosphate chains with Ca/P ratio of 0.5. CPP is easily hydrolyzed into the naturally-occurring calcium orthophosphate [71, 72]. Recent studies, including our research group's work, found that CPP represents a promising bone substitute because of its biocompatibility [62], mechanical strength, and stimulation of bone healing [71, 94]. The unique structure of CPP allows CPP to behave as an inorganic polymer to some extent [95]. In this study, CPP was prepared in amorphous structure rather than any crystalline structure (gamma-, beta-, or alpha-phase).

Recently, it has been found that CPP gel can be formed by soaking amorphous CPP (ACPP) in the presence of water [72]. The increased water availability accelerates the water molecule

ingress and microstructural transformation of CPP gels. In our research group by using Raman spectroscopy, it has been demonstrated that the mechanism of CPP gelation is mainly due to the bridging network between linear polyphosphate chains and calcium (Ca^{2+}) in the water and entanglement of polyphosphate chains [72]. In another attempt in our research group, a novel and simple method to prepare injectable and self-setting P-DCPD cement by the reaction of CPP gel with tetracalcium phosphate ($\text{Ca}_4(\text{PO}_4)_2\text{O}$, TTCP) were described. In contrast to the classical CPC setting formula (reaction of monomeric acid calcium source with alkali calcium source) [78], Song et. al. used CPP gel as the acidic calcium source. They found that the setting mechanism of P-DCPD is completely different from the classical calcium phosphate cement (CPC) that achieves crystallization by monophosphates reaction. P-DCPD introduces a new type of poly-CPCs with some superiorities, including strong mechanical strength, excellent cohesion and easy of handling. More extensive experiments to further evaluate the performance of P-DCPD cement, including biocompatibility and degradation behavior, were addressed here.

1.6 Summary of Dissertation & Specific Aims

My goal is to comprehensively investigate physicochemical properties and bioactivity of CPP hydrogel itself as well as P-DCPD forming cement. Thus, in the previous studies, our group developed and characterized CPP hydrogel [72]. Further in **Chapter 2**, I study the drug delivery capacity of CPP hydrogel to determine whether fully hydrated polyphosphate chains improve antibiotics encapsulation to address a fairly common burst release issue. I test various factors that impact drug loading efficacy. Investigation on parameters such as antibiotics' chemical structure (hydrophobic and hydrophilic), incorporation techniques (powder or gel), and finally change in viscoelastic properties of ACPP gel with and without antibiotics, is valuable in terms of taking one

step toward improvement of antibiotic incorporation in the bone infection area. In **Chapter 3**, I study antibacterial response of P-DCPD cement loaded with antibiotics in agar plate. In this way the bacterial inhibition area is measured and the effect of antibiotic retained within the bone cement is tested. In **Chapter 4**, the classical DCPD cement that was upgraded by CPP hydrogel instead of monomeric calcium phosphate material is under investigation by developing a series of characterization experiments. Physiochemical variations between DCPD and P-DCPD is fully understood. Individually, I perform a series of characterization measurements such as; Raman spectroscopy, contact angle, zeta potential, and pH measurements of P-DCPD and DCPD particles. As the last and most important piece in the puzzle of understanding the P-DCPD qualification as a biocompatible bone cement material, in **Chapter 5**, I conduct in Vitro and in Vivo biocompatibility study of P-DCPD and DCPD, physiochemical differences (**Chapter 4**) may play an important role in biocompatibility characteristics of these materials.

1.6.1 Specific Aim 1: Develop a Strategy to Study Antibiotics Effect on Structural and Physiochemical Properties of Calcium Polyphosphate Matrix

In this aim, we study the nature of any physiochemical interaction between EM/VCM and ACPD hydrogel.

Hypothesis: Antibiotics interact with a fully hydrated ACPD matrix by physical and ionic interaction which leads to delayed antibiotic release.

- a) Antibiotic loading comparison for two incorporation methods demonstrates the role of fully hydrated polyphosphate chains in antibiotic-hydrogel interaction
- b) Raman Spectroscopy and identify molecular-level interaction between antibiotics and ACPD hydrogel

- c) Viscoelastic properties of ACPH hydrogel was affected upon antibiotic incorporation
- d) Antibiotics release mechanism from ACPH hydrogel further confirms the interaction between antibiotics and hydrogel
- e) Antibacterial activity of released antibiotics depends on the sensitivity of antibiotics to the elution medium.

1.6.2 Specific Aim 2: Antibacterial Activity of Polymeric Dicalcium Phosphate Dihydrate (P-DCPD) Loaded with Antibiotics

Next, I implement, for the first time, antibiotics within P-DCPD bone cement by 2 approaches. Mix antibiotic with ACPH hydrogel first and then add complementary powders to prepare P-DCPD bone cement. In second approach I add antibiotic powder to complementary powder portion of P-DCPD cement and then add ACPH hydrogel. In this way I investigate which way more effectively retains antibacterial activity of antibiotics during the Agar plate experiment. made by ACPH hydrogel would be tested for antibiotic interaction with material and its activity stage. I measure the bacteria growth inhibition area by diffused antibiotics from P-DCPD cement discs using Kirby-Bauer method.

Hypothesis: P-DCPD antibiotic preserves the antibacterial activity of VCM and EM due to neutral pH of release medium higher than what has been reported for CPP hydrogel.

- a) Preparing P-DCPD discs loaded with antibiotics using two methods
 - Antibiotic mixed with ACPH hydrogel
 - Antibiotic mixed with sodium citrate and TTCP powder
- b) Antibacterial activity of P-DCPD thin disc using Kirby_Bauer method

1.6.3 Specific Aim 3: Physiochemical Comparison of DCPD and P-DCPD

Previously a study was conducted to reveal P-DCPD advantages over DCPD material in terms of mechanical stability, cohesion and handling properties. I conduct, contact angle, Raman spectroscopy, zeta potential, and pH measurements on mature DCPD and P-DCPD particles to understand the setting mechanism and morphology of particles.

Hypothesis: P-DCPD particles (<75 μm) as a new self-setting reaction system is completely different from the classical DCPD (<75 μm) setting-reaction system that achieves crystallization by monophosphates reaction. Also upon addition of citrate to PDCPD handling properties, mechanical stability represents a new type of poly-CPCs with significant advantages over current CPC products.

- a) To differentiate the particles, Scanning Electron Microscopy (SEM) and Energy Dispersive Spectroscopy (EDS) were utilized to characterize the particles' morphology and Ca/P ratio.
- b) Dynamic change of bonding (vibrational) mechanism through incubation times were studied by Raman spectroscopy
- c) Phase changes and molecular identification were investigated through XRD
- d) Measurement of net charge of particles in H_2O immersion has been conducted using Zeta Potential
- e) Relative surface hydrophilicity and absorbance rate is another important factor for the cement to be qualified as a favorable material for cell attachment, which can be measured by a surface contact angle.

1.6.4 Specific Aim 4: Biocompatibility comparison studies of P-DCPD and DCPD in Vitro and in Vivo

The growth and differentiation of different cells need appropriate microstructures of ECM. However, it is still unclear how the cells choose and what kinds of microstructures the specified cells prefer. After defining the physicochemical properties of ACPP and P-DCPD, we should be able to investigate the cellular behaviors of these well-defined materials.

More importantly, after in vitro biocompatibility testing, and in vivo biocompatibility study for testing tissue response on both P-DCPD and DCPD scaffolds is needed. As such, for further extending the results to show P-DCPD performance in a mouse air pouch model, I design an animal study with different steps, based on my hypothesis.

Hypothesis: Several factors such as surface charge, microporosity, composition and changes of molecular composition, affect osteoblast cell adhesion and migration process to the surface. Based on preliminary results from physiochemical differences between DCPD and P-DCPD, it is expected that cells behave differently in terms of proliferation and differentiation on each material. Based on previously studied unique properties of P-DCPD and DCPD, mouse air pouch tissue represents different inflammatory responses. To support our hypothesis we performed the following steps;

- a) One key requirement for calcium phosphate materials to be bioactive and bond to the living bone is the formation of a bone-like apatite layer on their surface. This phenomenon can be reproduced in vitro using simulated body fluid, a protein-free solution with ion concentrations similar to those of human blood plasma.
- b) Cell culture: Use osteoblast-like cells, to study the cell proliferation on the samples
- c) To examine cytotoxicity and cell growth on the substrates, LDH and MTT assays were designed for quantitative evaluation.
- d) Histological analysis of air pouch tissue to determine any inflammatory response

CHAPTER 2

Comparing the Release of Erythromycin and Vancomycin from Calcium Polyphosphate Hydrogel Using Different Drug Loading Methods

Disclosure statement

Chapter 2 of this dissertation is derived from *Chehrehghanianzabi, Y., Barua, R., Shi, T., Yurgelevic, S., Auner, G., Markel, D. C., & Ren, W. (2019). "Comparing the release of erythromycin and vancomycin from calcium polyphosphate hydrogel using different drug loading methods"*. The following article and data are published in the Journal of Biomedical Materials Research Part B: Applied Biomaterials and have been reused with permission from the publisher. All rights are reserved.

2.1 Purpose and Hypothesis

The purpose of this aim is to acquire a comprehensive understanding regarding antibiotic-ACPP hydrogel interaction as well as ACPP hydrogel properties upon antibiotic incorporation. In this study two types of commonly used antibiotics namely EM and VCM for Osteomyelitis were studied. The intention behind choosing EM and VCM was to demonstrate that hydrophobicity and hydrophilicity of antibiotics can impact the elution. Preliminary experiments evaluate microstructure, physicochemical properties, and activity of eluted antibiotics after release.

2.2 Introduction

The bacterial infection is one of the most challenging topics in orthopedic tissue engineering.[96-98] Osteomyelitis has been recognized as an inflammatory response that can actively transmit a local infection to surrounding tissue and lead to bone loss.[99, 100] To address such a challenging issue, localized antibiotics delivery from biocompatible bone cement material is one of the best-proposed solutions.[101] However, a desired and slow eluting antibiotic release method has not been previously achieved.

Calcium phosphate cement (CPC) has been studied for more than 2 decades to address common bone infections [102-105]. CPCs such as hydroxyapatite and tricalcium phosphate have been widely studied as local antibiotic delivery carriers [30, 106-109]. However, the rate of degradation and resorption of CPCs do not match well with the drug release and bone formation rate. In addition to weak antibiotic binding to CPCs, hydroxyapatite restricts full antibiotic release due to its low resorption rate [98, 110] as opposed to fast degrading tricalcium phosphate that initiates early burst release of antibiotics [16, 111].

Currently, polymer additives are the approved materials to prolong drug liberation.[112-116] These additives have emerged in bone tissue engineering to address CPC's limitations and to strengthen drug release capability of CPCs.[116-118] However, due to the non-biodegradability of some of these polymer additives, surgical removal is required. Thus, a polymeric biomaterial, similar to bone material, with the ability to resorb in time is expected to resolve these limitations.

Calcium polyphosphate (CPP) is a biocompatible and biodegradable ceramic material. CPP is osteoconductive and enables new bone formation on the surface both in vitro and in vivo. [71, 94, 119, 120] In 1977, Fukui et al. [121] at the first time reported the bone healing capacity of CPP in a rat femur implantation model and noticed that CPP represents one of the desired bone graft

substitutes because of its safety and high affinity to the bone. Current studies have shown that CPP can be used as a ceramic-based local drug-eluting device [43, 58, 59, 94, 122]. Initial observation on gelled CPP matrix showed the ability of linear CPP to delay antibiotic release using repeated gelling protocol [43]. Dion et. al reported that VCM release was significantly reduced during the first 2-4 h of elution, while it retained its bactericidal activity.[43] In a separate study, they demonstrated by P-NMR and Raman Spectroscopy that antibiotic incorporation does not transform the gelling-drying process.[58] However, polyphosphate chains presented in their studies have not been fully hydrated, thus the antibiotic interaction with polyphosphate chains may not be fully revealed in the gelled CPP, developed by Dion et. al. Recently, Song et. al. [72] introduced a simple process to prepare CPP hydrogel that suggests a unique gel formation process based on intermolecular ionic interaction and polyphosphate chain entanglement. The unique interaction abilities of CPP hydrogel requires a deep understanding to reveal the antibiotics' reaction mechanism. EM is known as a hydrophobic antibiotic with the ability to enhance bone formation[123] and VCM is the most common hydrophilic antibiotic to treat osteomyelitis.[124-127] In this study, the reaction mechanism of EM and VCM with fully hydrated polyphosphate chains was investigated.

The goal of this study was to describe the drug delivery potential and properties of a novel CPP hydrogel matrix made by exposing amorphous CPP to the large volume of water and applying subsequent gel formation procedure. In this study, we demonstrate the effectiveness of fully hydrated polyphosphate chains of CPP hydrogel on the interaction mechanism of antibiotic with the hydrogel matrix.

2.3 Materials and Methods

2.3.1 Synthesis of CPP powder and CPP hydrogel

Calcium phosphate monobasic monohydrate, ($Ca[H_2PO_4]_2 \cdot H_2O$; Sigma-Aldrich, St. Louis, MO) were calcined for 10 h at 500°C followed by melting for 1 h at 1200°C to produce an amorphous glass and quenched at room temperature for cooling. The resulting material was hammered to make small particles prior to grind in a planetary ball mill (Across International, Berkeley, NJ). The resulting particles were sieved (Laboratory Test Sieves, Fisher Scientific, Pittsburg, PA) continuously to segregate particles less than 75 μm . A Quanta FEG 450 scanning electron microscope (FEI, Hillsboro, OR) and a Beckman Coulter particle size distribution analyzer (LS 13 320 Series, Lakeview Parkway S Drive, Indianapolis, IN) show that particle sizes obtained in this study are less than 10 μm (**Figure 2.1 A-B**). Prior to usage, CPP powders were stored in a vacuum desiccator to avoid moisture absorption. For hydrogel preparation, CPP powder was added to distilled water ($0.1 \text{ g}\cdot\text{ml}^{-1}$), stirred for 90 min at 700 rpm at room temperature (25 °C) and suspended for 24 h until produced gel become precipitated and water phase becomes clear. There is a phase separation between CPP gel and water after gelation.

2.3.2 Antibiotic loading

VCM and EM were selected as common clinically relevant treatments for methicillin-resistant forms of *Staphylococcus aureus* (MRSA) infections. Noting that specific physiochemical properties of antibiotics may influence their release profile accordingly. The influence of hydrated polyphosphate chains on antibiotic binding mechanisms was studied by comparing two antibiotic loading methods, namely “Powder_Mixture” and “Gel_Mixture” method. In Powder_Mixture method antibiotics and CPP powders were mixed (1:10) (10 % (w/w)) by spatula for 10 min before

gel preparation. In Gel_Mixture method, the antibiotic powder was added to the formed CPP hydrogel (1:10) (10 % (w/w)) and mixed well to obtain a homogeneous gel as much as possible, before testing.

2.3.3 Antibiotic release measurements

Gels prepared by both methods were submerged in 50 ml ultra-pure water and the volume remained fixed throughout the experiment in static condition. To measure the released amount of antibiotics, the antibiotic assay was run for 1ml of supernatant which was collected in 2, 24, and 48 h for both methods. The amount of VCM and EM released into the supernatant was measured by absorption using an ultraviolet-visible spectrophotometer (BioTek Instruments, Inc., Winooski, Vermont, USA). EM concentration was determined at 485 nm using regular 96-well plates, by adding 0.1 ml of 3M sulfuric acid and 0.1 ml of supernatant to the plate and by heating it up to 50 °C for 30 min as well as by warming the plate reader up to the same degree in advance. This reading method has been studied for EM by Arayne et. al. [128] and they found that 30 min of warming up the plate reader can significantly enhance the absorbance at 485 nm.

VCM concentration was determined in a UV plate by a slightly different protocol. Briefly, 100 µl of the sample solution was loaded in the UV plate and absorbance at 295 nm was measured. Ultra-pure water was used as the assay solution. The experiment was repeated three times with duplicate for each gel preparation method. Data were compiled for “VCM_Powder_Mixture” and “VCM_Gel_Mixture”.

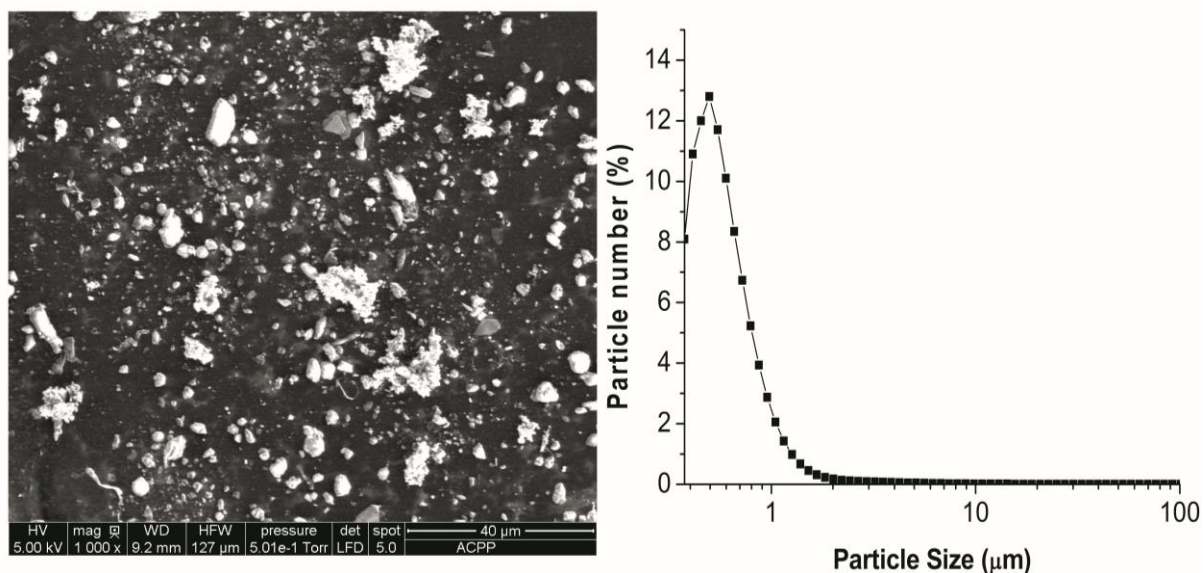


Figure 2.1. ACPP Particle size analysis. (A) SEM analysis (1000 x magnification) demonstrated that the particle sizes were less than 10 μm ; (B) Particle size distribution test uses a dry powder system and Fraunhofer optical method. The average number particle sizes are $0.68 \pm 0.53 \mu\text{m}$

2.3.4 Raman spectroscopy

An Invia Raman microscope (Renishaw, Gloucestershire, UK) with a 785 nm excitation laser, and WiRE 3.3 software was used to measure the vibrational pattern of CPP hydrogel, Gel_Mixture, and Powder_Mixture. A 50x N-plan Leica microscope objective with a numeric aperture of 0.75 and a working distance of 0.75 mm was used for measurements. The laser power was approximately 115 mW at the measurement site of 100% energy. Spectra were measured at 50% laser power for three accumulations of 10 s each over a spectral range of 200–1600 cm^{-1} with spectral resolution varying from 0.87 to 1.11 cm^{-1} . To eliminate background noises, the spectra were preprocessed by applying an in-house developed LabVIEW procedure for background subtraction and further normalizations.[129] Measurements were taken from each sample and

averaged to achieve minor variations within the measurement system. The Raman spectra of CPP hydrogel were measured immediately after antibiotic loading.

2.3.5 Rheological evaluation

Rheological experiment (ARG2, TA Instruments Inc., New Castle, DL) was performed to measure the impact of antibiotics on the viscoelastic properties of CPP hydrogel. A standard 40 mm diameter parallel plate was used in this study. Gel_Mixture and CPP hydrogel were prepared and submerged in water to stay fully hydrated. 1 mL of the fully hydrated gel was placed on Peltier plate. An oscillatory stress sweep (from 0.001 to 1 Pa) at a fixed frequency (0.16 °Hz) was applied to the sample. Frequency stress sweep and finally creep-recovery experiment with the fixed stress and time values were performed. The viscoelastic measurements such as; storage modulus (G'), loss modulus (G''), and complex viscosity $|\eta^*|$ as well as strain, were conducted for each sample. For frequency sweep, all G' , G'' , and $|\eta^*|$ were measured across a frequency range of 0.1-100 rad s^{-1} . The experiment was conducted at 25°C to evaluate dynamic viscosity of CPP hydrogel vs. Gel_Mixture. Also, the manufacturer provided a solvent trap bar to be loaded at the first 300 s of the experiment to avoid evaporation. Hydrogels loaded with antibiotics were prepared freshly prior to the experiment.

2.4 Statistical analysis

The influence of the gelling process on the release rate of VCM and EM, throughout the elution study, were analyzed by Paired Student T-test using excel where significant differences were identified between antibiotic release from two treatment groups namely, Powder_Mixture and Gel_Mixture. The release amount of EM and VCM from the powder_mixture method was

significantly higher than release of the same antibiotic from gel_mixture method within the early elution time points ($p < 0.05$).

2.5 Results

2.5.1 Antibiotic assay

The accumulated antibiotics release from Gel_Mixture and Powder_Mixture are shown in **Figure 2.2**. As the data suggests, the antibiotic release was restricted more for the Gel_Mixture method. The Gel_Mixture shows a significantly lower release of both EM and VCM [solid line] as compared to Powder_Mixture up to 48 h of submerging in water [dashed line]. The 48 h cumulative release of EM was ~7.5 % in Gel_Mixture, as compared to ~27.5 % in the Powder_Mixture method. A similar pattern was observed for VCM. The 48-h cumulative release of VCM was ~ 12.5 % in Gel_Mixture, as compared to ~ 22.5 % in Powder_Mixture method.

There is a release pattern difference between EM and VCM using both Gel_Mixture and Powder_Mixture methods. Though the trend of release pattern of EM and VCM is similar using the Gel_Mixture method, a higher release rate of EM was observed comparing to VCM using the Powder_Mixture method. The drug release curves of EM and VCM was merged at ~27 h. The release rate of VCM started to reduce post 27 h and remained at a lower rate of release for up to 48 h.

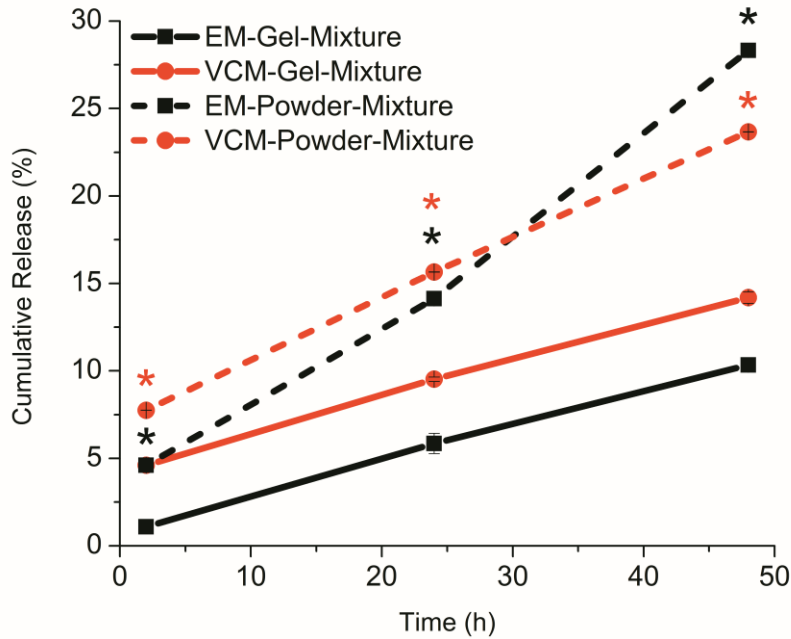


Figure 2.2. Erythromycin (EM) and vancomycin (VCM) release (10 wt.%) from CPP hydrogel prepared with both “Gel_Mixture” and “Powder_Mixture” methods for 2, 24, 48 hrs. EM and VCM cumulative release concentration (%) in “Gel_Mixture” supernatant indicated by black and red solid lines, respectively and EM and VCM cumulative release concentration (%) in “Powder_Mixture” supernatant indicated by black and red dashed lines, respectively. The initial concentrations of the antibiotics in the gel were 150 mg/ml, $n=3$ for each time point. Paired Student T-test was performed and antibiotic release from powder_mixture was significantly different than gel_mixture method for all the time points ($p < 0.05$).

However, antibiotic release in the Gel_Mixture method is 5% lower as compared to the corresponding results from the Powder_Mixture method for the 2 h time point. This difference increases for the 24 h and 48 h up to ~7% and ~20% for EM and ~7% and ~15% for VCM between the two treatment groups, respectively. Thus, the rate of antibiotic release from the

Powder_Mixture method is higher than their peers in the Gel_Mixture method, with respect to a significant release rate increase of EM.

2.5.2 Raman Spectroscopy

Raman spectra of CPP hydrogel in isolation and in combination with antibiotics for both Gel_Mixture and Powder_Mixture methods are shown in **Figure 2.3**.

Raman spectra of CPP hydrogel (**Figure 2.3 Ab, Bb**) contains three frequency regions to provide distinctive features of the CPP structure. CPP spectra indicate linear P-O-P bonds at $\sim 700\text{ cm}^{-1}$. The bands at $\sim 1170\text{ cm}^{-1}$ and $\sim 1290\text{-}1350\text{ cm}^{-1}$ represent symmetric and asymmetric stretching of the PO_2 bonds, respectively. These peaks correspond to our previous studies on Raman spectral analysis.[72] The bands between 1170 cm^{-1} and $\sim 1290\text{-}1350\text{ cm}^{-1}$ represent two non-bridging oxygens (NBOs) bonded to phosphorus creating PO_2 with symmetric and asymmetric vibrations, respectively.[130]

Raman spectra of CPP hydrogel in isolation and in combination with EM for both Gel_Mixture and Powder_Mixture methods are shown in **Figure 2.3[A(a-d)]**. EM has three structural components: a lactone ring, a desosamine sugar, and a cladinose sugar. The reactive groups of the desosamine sugar and the lactone ring mediate all the hydrogen-bond interactions of EM. The dimethylamino group of the desosamine sugar can be found in both protonated (>96–98%) and neutral (2–4%) forms. The protonated form of this group can easily interact, via an ionic bond, in a pH-dependent manner with the oxygen.[131] The Raman spectrum of EM, as indicated in **Figure 2.3[Aa]**, contains lactone rings and two sugars: L-cladinose and D-desosamine. The lactone is indicated around the $2800\text{-}3100\text{ cm}^{-1}$ region. Absorption at the range between 1650 cm^{-1} and 1750 cm^{-1} corresponds to the C=O stretching vibrations of the hydrogen-bonded lactonic group. The spectral region between $2800\text{-}3100\text{ cm}^{-1}$ may be attributed to the C-H stretching mode.

Spectral vibration between 600- 900 cm^{-1} was observed due to the vibration of C-C, C-O and C-O-C stretching of branched-chain monosaccharide, E-cladinose.[132]

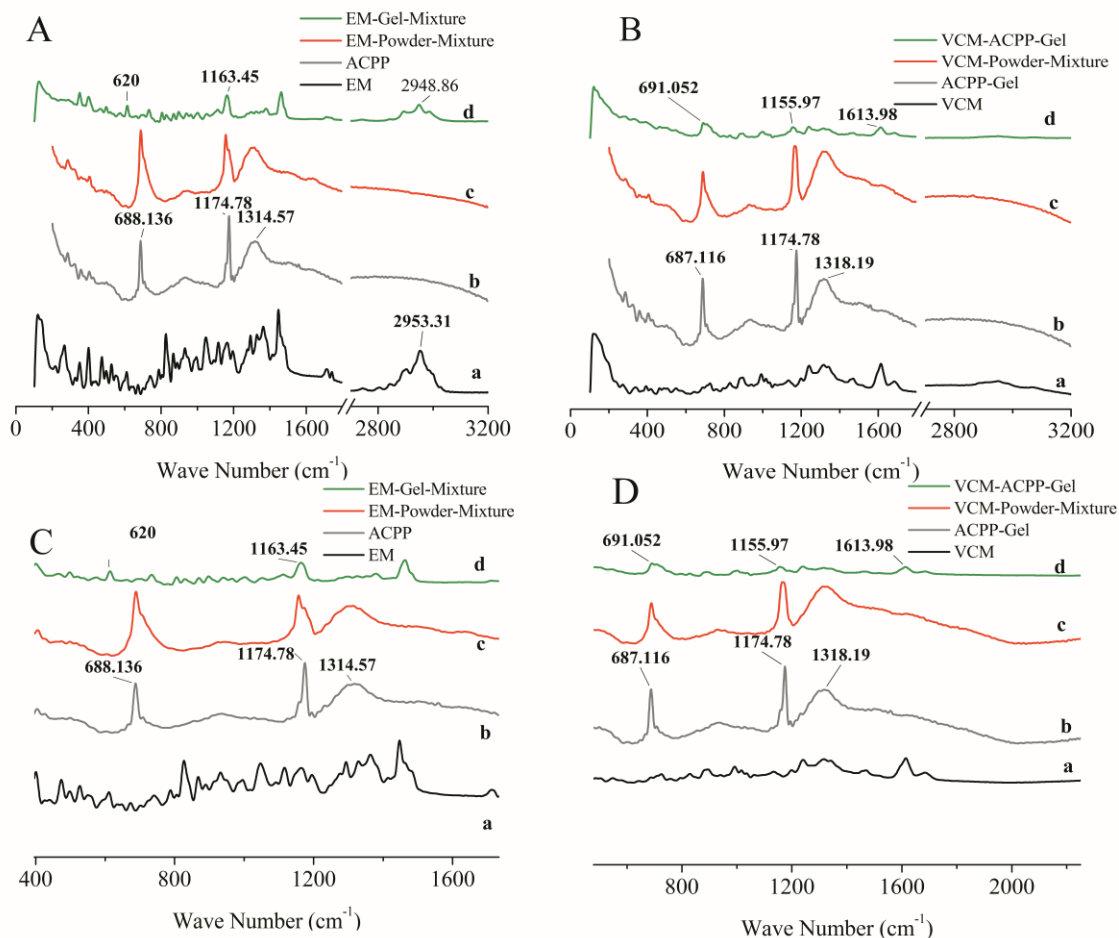


Figure 2.3. Raman spectra of antibiotics isolation and combination with CPP hydrogel. CPP hydrogel loaded with EM (10 wt.%) in both “Gel_Mixture” and “Powder_Mixture” methods. The characteristics peaks of CPP are P-O-P, symmetric and asymmetric PO_2 at ~ 700 , 1170 , and 1290 cm^{-1} bands at ~ 842 , ~ 900 and ~ 1004 represents C-O-C deformation, C-C bond stretching and breathing of aromatic rings, respectively (A), blank CPP hydrogel, and CPP hydrogel loaded with VCM (10 wt.%) in “Gel_Mixture” and “Powder_Mixture” methods (B), the powdered discs loaded with EM for both methods were tested after elution for presence of any antibiotic peaks

(C), the powdered discs loaded with VCM for both methods were tested after elution for presence of any antibiotic peaks (D)

Incorporation of EM on CPP hydrogel represented as 'EM_Gel_Mixture' in **Figure 2.3[Ad]**, exhibits reduced peak intensity at the 600- 3100 cm^{-1} range. This can be attributed to the reduction of most of the bands and stretching obtained in EM spectra may indicate an interaction between CPP and EM. In addition, the missing distinguishing peaks of CPP hydrogel and lactone (2800-3100 cm^{-1}) shift to a lower wavenumber is an indicator of CPP interaction with EM (**Figure 2.3C**). Generally, if the chemical bond length of molecules changes due to any internal or external effects, then it may cause a shift in wavenumber. However, the shift directed to lower wavenumbers may be attributed to the expansion of the C-H bond in the lactone group. The decrease in particle size may cause peaks to shift to a lower wavenumber as well.[133] Further, peaks between 600-1600 cm^{-1} shifted to a higher wavenumber. These peaks correspond to C-C, C-O, and C-O-C stretching of branched-chain monosaccharide, E-cladinose. In our experimental conditions, the temperature and particle size are considered constant during the measurements. The peak shift to the higher wavenumber in this region is associated with axial compression of bonds in these stretching groups.

Subsequently, in the Powder_Mixture method [**Figure 2.3(Ac)**], the Raman spectrum of the EM-CPP combination indicates missing EM peaks, followed by a shift in CPP distinguishing peaks to the higher wavenumber. Linear P-O-P bond, symmetric and asymmetric stretching of the PO_2 bond shifting to higher wavenumber is attributed to the contraction of polyphosphate chains due to continued polymerization of CPP hydrogel which has been delayed due to the intervention of EM in the hydrogel preparation process.

Raman spectra of CPP hydrogel in isolation and in combination with VCM for both Gel_Mixture and Powder_Mixture methods were shown in **Figure 2.3(B)**. Raman spectra of VCM, as indicated in **Figure 2.3(B)**, exhibited peaks at $\sim 830\text{ cm}^{-1}$, $\sim 800\text{ cm}^{-1}$, $\sim 1000\text{ cm}^{-1}$, $\sim 1240\text{ cm}^{-1}$, $\sim 1315\text{ cm}^{-1}$, 1475 cm^{-1} , $\sim 1615\text{ cm}^{-1}$, and $\sim 1696\text{ cm}^{-1}$. Peaks at $800\text{-}1200\text{ cm}^{-1}$ can be assigned to several stretching vibrations of the carbon chain. The bands at $\sim 842\text{ cm}^{-1}$, $\sim 900\text{ cm}^{-1}$ and $\sim 1004\text{ cm}^{-1}$ represent C-O-C deformation, C-C bond stretching and breathing of aromatic rings, respectively.[130] The peaks at $\sim 1252\text{ cm}^{-1}$, $\sim 1327\text{ cm}^{-1}$, $\sim 1475\text{ cm}^{-1}$, $\sim 1625\text{ cm}^{-1}$, and $\sim 1696\text{ cm}^{-1}$ represent characteristic of amide III (C-N stretching), deformation at CH_2 and CH_3 group, CH_3 bending, carbonyl group (C=O stretching) of amide I and C=C stretching, respectively. **Figure 2.3(B)** indicates a broad peak at around $\sim 2850\text{ cm}^{-1}$ to 3050 cm^{-1} . This is indicative of CH_3 and aromatic CH_2 groups at the VCM molecule.

Incorporation of VCM on CPP hydrogel (Gel_Mixture), represented as 'VCM_Gel_Mixture' in **Figure 2.3(B)**, exhibits a reduction in peaks at the $800\text{-}1800\text{ cm}^{-1}$ range which can be attributed to the reduction of most of the bands and stretching obtained in VCM spectra. The low-intensity level of the spectrum is observed for an addition of only 10 wt. % VCM in CPP. This can be an indicator of the interaction between CPP and VCM. CH_2 and CH_3 peaks of VCM at $\sim 2850\text{ cm}^{-1}$ to 3050 cm^{-1} shifted to the higher wavenumber which indicates a bond shortening for C-H due to an interaction. The C-O-C deformation, C-C bond stretching and breathing of aromatic rings, amide III (C-N stretching), deformation at CH_2 and CH_3 group, CH_3 bending, carbonyl group (C=O stretching) of amide I and C=C stretching from $600\text{-}1700\text{ cm}^{-1}$ slightly shift to the higher wavenumber due to a shortening of bond length. Furthermore, VCM incorporation on CPP hydrogel based on Powder_Mixture method indicates similar Raman spectrum as compared with the spectrum of CPP, except a tangible shift to the lower wavenumber

which is attributed to the expansion of polyphosphate chains due to continued polymerization of CPP hydrogel which has been delayed due to the intervention of VCM in the hydrogel preparation process (**Figure 2.3D**). The absence of characteristic peaks in 10 wt. % of VCM doped CPP represents either weak spectra or missing of VCM observed in CPP hydrogel.

2.5.3 Viscoelastic properties

A standard Oscillatory series sweep test was performed to evaluate the viscoelastic performance of CPP hydrogel and Gel_Mixture after antibiotic incorporation. In separate measurements, the gel was subjected to an oscillatory stress sweep to find the linear viscoelastic region (LVR), as shown in **Figures 2.4(A)** and **Figure 2.5(A)**.

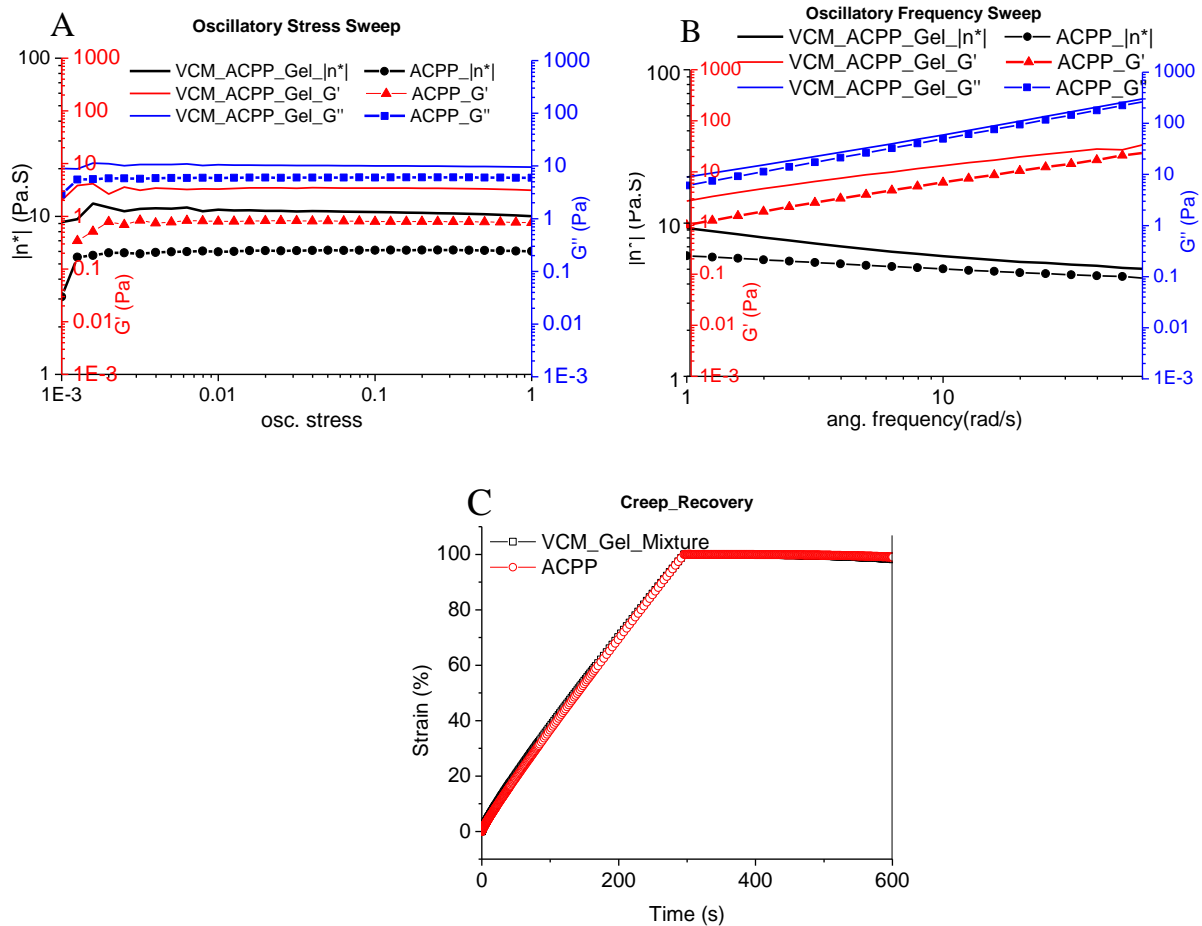


Figure 2.4. Viscoelastic properties of EM loaded CPP hydrogel with “Gel_Mixture” method. An oscillatory stress sweep test in an oscillatory range 0.001 to 1 rad/s at 25°C (A), an oscillatory frequency sweep test with stress value from LVR at 25°C (B) Creep-recovery test under nondestructive predetermined stress (MPa) and safe region of applied time. The recovery test was designed after stress released for the same applied time as the creep test. Strain (%) was normalized to be able to compare different conditions (C).

As shown in **Figure 2.4**, the viscoelastic property of CPP hydrogel was measured for as-synthesized CPP and “EM_Gel_Mixture”. Storage modulus (G'), loss modulus (G'') and complex viscosity ($|\ast\eta|$) were indicated by red, blue, and black colors, respectively. CPP hydrogel indicated a viscous fluid property with a loss modulus (G'') higher than the storage modulus (G'). G' observed around 1 Pa was slightly lower than G' (~ 2 Pa) reported elsewhere.[72] However, G'' observed less than 7 Pa was almost seven times higher than as reported G'' (~1 Pa).[72] High G'' increases G''/G' ratio termed as $\tan\delta$ which is a measure of internal friction of the material. The $\tan\delta$ of CPP obtained approximately more than an order of magnitude higher than as reported $\tan\delta$ (7 vs. 0.5).[72] This increased value of $\tan\delta$ was responsible for highly complex viscosity $|\ast\eta|$ of CPP hydrogel as high as 6 Pa.s, which were three times higher than the $|\ast\eta|$. From a physiochemical standpoint, high internal friction represents a strong particle interaction.

Oscillatory stress sweep test performed on EM_Gel_Mixture are shown in **Figure 2.4(A)**. Values of G' , G'' , and $|\ast\eta|$ are larger as compare to CPP hydrogel which indicates an elevated viscosity because of EM incorporation. As shown in **Figure 2.5(A)**, G' and G'' increased further after VCM incorporation to CPP on VCM_Gel_Mixture, which is obvious due to the addition of dissimilar particles with a complex chemical structure in the gel. However, the increase of G' , G'' , and $|\ast\eta|$ in EM_Gel_Mixture [**Figure 2.4(A)**] is much higher than the values that have been

monitored for VCM loaded CPP [Figure 2.5(A)]. The difference in chemical structure between VCM and EM may play a key role. Another reason is that EM is a hydrophobic drug that cannot be dissolved in water. Complex viscosity ($|\ast\eta|$) of VCM loaded CPP increased as compared to the complex viscosity of CPP hydrogel which indicates that the addition of VCM in CPP hydrogel becomes slightly thicker. The viscosity of gel increased as the particle size decreases, as we described before.[72] A large portion of CPP particles in the range between 1-5 μm , obtained from particle size distribution analysis, may have an impact on the viscosity of CPP hydrogel. Higher loss modulus (G'') than elastic modulus (G') was observed for both cases, which confirms the viscous material properties.

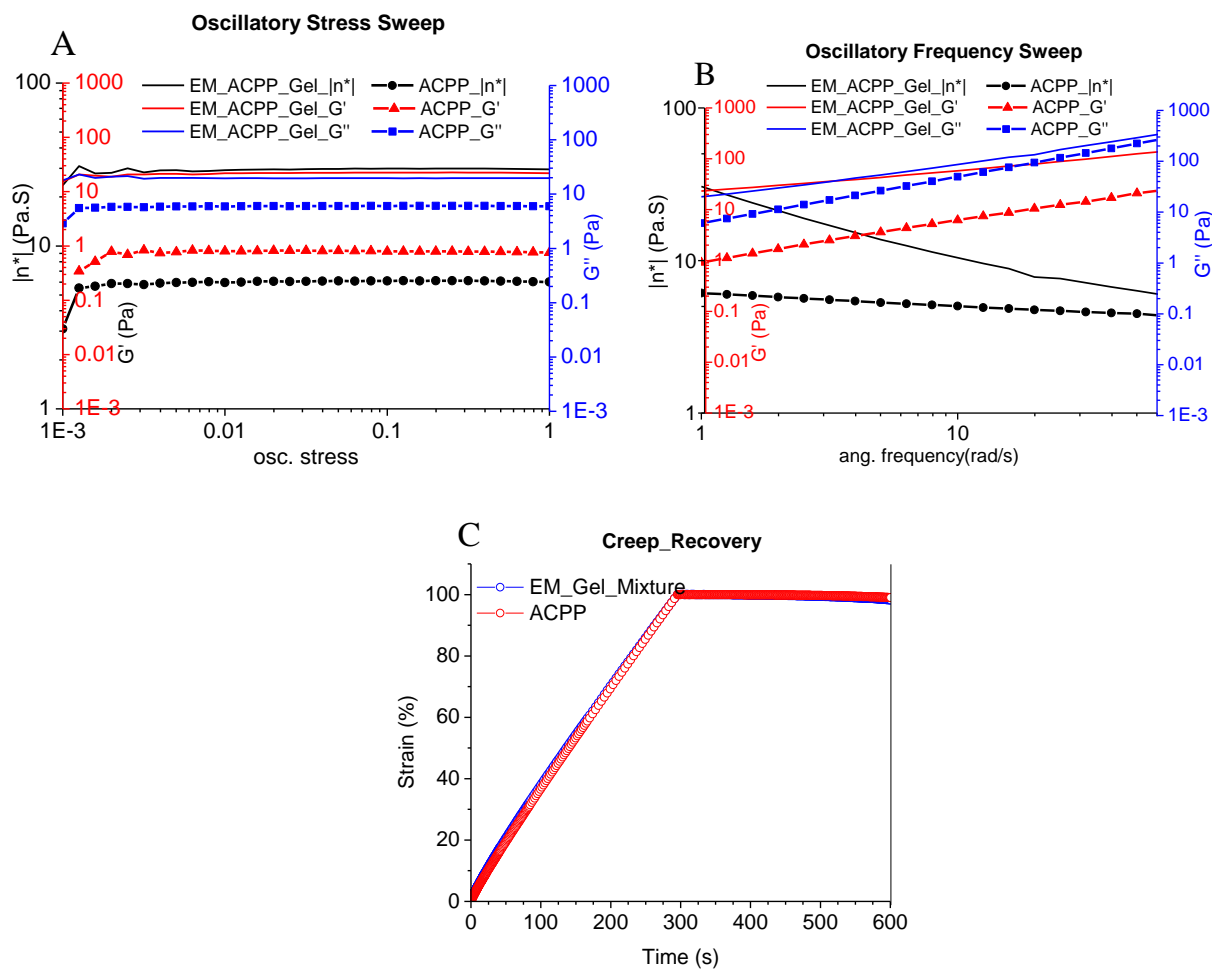


Figure 2.5. Viscoelastic properties of VCM loaded CPP hydrogel with the “Gel_Mixture” method. An oscillatory stress sweep test in an oscillatory range 0.001 to 1 rad/s at 25°C (A), an oscillatory frequency sweep test with stress value from LVR at 25°C (B) Creep-recovery test under nondestructive predetermined stress (MPa) and the safe region during the applied time. Recovery tests were designed after stress released during the same applied time as the creep test. Strain (%) was normalized to be able to compare different conditions (C)

To obtain information on the rubbery state of the hydrogel, it was subjected to an oscillatory frequency sweep test shown in **Figures 2.4(B)** and **Figure 2.5(B)**. The samples exhibit Maxwell-type behavior during the experimental frequency range (1- 100 rad/s), which is also reported, [72] with a slight decrease in G' at 1 rad/s angular frequency. However, G'' showed a higher modulus when parallel to G' which represents a high G''/G' ratio indicating a high viscosity as compared to results reported elsewhere.[72] The rheological behavior of CPP hydrogel indicates a viscous polymeric hydrogel behavior as compared to typical polymeric hydrogel behavior reported.[72] Therefore, results of oscillatory stress sweep [**Figure 2.4(A)**, **Figure 2.5(A)**] and oscillatory frequency sweep [**Figure 2.4(B)**, **Figure 2.5(B)**] are comparable in the sense that increased value of G'' as compared to G' was observed in both tests. However, increased values of G' , G'' , and $|\ast\eta|$ on VCM and EM loaded CPP during frequency the sweep test suggests that antibiotics increase internal friction. This is elucidated by the fact that a significant increase of corresponding values in EM loaded CPP, influenced by EM hydrophobicity, and avoids its full interaction with the hydrogel matrix as opposed to the hydrophilic VCM case.

Finally, the creep-recovery of CPP hydrogel was tested and shown in **Figures 2.4(C)** and **2.5(C)**. A predetermined non-destructive oscillatory stress was applied in this test and the strain values were measured over time. Recovery was tested after releasing the stress at the same time as

a creep. The strain values were normalized and reported as strain (%). The creep-recovery profile of CPP hydrogel, VCM, and EM loaded CPP overlapped. Particle size may play a crucial role in overall viscosity results which can also explain the recovery result. Small (<75 μm) particles exhibit higher viscosity as compared to large (>75 μm) particles because small particles have a high surface area and exhibit high ionic interaction or chain entanglement due to chain agglomeration of the particles with the high surface area. Particle size analysis [**Figure 2.1**] indicates that synthesized particle sizes were less than 10 μm which may induce higher viscosity as well as exhibit the slowest recovery. Gelation time after stirring the particles is also an important factor to explain the high viscosity of the CPP hydrogels. CPP hydrogel prepared after seven days of setting exhibited almost 75% recovery as compared to less than 10% recovery right after stirring for 1.5 h.

Overall, the rheology results confirm that in the liquid phase, the active polyphosphate chains of ACPP particles interact with each other, leading to the formation of a 3D network structure via ionic bonds and/or chain entanglement. Upon VCM incorporation the viscosity and rubbery properties of the CPP gel remain the same, however, the EM changes the CPP gel viscosity and rubber-like structure based on its poor solubility.

2.6 Discussion

The purpose of this study was to determine the role of fully hydrated polyphosphate chains on the interaction between the CPP matrix and antibiotics as well as the impact of antibiotics on viscoelastic properties of the hydrogel. Regardless of antibiotic type, cumulative release (%) of antibiotics into supernatant in the Gel_Mixture method demonstrated the lower tendency of antibiotics to mix with water as opposed to the Powder_Mixture method as shown in **Figure 2.2**.

This may have attributed to the formation of an early ionic bond between antibiotics and fully formed and hydrated polyphosphate chains as well as physical wrapping of antibiotic molecules by polyphosphate chains. Overall, the difference in release (%) of hydrophobic (EM) and hydrophilic (VCM) antibiotics indicates that EM molecules tend to escape from water molecules, therefore a less cumulative % of EM was observed in the supernatant as opposed to VCM. The large complex viscosity of CPP gel loaded by EM also confirms the poor solubility of EM and indicated coupling with hydrated polyphosphate chains as shown in **Figure 2.4(A-C)**. Note that unexpected EM release increments by approximately 5% as compared to VCM in Powder_Mixture method indicated that the higher release of EM, which has smaller molecules as compare to VCM, is based on matrix expansion as shown in **Figure 2.2**. Otherwise, the release of VCM is higher, since VCM as a hydrophilic molecule can readily form a bond with water molecules taking into account that VCM is highly soluble at a pH of 4.[134] This indicates that the elevation of pH rapidly decreases the solubility of VCM to a minimum of approximately 15 mg/ml with a near neutrality charge equal to zero . It is worth to mention that CPP gels exhibit low pH that constrains its clinical application as local drug-eluting device alone. Therefore, we have developed an injectable poly-dicalcium phosphate dihydrate (P-DCPD) forming cement by the reaction of acidic CPP gel with alkali tetracalcium phosphate (TTCP)[135]. This neutral injectable P-DCPD cement has been confirmed as an excellent drug-eluting bone graft substitutes for antibiotics and other drugs (unpublished data).

In the Powder_Mixture method, most antibiotic molecules readily bond to water molecules as soon as they contact with water molecules. Thereby, antibiotic interaction with polyphosphate chains is restricted until the CPP gel is formed and the fully hydrated polyphosphate chains are available for binding. Raman spectroscopic analysis similarly suggests that the antibiotic and the

CPP hydrogel matrix do not initiate any interaction in the Powder_Mixture method. This is indicated by the observation that antibiotics peaks appearing in the spectrum shown in **Figure 2.4(A_c, B_c)**. Thus, the presence of the CPP peaks and the absence of antibiotics peaks in the Raman spectrum of Powder_Mixture method indicates that antibiotics did not bind to the CPP matrix prior to complete gel formation. The shift of CPP distinguished peaks to higher wavenumber must result from continuous polymerization and contraction of CPP hydrogel which was delayed by antibiotics intervention during the gelling process.

In contrast, the spectrum of Gel_Mixture indicates intensity reduction and the antibiotic peaks appeared, which suggest antibiotics interaction with fully hydrated polyphosphate chains in the formed hydrogel. In addition to the ionic bonds, fully hydrated polyphosphate chains create a mesh-like structure that improves physical wrapping caused by polyphosphate chain entanglement. Thereby, antibiotic loading effectively improved as opposed to the formed hydrogel in the Powder_Mixture method. Nevertheless, the viscoelastic property measurement of CPP hydrogel depicts the property alteration of the hydrogel where VCM shows lower complex viscosity because of good solubility and interaction with CPP hydrogel than EM **Figures 2.4,2.5 (A-C)**.

2.7 Conclusion and Future Work

The results of this study indicate that CPP hydrogel loaded by the clinically relevant concentration of antibiotics retains EM and VCM (10 wt. %) within the matrix by 18% and 9%, respectively, which are higher than antibiotic incorporation prior to hydrogel matrix formation. The vibrational pattern of the Gel_Mixture method confirms that fully hydrated polyphosphate chains in CPP hydrogel are a key element to initiate ionic interactions between antibiotics and the

hydrogel matrix. It is evident immediately from emerging new peaks in the Raman spectrum of Gel_Mixture method. In contrast to hydrophobic EM, the hydrophilic VCM can significantly impact the viscoelastic properties of the hydrogel, suggesting that the molecular properties of loaded antibiotics are another key element in hydrogel performance as a local antibiotic delivery device. Loading antibiotics in fully formed CPP hydrogel enhances the antibiotic retention within the matrix rather than adding antibiotics to the CPP powder prior to gelation.

CHAPTER 3

Impacts of Compaction Methods on the Delivery Capabilities of Erythromycin and Vancomycin from Calcium Polyphosphate Hydrogel Matrices

3.1 Purpose and Hypothesis

The purpose of this Chapter is to acquire a comprehensive understanding, regarding the effect of molding methods on antibiotic release and activity. In this study two antibiotics namely, EM and VCM were used. The long term release of antibiotics from ACPP discs made with two different molding methods reveals the interaction properties of antibiotics with ACPP hydrogel and is a good comparison for the interaction of hydrophobic and hydrophilic antibiotics during the elution studies.

3.2 Introduction

It is known that more than two million bone graft procedures are being performed worldwide each year with a high risk of infection [136]. Chronic osteomyelitis is one of the major issues which is caused by a bacterial infection, post-surgery [137]. To prevent this prevalent problem, besides systemic antibiotic administration, local antibiotic delivery is highly recommended. To this goal, many bone cement materials loaded with a clinically relevant concentration of antibiotics have been studied [138-141]. One of the most extensively studied synthetic bone grafts is calcium phosphate cement (CPC) which has been widely used as injectable

bone cement for bone defect fillings [16, 142-144]. Although CPCs are biocompatible and set in room temperature, they do have some limitations, including weak mechanical strength [85, 145] and inability to release the antibiotic in a concert with the treatment period [16, 110]. The weak binding between loaded drugs and CPCs matrix surface is one of the main drawbacks. Thus a polymeric bone cement material that can initiate a potent bond with antibiotics may be suitable.

Calcium polyphosphate (CPP) is composed of linear polyphosphate chains that possess interesting mechanical and chemical properties in solution and in the solid-state and offers a wide range of applications for tissue engineering and drug delivery devices [72]. Owing to the importance of the subject, CPP's capacity as an antibiotic delivery system has been addressed by several studies, including investigation on VCM release behavior from amorphous CPP matrices [43], the effect of processing on the structural characteristics of VCM-loaded amorphous CPP matrices [58], effect of gelled calcium polyphosphate matrices on delayed antibiotic release [122], compaction strategies for modifying the drug delivery capabilities of gelled calcium polyphosphate matrices [59]. Dion et al. [43] claimed that a repeat gelling process on antibiotic-loaded CPP significantly reduces the burst release of VCM during the initial 2–4 h of elution while extending the effective antibiotic release period only by 80 h. The same group observed more homogenous and prolonged drug release of VCM from compacted CPP discs as compared to their previous drug release study. Before the last gelling step of repeated gelling protocol they compacted CPP powder then exposed the discs to high humidity for the final step [59]. In repeated gelling procedures the CPP and antibiotic molecules cannot make enough ionic bonds due to the lack of water molecule availability, thus the release of antibiotic is with higher rate than when the complete hydrogel formed.

The CPP hydrogel has been developed in our research group with a unique technique and in the presence of an excess volume of water [72]. One of the enhanced features of CPP hydrogel is the bulk gelation and not the surface gelation only. Thus we recently have showed that antibiotic loading efficiency increases through addition of antibiotic to fully formed CPP hydrogel rather than powder to powder addition [146], and we will later show more precisely in this chapter that water availability to CPP chains due to accelerating water molecule ingress and microstructural transformation of CPP hydrogel, enhances antibiotic loading efficiency through the mechanisms of intermolecular ionic interaction and entanglement of polyphosphate chains with antibiotic molecules. As a result, we believe that CPP hydrogel can be a promising local antibiotic delivery device for sustained antibiotics release with minimal impact on the material mechanical properties. We also note that the CPP matrix formation can be a determining factor for sustained drug release [146]. However intermolecular ionic interaction majorly effects antibiotic release, inconsistent pore distribution throughout the condensed matrices in manually molded discs (M-discs) may cause non-uniformity of the discs and thereby result in lack of mechanical strength of the matrix and the burst release of the antibiotics. Nevertheless, discs made by compression molding method (C-discs) which are expected to be more uniform and dense show prolong antibiotic release. Petrone et. al. [59] also have demonstrated the improvement of antibiotic release by developing a new compaction method in addition to the repeated gelling process previously mentioned in Dion et. al study [43]. In this study, we are going to quantify the effect of the compaction strategies on antibiotic release by performing release studies on discs that are prepared by compression molding and manual molding methods.

In order to prove that water molecules, contribute majorly to the interaction processes of antibiotic and CPP matrix, the effect of hydrophobic and hydrophilic antibiotics on the release

efficiency has been tested. Based on this fact, the release of VCM as a hydrophilic antibiotic and the EM as a hydrophobic antibiotic were investigated. The unique interaction abilities of CPP hydrogel requires a deep understanding to reveal the antibiotics' reaction mechanism. EM [147] (EM, 733.937 g/mol) is known as a hydrophobic antibiotic with ability to enhance bone formation [123] and VCM [148] (VCM, 1449.265 g/mol) is the most common hydrophilic antibiotic with larger molecule to treat osteomyelitis, both were used in clinical practice.[124-127] In addition to matrix preparation impact on drug release, in this study potential impacts of antibiotic size and wettability on antibiotic release were investigated.

3.3 Materials and Methods

3.3.1 Synthesis of CPP powder and CPP hydrogel

CPP hydrogel was prepared as we reported elsewhere. [72] Briefly, Calcium phosphate monobasic monohydrate, ($\text{Ca}[\text{H}_2\text{PO}_4]_2 \cdot \text{H}_2\text{O}$; Sigma-Aldrich, St. Louis, MO) was calcined for 10 hours at 500°C followed by melting for 1 hour at 1200°C to produce an amorphous glass and quenched at room temperature for cooling. The resulting material was hammered to make small particles prior to grind in a planetary ball mill (Across International, Berkeley, NJ). The resulting particles were sieved (Laboratory Test Sieves, Fisher Scientific, Pittsburg, PA) continuously to segregate particles less than 75 μm . Prior to usage, CPP powders were stored in a vacuum desiccator to avoid moisture absorption. For hydrogel preparation, CPP powder was added to distilled water ($0.1 \text{ g}\cdot\text{ml}^{-1}$), stirred for 90 minutes at 700 rpm at room temperature (25 °C) and suspended for 24 hours.

3.3.2 Drug loading

EM and VCM [147] [148] (purchased from Sigma) were mixed with CPP hydrogel (1:10) (10 weight % (w/w)) by a spatula, separately.

3.3.3 Disc compaction methods

EM and VCM were mixed with CPP hydrogel (1:10) (10 weight % (w/w)), separately. In order to enhance handling properties of the mixture, the resulting pastes were placed in room temperature for 24 hours to obtain semi-dried gel pre-molding.

To understand the role of matrix structure on antibiotic elution, for each antibiotic two types of elution matrices were designed and the discs' properties and a schematic of disc preparation procedure were summarized in **Table 3.1** and **Figure 3.1**, respectively.

Manual method

Like the first type, Semi-dried gel mixtures were weighted and separated into four equal portions, then manually filled in disc-shaped plastic molds (**Figure 3.1**). The filled material was placed in room temperature for 1 week to dry.

Compression method

The compressed discs (C-discs) were prepared via a mechanical compressor (CARVER, Wabash, IN. USA) with a mean pressure of 3000 psi (**Figure 3.1**). All the samples from both groups were placed at room temperature for 1 week to stabilize their weights. The amount of water added to each disc was calculated based on the weight of each disc.

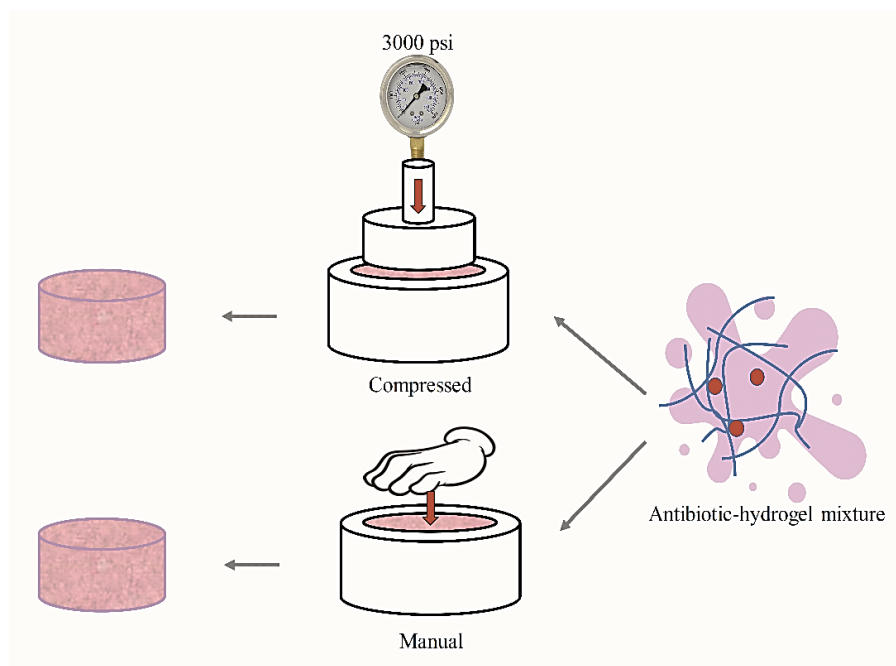


Figure 3.1. Schematic of molding methods used in this study; compressed and manual.

3.3.4 Structural evaluation of discs' pre-elution

Micro-computed tomography

A structural difference between the two types of discs was evaluated by microcomputed tomography (μ -CT) (vivaCT 40, Scanco Medical AG, Bruttisellen, Switzerland) analysis. The CT scan was performed at an energy of 70 kVp and an intensity of 114 μ A. The slice thickness was set at 10.5 μ m and data collected with an integration time of 320 ms. Following reconstruction, the specimen volume of interest was selected and pore structures analyzed using the built-in software. Briefly, a binary threshold was applied to separate sample material from pores, and image processing techniques used to calculate the diameter of pores in three dimensions. The results were summarized in **Table 3.2**.

Scanning electron microscopy

Discs were fixed on a strip of carbon tape (Ted Pella, Redding, CA). A Quanta FEG 450 scanning electron microscope (FEI, Hillsboro, OR) was used to collect images of each sample at magnifications of both 50x and 1000x (**Figure 3.2**). For all samples, the power was set to 10 kV and the spot size was set at 4 for imaging. All samples were imaged and analyzed in a low-vacuum setting of approximately 0.45 torr with no coating.

3.3.5 Antibiotics release and bactericidal activity assay

Upon curing, antibiotic-loaded CPP hydrogel discs were submerged into the 1:10 ratio (1 g disc submerged in 10 ml ultra-pure water) ultra-pure water in sealed containers and maintained in 37 °C. Supernatants were collected completely at predetermined time points and replaced with the same amount of fresh media. At the completion of the release study, the discs were dried and weighted to calculate the total mass loss. weight before soaking (W_1) and weight after soaking (W_2), the weight loss: $\Delta W = (W_1 - W_2) / W_1$. A summary of weight loss values is shown in **Table 3.3**.

The concentrations of EM and/or VCM released from discs were measured via a microplate reader (Synergy HT, BioTek Instruments, Inc., Winooski, Vermont, USA) at the absorbance wavelength of 486 nm and 295 nm, respectively and converted to a known concentration of each antibiotics using internal standard curve. The antibiotic cumulative concentration (%) measured by the microplate reader was calculated based on the concentration of loaded antibiotics of each disc. Due to UV properties of VCM, the elution from VCM-loaded discs was transferred into a UV transparent 96 well plate for microplate reader measurements.

A modified minimum inhibitory concentration (MIC) assay was developed to measure the antibacterial activity of eluted EM and VCM in pre-determined time points. The MIC was determined by the lowest concentration that inhibited the growth of bacterium as characterized by a lack of turbidity and lower OD readings. Briefly, a Mueller–Hinton broth inoculated with *S. aureus* spores (CDC 587, #49230 American Type Culture Collection, Manassas, VA) was cultured at 37°C until an absorbance reading of 0.08–0.1 was attained at 625 nm, corresponding to roughly 1×10^5 CFU/mL. Then 100 μ L of VCM eluent from M and C discs (VCM-M and VCM-C) and 100 μ L of EM eluent from M and C discs (EM-M and EM-C) were collected at various time points and added into 900 μ L of the bacterial broth. All the bacterial samples incubated at 37°C for 22 h, followed by OD measurement at 625 nm. Bacterial culture in Mueller–Hinton broth without antibiotics considered a positive control. Antibacterial activity assays were conducted in duplicate for both the blank and testing samples. The MIC₁₀₀ was determined 2 mg/L for both EM and VCM. In parallel, the pH of the elution medium was measured at each time point and summarized in **Figure 3.6**.

3.3.6 Structural analysis of remnants post-elution

Raman spectroscopy analysis

The composition of CPP discs residues (after the drug release experiments) was evaluated by Raman spectroscopy to qualitatively assess any structural changes that might have occurred during aging. To this goal, the residuals of M and C discs were centrifuged, and the supernatant was removed and the remnants were dried after collecting the last time point. Then dried samples were ground to obtain a fine powder for further studies.

An In Via Raman microscope (Renishaw, Gloucestershire, UK) with a 785 nm excitation laser, and WiRE 3.3 software was used to measure the vibrational pattern of the remnant of post-elution matrices. A 50x N-plan Leica microscope objective with a numeric aperture of 0.75 and a working distance of 0.75 mm was used for measurements. The laser power was approximately 115 mW at the measurement site of 100% energy. Spectra were measured at 50% laser power for three accumulations of 10 s each over a spectral range of 200–1600 cm^{-1} with spectral resolution varying from 0.87 to 1.11 cm^{-1} . To eliminate extra noises, spectra were preprocessed by applying an in-house developed LabVIEW procedure for background subtraction and further normalizations [129]. Measurements were taken from each sample and averaged to achieve minor variations within the measurement system. The Raman spectra of powder samples were measured for each group.

3.3.7 Eluent pH

Eluent pH of antibiotic-loaded ACPD discs immersed in distilled water was measured via a Fisher Scientific accumet AE150 pH meter (Hampton, NH) with accumet 13-620-AE6 electrode. The pH values of all discs were measured for all time points and up to two weeks were summarized in **Figure 3.6**.

3.4 Statistical analysis

The influence of the compacting method on the release rate of VCM and EM, throughout the elution study, were analyzed by Student T-test using excel where significant differences were identified between 2 treatment groups namely, manual and machine compressed ($p \ll 0.05$). Also, the influence of antibiotic type on the release amount within each compaction method was

analyzed by the same test, where no significant difference was identified ($p > 0.05$). A significant difference was detected ($p < 0.05$) in the antibacterial activity of released VCM between M and C discs.

3.5 Results

3.5.1 Structural evaluation of discs' pre-elution

The influence of the compaction method on CPP matrix microstructure was evaluated by Scanning electron microscopy (SEM) and Microcomputed tomography (μ -CT).

Table 3.1. Physical properties of compressed and manual samples used in elution study

Properties	Manual			Compressed			*P value
	Blank	VCM	EM	Blank	VCM	EM	
Thickness	0.422 ± 0.025	0.492 ± 0.053	0.522 ± 0.04	0.806 ± 0.002	0.880 ± 0.062	0.904 ± 0.036	< 0.05
Diameter	1.386 ± 0.004	1.366 ± 0.026	1.377 ± 0.011	1.308 ± 0.002	1.292 ± 0.005	1.306 ± 0.004	> 0.05
Weight. (g)	1.036 ± 0.101	1.150 ± 0.145	1.177 ± 0.104	2.057 ± 0.11	1.992 ± 0.181	2.092 ± 0.121	< 0.05

Micro-computed tomography

The values of structural properties reported in **Table 3.2** showing that M discs have higher porosity and the mean pore size is larger than C discs and statistically, there is a significant difference in porosity (%) of these two groups ($n = 4, p < 0.05$). However, there is no significant difference in the mean pore size of these 2 groups ($n = 4, p < 0.05$).

Table 3.2. Structural Properties of Discs by μ -CT

Group	Porosity (%)	Mean Pore Size (mm)
Manual (M)	9.313 \pm 3.351	0.235 \pm 0.219
Compressed (C)	4.837 \pm 2.197	0.085 \pm 0.033
*P value	<0.05	<0.05

Scanning electron microscopy

SEM observation revealed micro-cracks and surface roughness on the surface of M-discs and C-discs (**Figure 3.2**). However, the micro-cracks observed on both discs, those are slightly deeper in M-discs, so the M-discs are structurally more fragile as compared to C-discs. Material agglomerations were detected on the surface of the M-discs as they can be found as white spots in **Figure 3.2**.

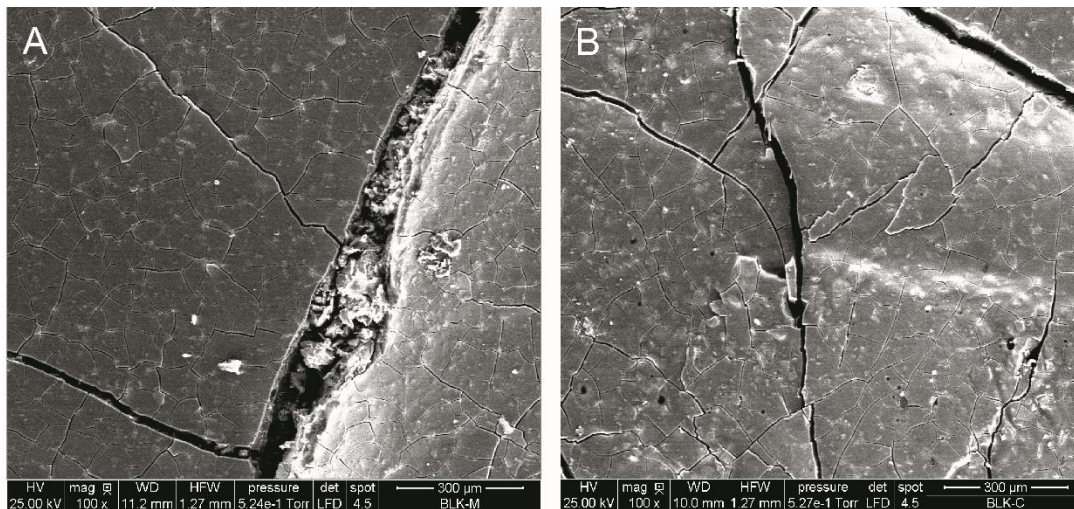


Figure 3.2. Surface morphology of antibiotic release samples prior to release for M (A) and C (B) discs. Magnification is 100x.

3.5.2 Antibiotic release and bactericidal activity assay

The cumulative release (%) of VCM and EM from M and C discs (VCM-M, VCM-C, EM-M, and EM-C) with the physical properties given in **Table 3.2** were measured throughout the predetermined time points and the results are shown in **Figure 3.3**.

The significant burst release was indicated in M discs for both EM (64.9 ± 11.5 %) and VCM (66.5 ± 8.5 %) within 2 weeks. The higher burst release was observed at early time points for the M discs. While the measured release of VCM up to 2 months for C discs showed no burst release in EM and VCM loaded discs. Also, the sustained release was observed in C-discs for EM (49.3 ± 2.9 %) within 4 weeks and VCM (55.5 ± 11.9 %) within 2 months as compared to M-discs.

Generally, C-discs show higher sustained release as compared to M-discs which have earlier and shorter sustained release. In addition, a more sustained release of VCM starting from 72 hours up to 9 weeks was observed as compared to EM in C-discs starting from 8 hours to 3 weeks. Comparing the burst release of EM and VCM over the course of 48 h (**Figure 3.3 (C,D)**), realized that manual samples are shown in **Figure 3.3 C**, immediately release almost 50% of antibiotics in 24 h and 65% in 48 h and there is no significant difference between the release of EM and VCM for manual samples. In **Figure 3.3 D**, antibiotics' burst release from C-discs reduced significantly due to compaction method. The EM and VCM release is almost the same at 24 h of release and it is around 1.5 %, however the EM release leveled up for the 48 h of release to ~4%.

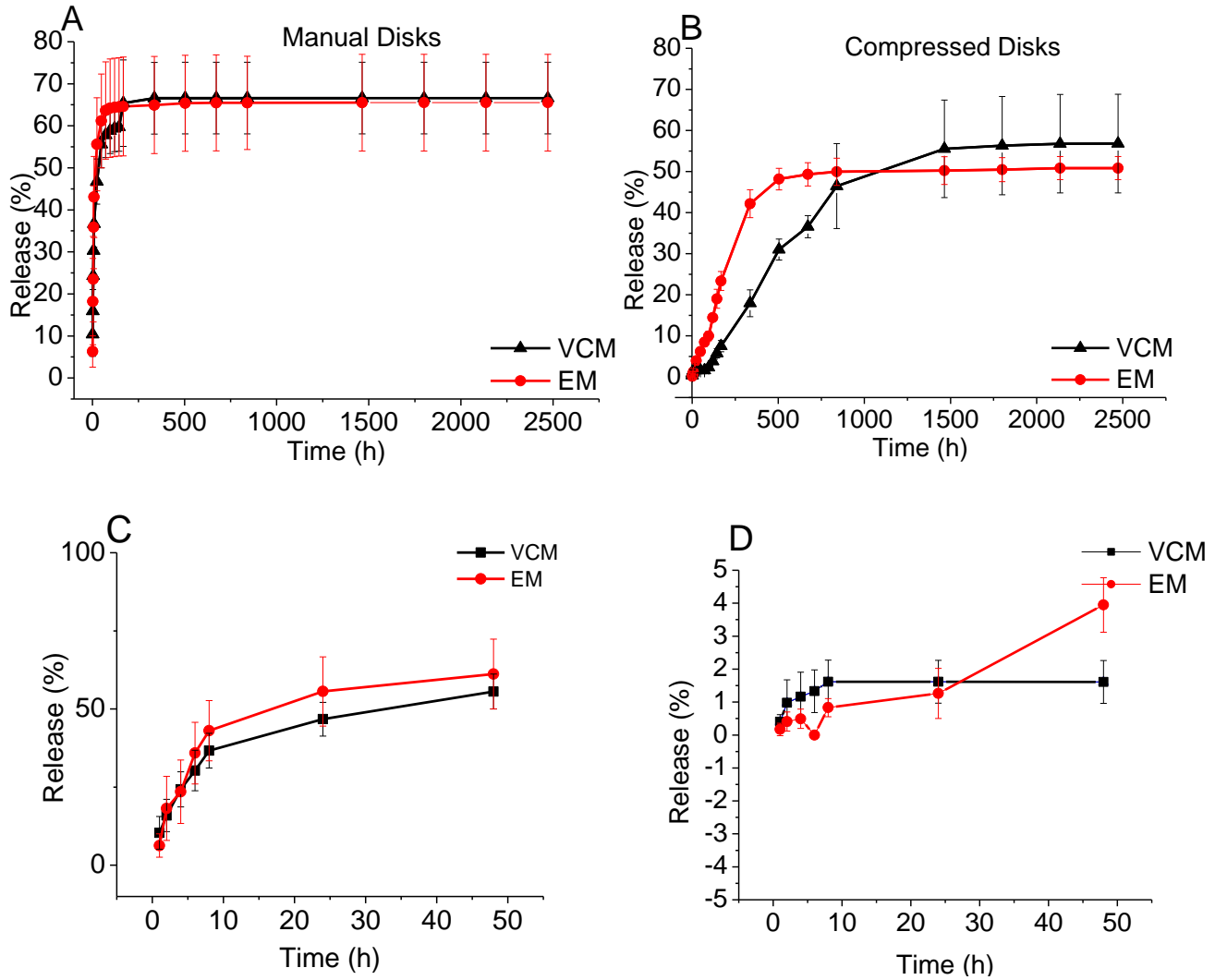


Figure 3.3. The release pattern of vancomycin and erythromycin from manually (A) and mechanically compressed discs (B), the burst release comparison for manual (C), and compressed samples (D) in seven time points over the course of 48 h. Statistical significant differences indicated by (*) ($n=4$, $p < 0.05$).

Released VCM is stable and retains its antibacterial activities, as shown in **Figure 3.4**. In agreement with the VCM release profile, C-discs has a slower and more sustainable release all above MIC concentration, thereby, a sustained and longer above MIC bacterial inhibition was observed. Released VCM from both C-discs and M-discs within the first week significantly

inhibited bacterial growth. However, bacterial growth inhibition of M discs was reduced ($49.9 \pm 53.4 \%$), whereas C discs retain their strong bacterial growth inhibition ($99.6 \pm 0.6 \%$) up to 2 months ($p = 0.005$).

The reported minimal inhibitory concentration (MIC) for EM and VCM against *S. aureus* (ATCC) is $2.0 \mu\text{g/ml}$, demonstrating that the antibiotic concentrations released from these discs construct the volume were always above the MIC.

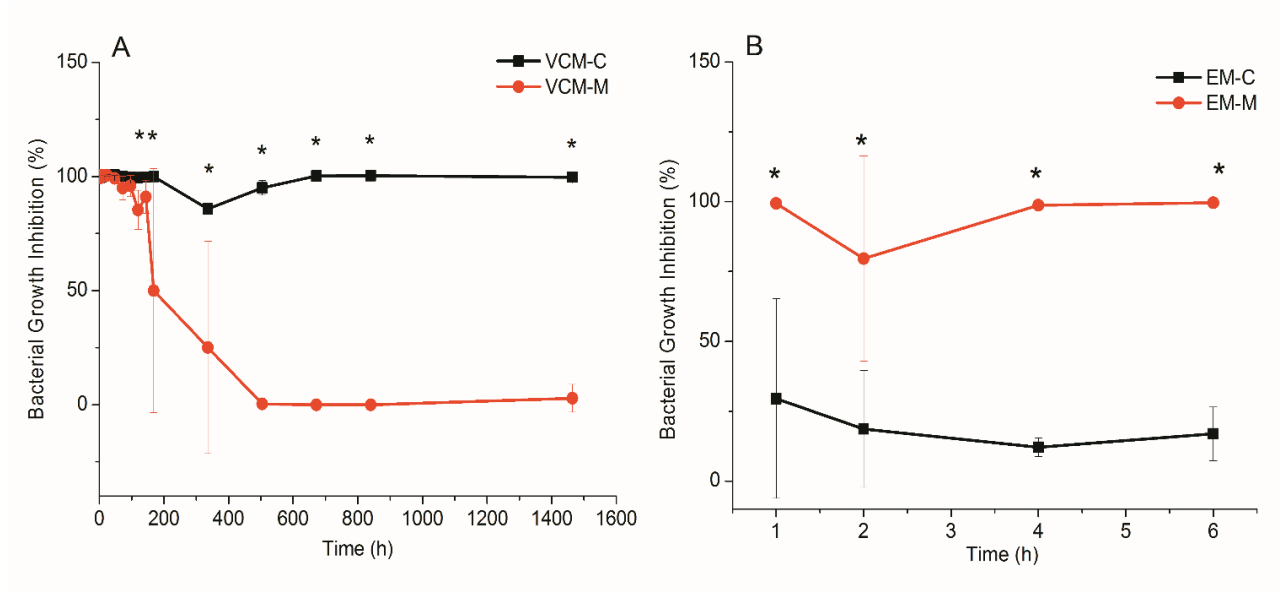


Figure 3.4. Bacterial growth inhibition percentage was obtained by normalizing bacterial growth inhibition without the presence of any release media. Statistical significant differences indicated by (*) ($n=4$, $p < 0.05$). Bacterial growth inhibition by VCM measured up to 2m (A), and for EM measured up to 6 h.

3.5.3 Structural analysis of remnants post-elution

Raman spectroscopy analysis

Pre-release and post-release Raman spectra of CPP discs in isolation and in combination with antibiotics for both manual and compressed discs are shown in **Figure 3.5**.

Generally, the Raman spectra of CPP disc pre-release, contains three frequency regions to provide distinctive features of the CPP structure. CPP spectra indicate linear P-O-P bonds at ~ 690 cm^{-1} . The bands at ~ 1170 cm^{-1} and 1340 cm^{-1} represent symmetric and asymmetric stretching of the PO_2 bonds, respectively. The bands between 1170 cm^{-1} and 1340 cm^{-1} represent two non-bridging oxygens (NBOs) bonded to phosphorus creating PO_2 with symmetric and asymmetric vibrations, respectively.

A significant post-release change of spectra was observed throughout the samples. As it has shown in **Figure 3.5**, the post-release Raman spectrum of VCM loaded samples indicates that VCM remained within the matrix by appearing the characteristic peaks of VCM. In contrast to EM loaded samples a few EM characteristic peaks were detected at ~ 400 , ~ 600 , and ~ 1100 and the strongest characteristic peaks belong to CPP gel.

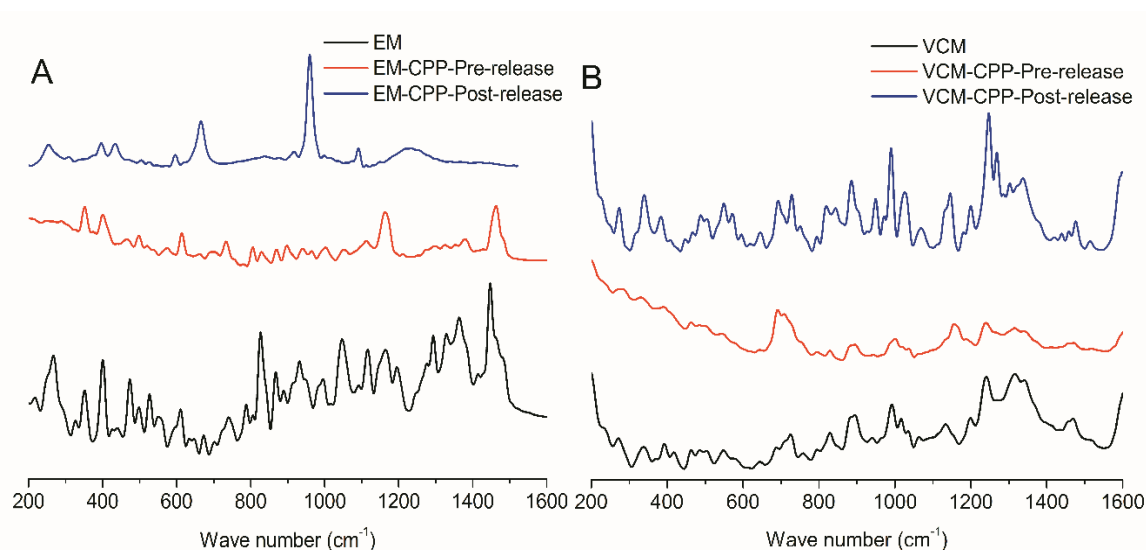


Figure 3.5. Raman spectra of VCM, VCM-C discs (A), EM, EM-C discs (B), pre-release and post-release is showing VCM remnants within matrix after ~ 3 months of release

As indicated in **Table 3.3**, the remnant of samples was used to determine the weight loss % at the completion of the release study. The C-discs retained higher percentage of their original mass and M-discs lost more weight upon washout. Blank samples lost less weight significantly in compare with antibiotic-loaded discs ($n = 4, p < 0.05$). The weight loss of EM loaded discs, also showed significant difference between C and M discs ($n = 4, p < 0.05$). However, the weight loss of VCM loaded discs is not significantly different within C and M discs, and the statement is true for EM as well (**Table 3.3**).

Table 3.3. Post-elution weight loss of discs

Properties	Manual			Compressed		
Weight (g)	1.036 ± 0.101	1.150 ± 0.145	1.177 ± 0.104	2.057 ± 0.11	1.992 ± 0.181	2.092 ± 0.121
Weight. loss (%)	95.174 ± 0.02	96.051 ± 2.329	95.88 ± 0.258	88.333 ± 0.03	94.285 ± 1.032	91.52 ± 1.529

3.5.4 Eluent pH

Eluent pH of ACPD discs in isolation and combination of antibiotics for both compaction methods is summarized in **Figure 3.6**. Overall compressed samples regardless of antibiotic types show a slow rise in pH, and EM loaded samples experiencing higher pH within first two weeks in comparison with blank and VCM loaded samples.

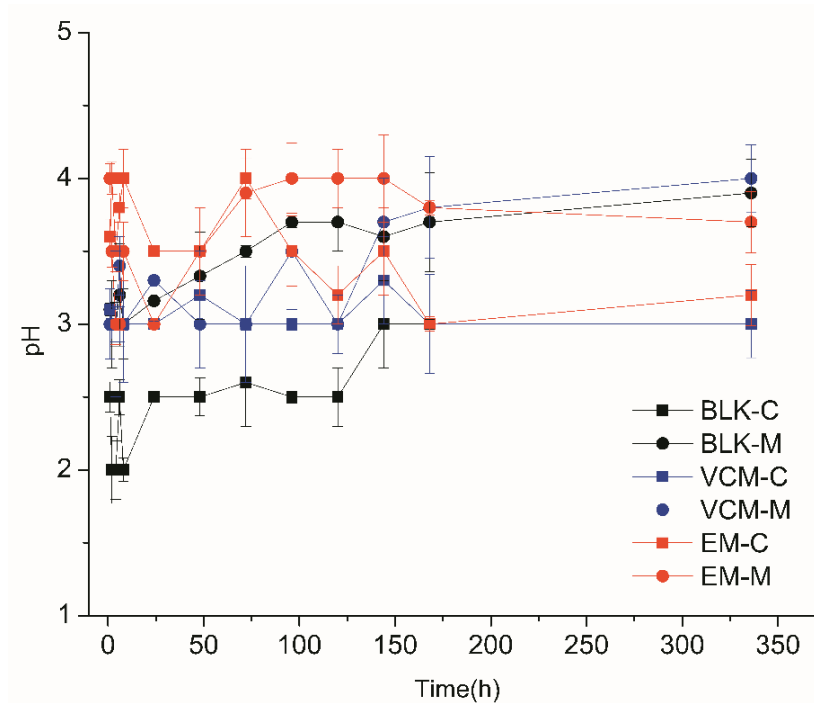


Figure 3.6. Monitored pH of elution within 2 weeks. the pH of manual discs is not significantly different within the manual samples ($p > 0.05$), while the pH of the compressed discs is significantly different between blank , VCM , and EM loaded discs. ($p < 0.05$)

3.6 Discussion

Many factors are involved to obtain a desired antibiotic delivery device which controls antibiotic release in a sustainable manner and in harmony with the material degradation. Here we proposed a delivery system which is capable of releasing an effective dose of antibiotic that remains above the MIC throughout the release period. Mainly, we explain how ionic interaction and compaction methods can improve the release of antibiotic. Principally, a challenging part of any localized drug delivery devices is the burst release of therapeutic within the initial hours of implantation. Antibiotic release from CPP was first studied by Dion et.al.[58] where the gelled CPP was prepared under humidified condition. Their study shows a high initial release of VCM in

0.5 h , with reaching a cumulative release of 72 % of the calculated amount of incorporated VCM. It is worth to mention that the cumulative release of VCM reaches above 50 % in less than 50 h. In our study, the CPP hydrogel as an antibiotic carrier was studied to compare two antibiotics and two compaction methods. Samples were divided into M-discs and C-discs. The larger pores and higher porosity % of M-discs rationalizing the higher release of antibiotics (**Table 3.3**). The surface morphology of discs was shown by SEM images (**Figure 3.2**) and clearly indicating the deeper fractures over the surface of the M-discs in comparison with C-discs.

The total cumulative release of antibiotics is reaching ~65 % and ~55 % of the calculated amount of incorporated antibiotics in M-discs and C-discs, respectively. In the CPP hydrogel formation, there is a strong ionic association between calcium (Ca^{2+}) or other multivalent cations and the linear polyphosphate ions in water, which can result in the formation of a hydrogel. The cations which are capable of bridging between linear polyphosphate chains, effectively create a polymer network, leading to hydrogel formation. Positively charged molecules such as VCM would show an affinity for the ionic bond.

Raman spectroscopy on post-release samples indicates that some EM still remain within the matrix since some characteristic peaks of EM appear in the post-release spectra (**Figure 3.5A**). Similarly, the VCM group post-release still contains characteristic peaks of VCM which is indicating that a strong ionic bond holds VCM and CPP matrix together even after 2 months of release (**Figure 3.5B**).

In C-discs the VCM and EM release reach 4% and 15% in 5 d, respectively, that shows the CPP matrix made by compression sustained the release of antibiotics.

However, the released amount of VCM from C-discs was very low at the initial time points, it's antibacterial activity remained above MIC level. EM's sensitivity to low pH [149, 150]

compromised its activity and the activity reduction was impacted by the cleavage of EM molecule in an acidic environment. Thus the low antibacterial activity of EM was not reported throughout the entire release period and **Figure 3.4B** indicates the prohibition for 1 w. While reports show that VCM has higher antibacterial activity in lower pH [151], thus the activity of VCM retained higher than 80% in C-discs.

Comparing the pH of elution obtained from C-discs and M-discs, the pH is significantly ($p < 0.05$) lower in blk-c vs blk-m samples due to more homogeneity of the samples. The pH during the release is not too significant ($p < 0.05$) between different time points of VCM loaded, and not significant between EM loaded samples.

Antibiotic loaded samples generally have higher pH indicating that the interaction of antibiotics with PP chains may accelerate the dissolution process of CPP and the released material raises the pH faster. Furthermore, pH significantly changed between blank, VCM and EM loaded samples in C-discs, while within manual samples pH remains constant.

In VCM loaded C-discs, pH value is significantly lower than VCM loaded M-discs. This may be due to the strong ionic bond that VCM makes with the CPP matrix and provides a more homogenous environment in comparison with M-disc. Indicating that hydrophilic VCM molecules bond well with hydrated PP chains in a way that intervenes less to the matrix structure.

In fact, the manufacturing process has a significant effect on the dissolution and degradation process of CPP discs and as result on pH. As it has been shown in **Figure 3.6**, in compressed discs the pH raises slowly in comparison with less dense samples (M-disc). Since compressive manufacturing only increased the matrix density due to compression pressure but not the structure at ionic level, so the slight pH increase might be due to the slow degradation of matrix lead to delayed acidic phosphate release.

3.7 Conclusion and Future Work

VCM ionic bond to the CPP matrix provides a more sustained release. Compressed samples as a denser disc may retain antibiotics more effectively within the matrix. Imbedding EM within the acidic CPP matrix compromised EM biological efficacy which may be addressed by elevating the pH of elution medium or by modifying EM to be more resistant therapeutic in further studies.

CHAPTER 4

Antibacterial Activity of Polymeric Dicalcium Phosphate Dihydrate (P-DCPD) Loaded with Antibiotics

4.1 Purpose and Hypothesis

In this aim, I perform a very well-known bacterial agar plate for determining bacterial inhibition zone. The releasing antibiotic from P-DCPD discs, prepared with different loading methods, inhibits the bacteria growth in the agar plate in a ring shape. I measure the inhibition zone and based on the inhibition area, I explain the release of antibiotics and relate it to previous release data from ACPP hydrogel (**Chapter 3**). The experiment is a complimentary set of experiment to confirm polymeric cement capability to perform as local antibiotic delivery matrix by retaining antibiotics antibacterial activity. In Chapter 3, the pH of ACPP impacts the antibacterial activity of EM completely, and VCM partially. As shown in **Figure 4.1** the pH of P-DCPD stays in neutral pH and differs significantly than the pH of ACPP for the same exposure time.

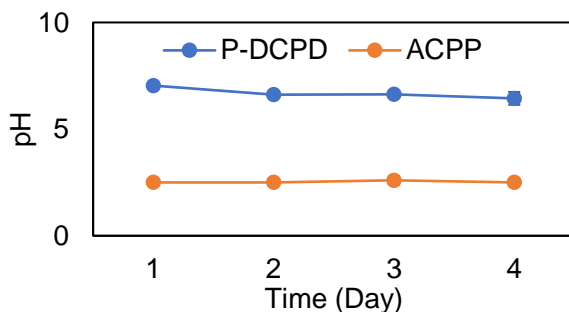


Figure 4.1. pH values for P-DCPD and ACPP elution medium (1 day, 2 days, 3 days, and 4 days).

The pH of ACPP hydrogel is very low and the acidic environment damages EM structure,

thus reduces EM's activity throughout the release period. In contrast, VCM is more resistance to an acidic environment and retains its activity even in a highly acidic environment.

4.2 Introduction

Owing to ACPH hydrogel's unique properties, P-DCPD with a novel formula makes a polymeric DCPD cement which forms completely different than monomeric classical CPCs. Previously many materialistic aspects of P-DCPD cement were analyzed in our research group [135]. As means to address antibiotic sensitivity and susceptibility as compared to ACPH, it is necessary to know that P-DCPD cement made by polymeric ACPH hydrogel as the acidic calcium source suggests a completely different setting reaction as compared to classical CPCs setting formula. The reaction of monomeric acidic calcium source with alkali calcium source provides a polymeric bone cement that not only has to be mechanically stable and biocompatible, also the therapeutics has to be delivered effectively. Previously, other polymeric bone cement materials such as poly (methyl methacrylate) (PMMA) were mixed with ACPH hydrogel and the release of VCM and tobramycin were significantly improved in a sense that the burst release reduced, with a minor reduction of antibiotics effect [152]. ACPH shows promising characteristics as a local antibiotic delivery carrier with a prolonged release and high activity of VCM. Although roughly the same release of antibiotics is expected from P-DCPD due to presence of fully hydrated polyphosphate chains, EM and VCM activity might be different in P-DCPD since the pH of P-DCPD is very neutral. This motivates me to explore the bacterial inhibition of P-DCPD cement discs loaded with EM and VCM.

One of the common approaches to test antibiotics sensitivity is via the disc-agar diffusion method. The Kirby-Bauer method is usually used for antimicrobial susceptibility testing. NCCLS

is an international organization composed of medical professionals who promote accurate antimicrobial susceptibility testing (AST). The Kirby-Bauer method is approved by NCCLS.

4.3 Materials and Methods

4.3.1 Discs Materials, Manufacturing, and Antibiotics Loading

I prepared a thin layer P-DCPD cement disc loaded by 10 wt. % of antibiotics. P-DCPD cement discs were prepared by mixing CPP hydrogel and tetra calcium phosphate (TTCP) and sodium citrate with a weight ratio of 1:0.87:0.15, w/w/w at room temperature. This mixture was molded in thin disc shape molds.

To test the idea that the presence of hydrated polyphosphate chains improves antibiotic interaction with the matrix, I decided to measure the inhibition zone for two antibiotic loading methods. In the first method, I added VCM and EM each in 10 wt. % of total cement weight to ACPH hydrogel and mixed it with hydrogel. Subsequently, to form the cement the TTCP and sodium citrate powder was added to the mixture of antibiotics and ACPH hydrogel. In the second method the antibiotic powder in 10 wt. % of total cement weight was added to the mixture of TTCP and sodium citrate powder and afterward the powder mixture was added to ACPH hydrogel to form the cement. The whole procedure was performed under sterile conditions. The average weight of the discs was $\sim 166.25 \pm 0.02$ mg and in this way we can estimate that $\sim 16.62 \pm 0.001$ mg of each disc was loaded by antibiotic. By calculating the volume of each disc and wt.% of drug, $\sim 0.6 \pm 0.003$ g/ml of antibiotic is loaded in each disc.

The summary of the type of discs was indicated below:

(a) P-DCPD/EM (hydrogel mix): P-DCPD cement disc, loaded with EM in a way that EM was mixed with the ACPH hydrogel phase.

(b) P-DCPDVCM (hydrogel mix): P-DCPD cement disc, loaded with VCM in a way that VCM was mixed with ACPH hydrogel phase.

(c) P-DCPDDEM (powder mix): P-DCPD cement disc, loaded with EM in a way that EM was mixed with TTCP and sodium citrate powder.

(d) P-DCPDVCM (powder mix): P-DCPD cement disc, loaded with VCM in a way that VCM was mixed with TTCP and sodium citrate powder.

4.3.2 Antibacterial Activity of P-DCPD Disc-Agar Diffusion Method

The assessment of the antibacterial activities was firstly conducted towards the *S. aureus* because it appears to be most commonly found in orthopedic implant infections.

Briefly, a Mueller–Hinton broth inoculated with *S. aureus* spores (CDC 587, #49230 American Type Culture Collection, Manassas, VA) was cultured at 37°C until an absorbance reading of 0.124 was attained at 625 nm, corresponding to roughly 1×10^5 CFU/mL. Then 0.5 ml of bacteria was dispensed onto the surface of the agar plate (**Figure 4.2 a**). Each disc was pressed down to ensure complete contact with the agar surface (**Figure 4.2 b**). Discs were distributed evenly so that they are no closer than 24 mm from the center to center. No more than 12 discs were placed on one 150 mm plate or more than 5 discs on a 100 mm plate. The plates were inverted and placed in an incubator set to 37°C within 15 minutes after the discs were applied (**Figure 4.2 c**).

After 22 hours of incubation, each plate was examined. Based on satisfactory experimental procedure, the resulting zone of inhibition is uniformly circular and there is a confluent lawn of growth. In detail, the *S. aureus* was used for the test, which was among the most formidable pathogens because of their ability to cause serious bone infections after implantation. The concentrations of bacterial inoculation solution applied in different test series were standardized by UV. After 22 h

incubation at 37 °C, the inhibition zone around the disc samples was defined and measured as the diameter of the inhibition zone excluding the samples. The antibacterial effect was assessed by the radius of the inhibition zone.

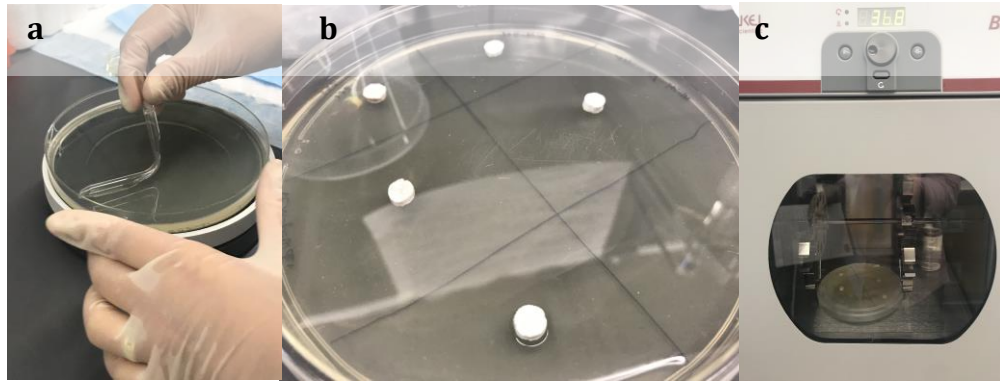


Figure 4.2. Disc-agar diffusion method. Dispensing 0.5 ml of the bacteria on the agar plate and try to be absorbed by the agar gel properly (a), macroscopic appearances of P-DCPD scaffolds which were press down into the agar gel (b), and finally flip over the agar plate and place the plate into an incubator with 37 °C for 22 h (c)

4.4 Data Analysis

All the experiments were repeated 3 times for each group for different time intervals and were summarized. The diameter of inhibition zones and the optical density of antibiotics within each plate were expressed as mean \pm SD. ANOVA was used as statistical analysis.

4.5 Results

4.5.1 Bactericidal Activity

Antibacterial activity of antibiotic-loaded P-DCPD discs with different loading methods was assessed by diffusion agar plate method. As it has shown in **Figure 4.3** inhibition zones are

clearly determined by creating a ring around the discs. As expected the diameter of inhibition zone around the blank P-DCPD disc is very tiny and is 1.5 ± 0.001 cm. The diameter of EM loaded discs is significantly larger than vancomycin loaded discs (**Figure 4.3 a, c**), but there is no significant difference between loading types for both VCM and EM loaded discs.

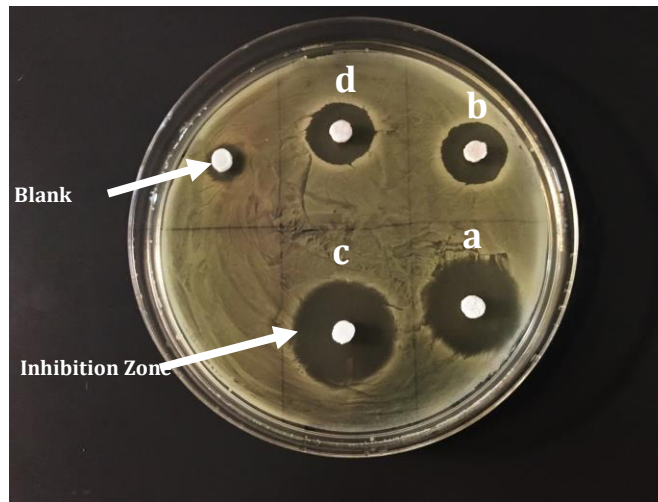


Figure 4.3. Growth of *S. aureus* on the agar plate. Scaffolds were incubated on the sterilized agar plate for 24 h. (a) P-DCPDEM (hydrogel mix) (b) P-DCPDVCM (hydrogel mix), (c) P-DCPDEM (powder mix), (d) P-DCPDVCM (powder mix)

The quantitative analysis of inhibition zones was assessed in **Figure 4.4**. The diameter of the inhibition zone was measured by ruler from 3 different angles then the average was taken between different measurements.

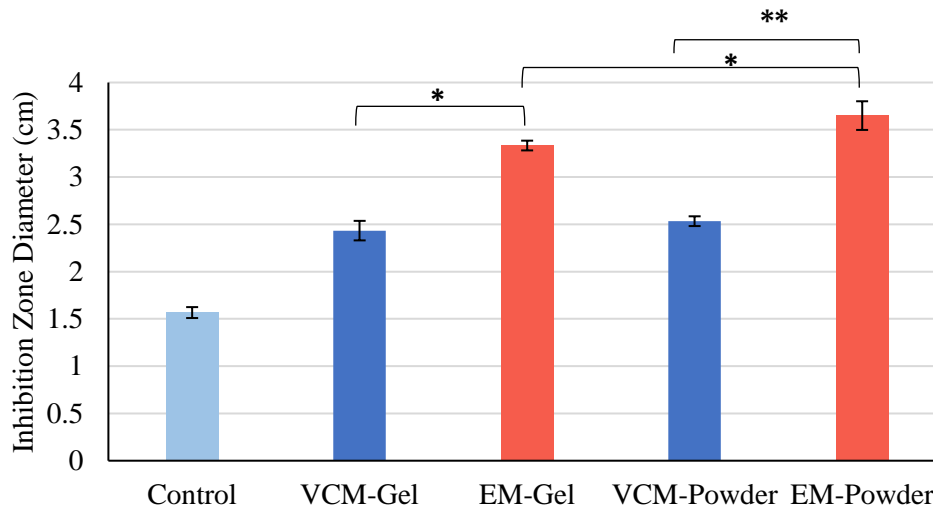


Figure 4.4. Quantitative analysis of the inhibition zone diameter for each disc. (X-Gel: x was mixed with gel phase, CPP gel, of P-DCPD bone cement, X-Powder: x was mixed with powder phase, TTCP, and sodium citrate, of P-DCPD bone cement). * indicates that the difference was significant where the $p < 0.05$.

4.6 Discussion

EM and VCM release from CPP hydrogel have been studied before and we described the results in **Chapter 3**. As it was shown, EM releases faster than VCM and the large amount of EM could kill ~90% of bacteria in the first week of release. Due to antibiotic depletion from CPP discs and acidic nature of CPP hydrogel the activity of EM decayed. In the agar plate experiment the EM inhibition zone appeared to be larger for 22 h of exposure to the same bacteria. Current results are in correlation with the previous antibiotic release results. The smaller inhibition diameter of VCM loaded discs, unlike EM loaded discs, is indicating the strong bond of antibiotics to the matrix.

4.7 Conclusion and Future Work

In conclusion, although results obtained from antibiotics release from ACPP hydrogel, demonstrated the higher activity of VCM in comparison with EM, here we observed that P-DCPD loaded antibiotic with neutral pH and within the shorter time (22 h) preserves antibiotic activity.

EM fast and large volume release was observed here again and it is evident from the significantly larger inhibition zone than VCM one.

VCM makes a strong bond to the CPP matrix and the antibiotic loading approach doesn't have significant effect on the antibiotic release and activity at all.

CHAPTER 5

Physiochemical Comparison of DCPD and P-DCPD

5.1 Purpose and Hypothesis

This aim was developed to study physiochemical differences between the structure of DCPD and P-DCPD particles upon incubation at different time intervals. P-DCPD prepared by ACPD hydrogel owns polymeric properties with completely different properties than DCPD which is made from monomeric calcium phosphate material. In this study, we utilized various techniques to study fine size particles of DCPD and P-DCPD cement, treated under humidified condition (37 °C) for 1, 4, 7, and 14 days.

Some of the key differences between P-DCPD and DCPD have been investigated previously. Based on this study, the setting reaction mechanism of P-DCPD is due to the intermolecular interaction between CPP gel and TTCP, which was supported by XRD, AFM, Raman spectra analysis and SEM. The setting mechanism of P-DCPD is completely different from the classical calcium phosphate cement (CPC) that achieves crystallization by monophosphates reaction. P-DCPD represents a new type of poly-CPCs with significant advantages, including strong mechanical strength, excellent cohesion and easy of handling. We are going to investigate more deeply the differences between P-DCPD and DCPD using various techniques. In this study, particle differentiation based on surface morphology was investigated by SEM and Ca/P ratio-based differentiation of particles has been analyzed by EDS. To determine the dynamic change of bonding (vibrational) mechanism through incubation times, Raman spectroscopy was utilized. Phase changes and molecular identification were investigated through XRD. Measurement of net

charge of particles in H₂O immersion has been done using Zeta Potential. Surface contact angle additional to surface hydrophobicity can reveal the relative absorbance rate on the surface of the cement which is another key factor to unravel information on physiochemical differences between P-DCPD and DCPD.

5.2 Introduction

P-DCPD is a new formula to make polymeric DCPD cement in which its physiochemical behavior is completely different than classical CPCs. In our research group, a study was conducted to compare injectability, cohesiveness, mechanical properties as well as setting mechanism of this newly developed cement.

Based on the reported results, P-DCPD has similar handling properties of classical CPCs. However, P-DCPD cement possesses stronger mechanical properties and excellent cohesion upon wash out. CPC can be divided into HA and DCPD cement. Dicalcium phosphate dihydrate (DCPD), has calcium to phosphate Ca:P ratio of 1 and hence calcium phosphates with Ca:P ratio higher than 1 can be utilized to make brushes. TCP is the most common basic calcium source in brushite cement (Ca/P ratio of 1.5).

It is known from the literature [135] that two processes involve in P-DCPD formation; first, dissolution–precipitation mechanism and second, by deprotonating of the phosphonate followed by the formation of intra- or inter-chained bonding of Ca²⁺ from TTCP with phosphonate ions from CPP. The reaction of an acidic CPP hydrogel with alkali TTCP powder during the setting mechanism at ambient temperature produces such an interaction. Clearly, dissolution of embedded TTCP particles within CPP hydrogel develops a continuous interaction until the TTCP particles convert into P-DCPD. From physical and microscopic scale aspects, we expect a mesh-like

hydrogel matrix within the porous cement structure. Molecular structural of P-DCPD determines its mechanical and cohesiveness superiorities to classical CPC since it was composed of interconnected P-DCPD crystal particles by interlocking to the polyphosphate chains, while CPC is composed of DCPD crystal particles with weak monomer to monomer binding.

5.3 Materials and Methods

5.3.1 P-DCPD and DCPD particle preparation

P-DCPD and DCPD cement were prepared based on previously mentioned protocol, briefly; P-DCPD cement was prepared by mixing of CPP gel with TTCP (weight ratio of 1:0.87, w/w) at room temperature. The mixture of CPP gel with TTCP powder is dough-like material which was placed into a cylindrical mold with an inner diameter of 6 mm. In addition, DCPD cement was prepared by mixing β -TCP, Monocalcium phosphate monohydrate [$\text{Ca}(\text{H}_2\text{PO}_4)_2 \cdot \text{H}_2\text{O}$] (MCPM) (weight ratio of 1:0.812), and 19.1 ml of 0.05 M citrate acid. The mixed material was pressed to yield a cylindrical specimen by uniaxial pressing for 10 days at room temperature. After cement dried, they were ground to the fine powders using mortar and pestle. The ground particles were evaluated under the microscope for particle size analysis ($<75 \mu\text{m}$).

P-DCPD and DCPD particles ($<75 \mu\text{m}$) were divided into 4 parts each, collected in plastic Petri dishes. A total of 8 samples were incubated in 37°C for 1, 4, 7, 14 days respectively. The first sample from each category was collected after 24 h (1st day) and placed under the hood to dry. The second sample from each category was collected after 96 h (4th day) and placed under the hood to dry, and the procedure was repeated until 14 days. After all samples were collected the further analysis was performed on the particles.

5.3.2 Phase determination of DCPD and P-DCPD using X-Ray Diffraction (XRD)

A Rigaku SmartLab Ultima IV x-ray diffractometer with a Cu K α X-ray source was used to measure diffraction peaks for each sample. Approximately 0.5 g of sample powder was loaded into the glass sample holder and flattened at the top. Data were captured every 2° between 10° and 80° at a rate of 5°/second. Analysis of XRD data was completed using PDXL 2.4.2.0 software and samples were referenced by DB card. % crystallinity.

X-Ray Diffraction (XRD) was used to characterize the phases of DCPD and P-DCPD at different time interval and XRD of DCPD powders were shown in **Figure 5.1**. DCPD at 1-day sample represented most of the peaks of brushite [$HCa(PO_4).(H_2O)_2$] and some of the peaks of tuite [$Ca_3(PO_4)_2$]. Small intensity peaks combined brushite and tuite peaks. Some single component tuite and very few hydroxylapatite peaks were also observed.

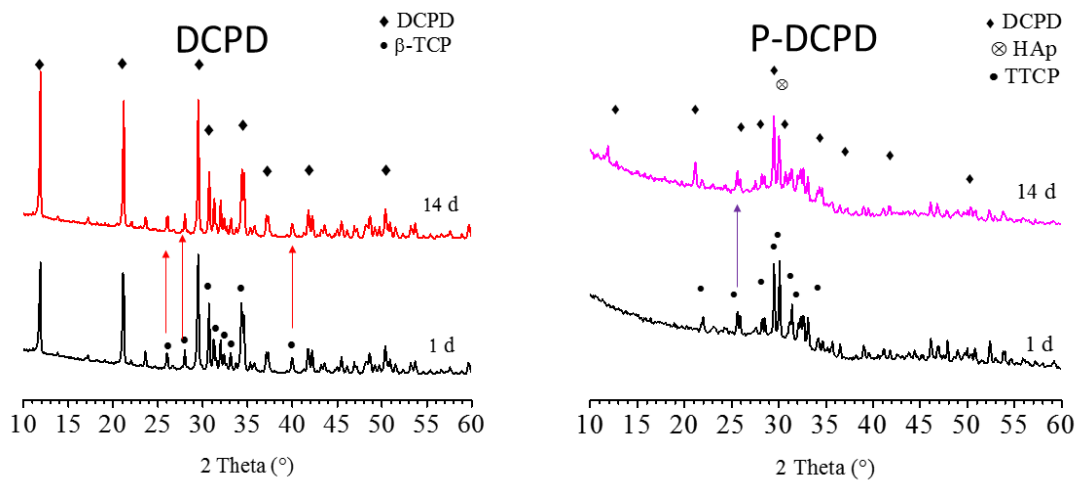


Figure 5.1. XRD peaks of DCPD and P-DCPD powders for 1, and 14 days of incubation considering the best figure of merit (FOM), DCPD particles represent brushite with ICDD# 04-013-3344.

5.3.3 Setting reaction mechanism study of DCPD and P-DCPD using Raman spectroscopy

Raman Spectra were gathered using a Renishaw inVia Raman Microscope with 50x N-Plan Lecia optics (Numerical aperture=0.75) and a working distance of 0.75mm. The 785nm excitation beam was reduced to 10% power (approximately 11.5mW). The powder was compressed into thin disks to achieve a solid surface for the collection interface and scanned using three-second accumulations for each point in a range of 200-1500 cm^{-1} . Five points were taken on each sample and averaged to compensate for a small radius of each collection point on the sample. Raman spectroscopy was used to characterize the setting reaction mechanism of P-DCPD at different time intervals after mixing of ACP and TTCP. Raman further supports the formation of DCPD and transition from initial materials to the final DCPD or HA materials, which was explained by XRD.

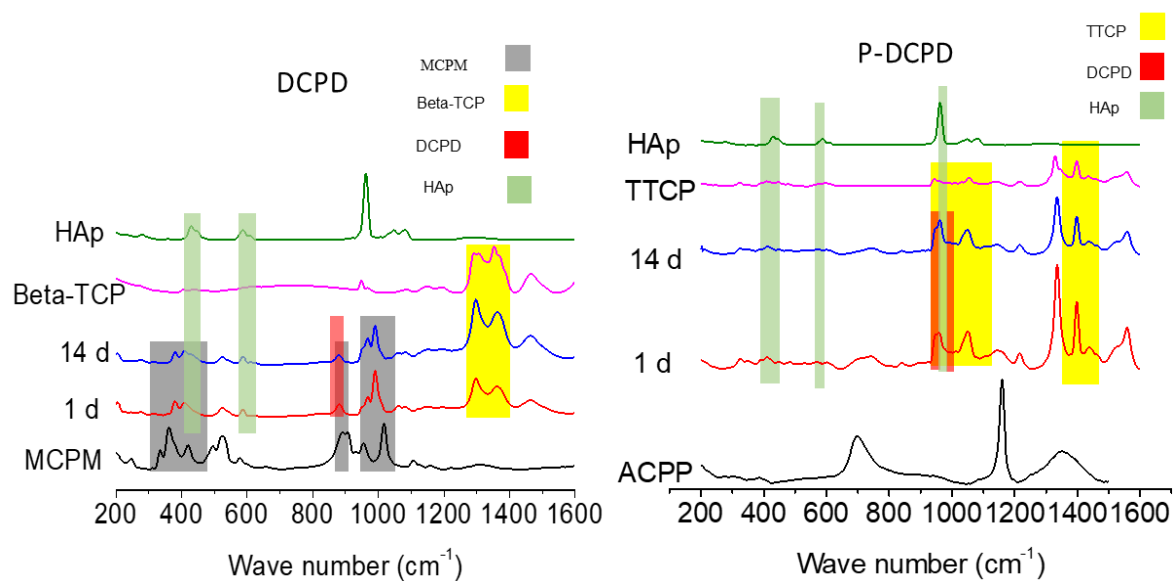


Figure 5.2. Raman Spectra of DCPD and P-DCPD powders for 1, 14 days of incubation.

5.3.4 Identification of particle morphology and content using scanning electron microscopy(SEM)

SEM was used to collect high-resolution images of particle morphology and identify particle contents using EDS analysis. While monomeric DCPD groups show very visible changes in the morphology of its aggregates over time, P-DCPD groups reveal much subtler morphological changes. Therefore, EDS analysis was an integral part of identifying particles and correlating morphology to suspected particle status. Energy Dispersive Spectroscopy (EDS) Analysis: Using the scoring key tolerances established by EDS negative controls, Ca/P ratios of particles were classified as either a pure or transitional. SEM images color marked with EDS data are shown in **Figure 5.3**.

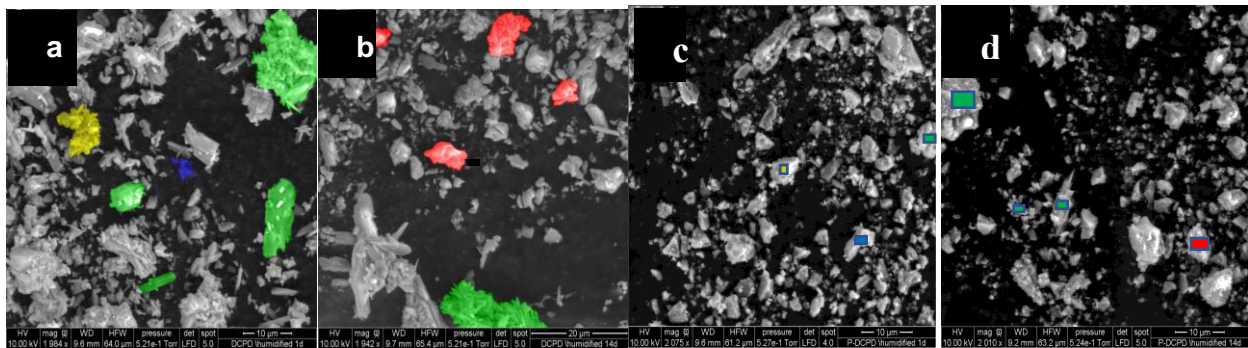


Figure 5.3. Morphologies of DCPD and P-DCPD with EDS data over time (a) DCPD humidified 1 day (b) DCPD humidified 14 days (c) P-DCPD humidified 1 day and (d) P-DCPD humidified 14 days

Ca/P averages were taken across both length scales without prejudice to determine key transitional trends in major particles. It was found that while less Hydroxyapatite (HA) was detected that the DCPD formation is higher for P-DCPD powder converge on the accepted range

for ‘pure P-DCPD’ with longer humidification, monomeric DCPD shows higher HA formation. **Figure 5.4** illustrates the progression of the average Ca/P values over time. Additionally, Using P-DCPD and DCPD mature particles resulted in observing less amount of material as transitioned DCPD.

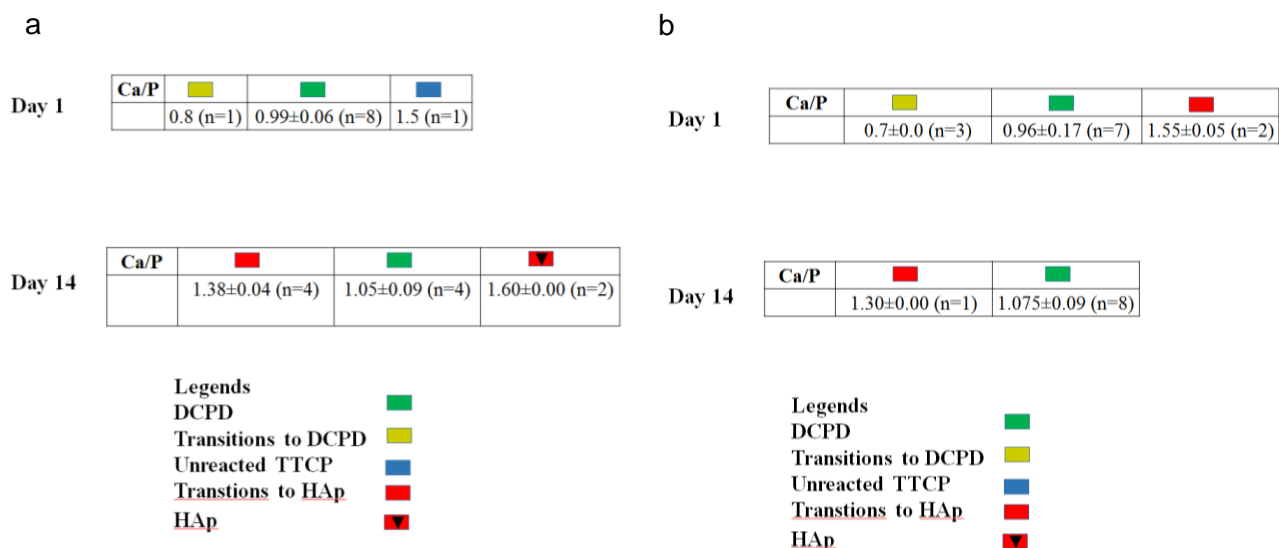


Figure 5.4. Average Ca/P ratio progression over time. (a) DCPD, (b) P-DCPD

Although it would be impossible to tell from a static timepoint whether Ca/P values in the 1.5-2.0 range represented Hydroxyapatite or the reactant β -TCP, the Ca/P trend over time suggests that P-DCPD forms the desired product in the prolonged presence of water molecules while DCPD formed a certain quantity of Hydroxyapatite crystals between the 4 days and 7 days timepoints. This crossing of Ca/P ratios into the HA or DCPD/HA transitional range accompanied by the appearance of new morphologically different aggregates (Shown in **Figure 5.4**) suggests the transformation of monomeric DCPD to larger hydroxyapatite aggregates.

Conversely, it is seen that particles showing Ca/P ranges of 0.85-1.14 for P-DCPD products become much more frequent in subsequent P-DCPD time groups. This is grounds to suspect that P-DCPD is not as susceptible to HA transformations in the presence of water.

5.3.5 Stability and adhesion of DCPD and P-DCPD particles using Zeta Potential

The ζ potential of P-DCPD and DCPD in the colloidal state were measured in the aging medium at 25 °C to determine and compare the stability and adhesion for both particles

As shown in **Table 5.1** and **Figure 5.5**, zeta potential values for both products have a slight descending trend in terms of approaching to a less negative value as interval time increases. The absolute zeta potential value is less negative for P-DCPD. Basically, when P-DCPD particles are placed in water, polyphosphate chains expose their negative charges. Since the polyphosphate chains expected to be depleted as result of P-DCPD formation, less negative potential can be predictable. As previously[72], indicated zeta potential value for ACPD particles was -32.92 ± 2.74 mV, which is a more negative value in comparison to P-DCPD and DCPD. This indicates presence of fewer polyphosphate chains in P-DCPD, as the overall potential decreases with greater numbers of exposed asymmetric P=O-P ends.

Table 5.1. Zeta potential values for P-DCPD and DCPD in water

Intervals (day)	ζ Potential (mean \pm SD) (mV)	
	P-DCPD	DCPD
1	-20.5	-28.60
4	-20.4	-30.5
7	-19	-28.05
14	-19.7	-23.35

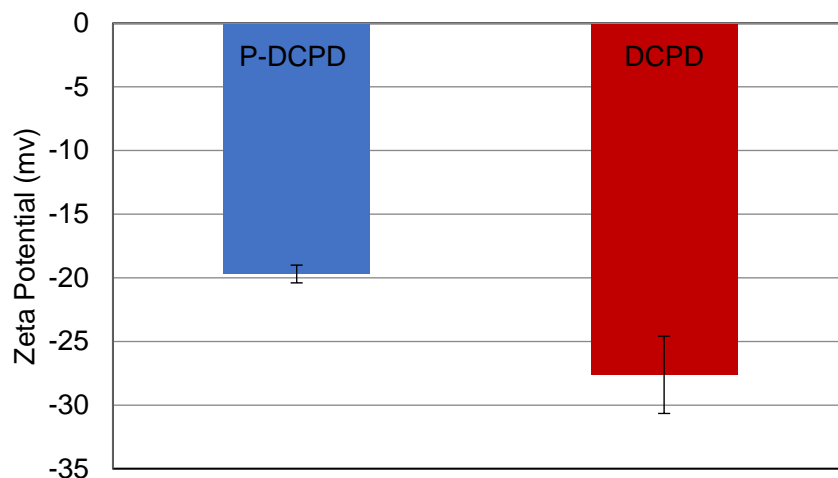


Figure 5.5. Average zeta potential values for P-DCPD and DCPD, indicating

5.3.6 Contact angle measurements

Water contact angle and absorption behavior on the surface of DCPD and P-DCPD were measured and analyzed for 4-time intervals of particle incubation. 20 μ l of deionized water was dropped on the surface of each compressed disc (CARVER, Wabash, IN. USA) made up of DCPD and P-DCPD particles.

Table 5.2. Water contact angle values for P-DCPD and DCPD

Sample	1-Day		4-Days		7-Days		14-Days	
	P-DCPD	DCPD	P-DCPD	DCPD	P-DCPD	DCPD	P-DCPD	DCPD
Angle[°] \pm	20.32 \pm	7.12 \pm	29.19 \pm	24.87 \pm	23.71 \pm	8.35 \pm	16.70 \pm	8.27 \pm
STD	1.03	0.13	1.22	3.23	0.10	1.25	0.67	0.42

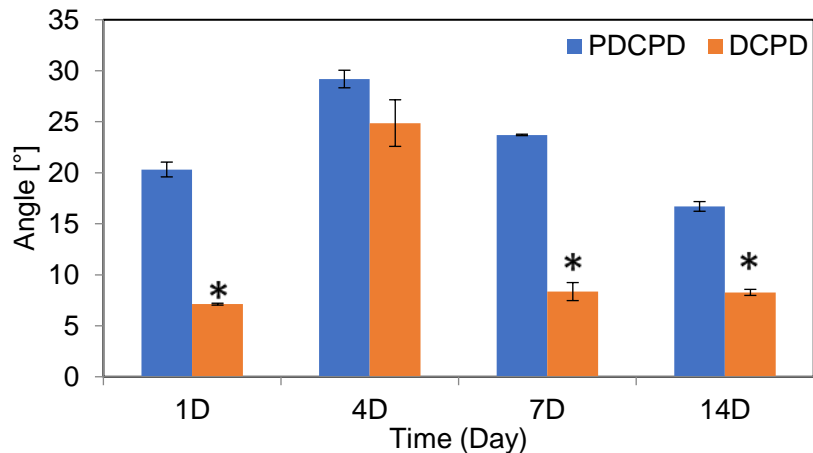


Figure 5.6. The water contact angle of P-DCPD vs. DCPD, indicating super hydrophilicity nature of DCPD

As shown in **Figure 5.6**, DCPD and P-DCPD contact angle results ($< 30^\circ$) confirms the hydrophilicity of both materials. DCPD with contact angle ($< 20^\circ$) shows super hydrophilic behavior. To further investigate how hydrophilicity degree of two materials varies in different time points; an experiment was performed to measure the alteration of contact angle during the absorption period.

Table 5.3. The water absorption rate for P-DCPD and DCPD

Sample	PDCPD		DCPD	
	d θ /dt	STD	d θ /dt	STD
1D	1.411	0.540	3.079	1.115
4D	0.944	0.237	1.004	0.414
7D	1.635	0.087	3.532	1.126
14D	1.296	0.058	8.000	3.020

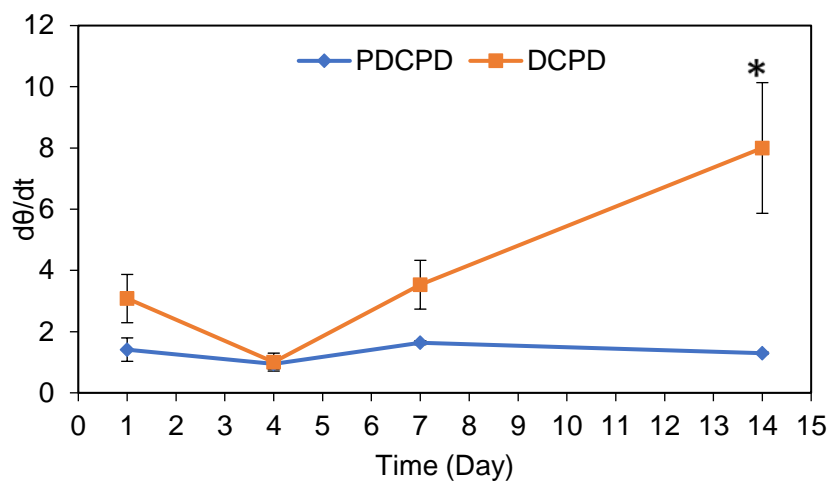


Figure 5.7. Water absorption behavior for DCPD and P-DCPD in 1 day, 4 days, 7 days, and 14 days after incubation.

As it has shown in **Figure 5.7** absorption rate for P-DCPD is lower than DCPD and it can be considered near-constant, overall. DCPD has a higher absorption rate, with an increased absorption rate over time of incubation. P-DCPD particles considered polymeric material, which known as material with less hydrophilicity degree over other monomeric materials.

A t-test was used to determine the statistical difference in the absorption rate between DCPD and P-DCPD particles ($P < 0.05$).

5.4 Data Analysis

All the experiments were repeated 3 times for each group for different time intervals and were summarized. Zeta potential and contact angle experiments were expressed as mean \pm SD. A t-test was used to determine the statistical difference in the absorption rate between DCPD and P-DCPD particles ($P < 0.05$).

5.5 Discussion

The self-setting reaction is initiated by mixing of monomeric acidic monocalcium phosphate (MCPM) and basic calcium phosphates (TTCP) in an aqueous solution, which undergoes setting in a continuous dissolution–precipitation reaction. P-DCPD is set by a synchronous gelation–polymerization process by the reaction of an aqueous acidic ACP gel with alkali TTCP powder at ambient temperature. The key molecular structural difference between P-DCPD and DCPD are the interconnected P-DCPD crystal particles via interlocking polyphosphate chains, compared to DCPDs crystal particles with weak mutual bonding.

In this chapter, we compared the physio-chemical and micro-structural performance of P-DCPD and DCPD particles. We found that P-DCPD was more stable than DCPD and showed much less transformation to hydroxyapatite crystals in a neutral reaction environment demonstrated by XRD, SEM and Raman spectroscopy.

XRD analysis carried out by Dr. Rajib Barua, demonstrated quick and steady DCPD formation from MCPM and β -TCP. The monomeric DCPD sample contained hydroxyapatite and β -TCP impurities (**Figure 5.1**). The β -TCP impurity was likely unreacted starting material. The hydroxyapatite impurity may have originated from the hydroxyapatite present in the β -TCP sample, as an impurity from the synthesis of β -TCP. It is also possible that DCPD decomposed to hydroxyapatite, due to its weak mutual bonding and absent chain formation. Thus DCPD was unstable and acts as a precursor of hydroxyapatite. The P-DCPD sample contained a mixture of DCPD, troemelite, monetite and trace hydroxyapatite. P-DCPD likely decomposed to troemelite, monetite and traces of hydroxyapatite. The trace amount of hydroxyapatite suggests that P-DCPD decomposes to hydroxyapatite very slowly. Therefore, it exhibits greater stability than its monomeric counterpart, DCPD. P-DCPD first dehydrates and forms monetite, CaHPO_4 . Since

monetite is still present, the P-DCPD is in the process of removing water molecules from their structure. Troemelite peaks are observed a much higher than hydroxyapatite means that P-DCPD forms troemelite higher than that of hydroxyapatite. Monomeric DCPD forms a high quantity of hydroxyapatite. P-DCPD is observed during a slow formation of bone cements. The reaction rate cannot be clearly identified due to a visible shrinkage of P-DCPD particles during the comparison. Therefore, the other characterization techniques were used to observe additional finding in addition to XRD analysis.

Raman intensities of DCPD indicated the partial formation of DCPD along with the peak of reactants and hydroxyapatite. This hydroxyapatite appears from the reactants and from the decomposition of DCPD due to their unstable nature. Therefore, the analysis by Raman spectroscopy supports the XRD studies. The conversion to hydroxyapatite is more pronounced in DCPD as compared to the conversion to hydroxyapatite in P-DCPD. The phenomenon can be rationalized by the chain formation in P-DCPD. The acidic reactant of P-DCPD mainly acts as a setting reactant due to its unique inter/intra polyphosphate chains. As shown in **Figure 5.2**, at the beginning of the setting, the main bands obtain are $\nu_s(\text{P-O-P})$, $\nu_s(\text{PO}_2)$ and the band between 1290-1355 cm^{-1} from ACPG gel and ν series from TTCP. With the time elapse, $\nu_s(\text{P-O-P})$ and $\nu_s(\text{PO}_2)$ becomes broader and shifts to a high wavenumber to accumulate more calcium ions from TTCP. However, the third band (1290-1355 cm^{-1}) shows TTCP peaks which indicates unreacted TTCP in P-DCPD. The results deviate in this part may be due to processing difficulties. This phenomenon indicates the possibility to obtain a double phase in P-DCPD. One phase contains regular P-DCPD with lacking calcium ions in their structure and the other phase contains unreacted TTCP with the high calcium content. This phenomenon may change the physicochemical properties of P-DCPD

explained elsewhere. However, this newly formed P-DCPD has higher stability than monomeric DCPD as the existence of hydroxyapatite is not observed.

In the SEM studies, performed by our Master's student, Conor Daly-Seiler, a small amount of transforming hydroxyapatite, absence of transformed hydroxyapatite and a significant decrease in Ca/P ratios in P-DCPD were observed (**Figure 5.3**). These indicate that P-DCPD is more stable than DCPD. SEM studies suggest a fundamental difference in the formation of DCPD and P-DCPD particles although both follow the same dissolution-precipitation mechanism. The decrease in DCPD structure and formation of transitioning and transitioned hydroxyapatite confirms their lack of stability. DCPD particles exhibit a very weak mutual bonding because reactants do not form any interconnection and interlocking of the interconnected chains which increases their rate of reaction. P-DCPD, on the other hand, tends to transform slowly after mixing reactants because an intermediate precursor phase of P-DCPD is formed. During precipitation, the newly formed P-DCPD crystals grow, while interconnecting and interlocking the entangled polyphosphate chains.

Although it would be impossible to tell from a static timepoint whether Ca/P values in the 1.5-2.0 range represented hydroxyapatite or the reactant β -TCP, the Ca/P trend over time suggests that P-DCPD forms the desired product in the prolonged presence of water molecules while DCPD formed a certain quantity of hydroxyapatite crystals over time. This crossing of Ca/P ratios into the hydroxyapatite or DCPD/hydroxyapatite transitional range accompanied by the appearance of new morphologically different aggregates suggests the transformation of monomeric DCPD to larger hydroxyapatite aggregates.

As it has shown in **Figure 5.5**, we also noticed that the Zeta potential of P-DCPD (-19.9 mV) was lower than that of DCPD (-27.6 mV). The key engineering factor for the change in zeta potential is the presence of polyphosphate chains in P-DCPD. Zeta potential represents the stability

of DCPD and P-DCPD particles. DCPD indicates more stability than P-DCPD because they exhibit a more negative zeta potential than that of P-DCPD particles. When these particles are placed in water, the particle surface exposes positively charged Ca^{2+} and negatively charged phosphates (*e.g.* monomeric phosphate for DCPD and polyphosphate for P-DCPD particles). DCPD obtains a higher negative value which indicates more negative adsorption of calcium ions. On the other hand, P-DCPD has a low negative value which indicates less adsorption of calcium ions because calcium ion needs time to adsorb in polyphosphate chains. Therefore, the Ca/P ratio in P-DCPD is lower than that of DCPD in the specific time period. This result is consistent with the EDS studies.

Another interesting finding is that the contact angle of P-DCPD (8.27°) is lower than that of DCPD (16.71°) (**Figure 5.6, Table 5.2**). The lower the water contact angle, the higher the hydrophilicity, wettability, and water absorption rate. DCPD provides a less contact angle than P-DCPD because DCPD, being super-hydrophilic undergoes faster dissolution than P-DCPD in an aqueous environment. The weak bonding in DCPD allows positively charged calcium ions dissolve fast. P-DCPD, on the other hand indicates high contact angle because highly entangled and interconnected polyphosphate chains in P-DCPD let calcium ions to dissolve slowly in aqueous solution. Therefore, a higher Ca/P ratio in DCPD than that of P-DCPD obtained from EDS study result can support the contact angle studies as well.

5.6 Conclusion and Future Work

DCPD exhibits a faster formation than the P-DCPD. Reactants exhibit a fast chemical reaction and form DCPD along with hydroxyapatite and β -TCP impurities. This hydroxyapatite may originate from reactant β -TCP or may decompose from DCPD due to the unstable nature of DCPD.

P-DCPD exhibits a slow and stable chemical reaction to form troemelite, DCPD, monetite and traces of hydroxyapatite. The amount and intensity of hydroxyapatite peaks are substantially lower in P-DCPD as compared to their monomeric counterparts. Conversion to hydroxyapatite is more pronounced in monomeric DCPD than in P-DCPD due to the unstable nature of DCPD.

The Raman spectroscopy supports the XRD studies of the appearance of hydroxyapatite. The formation of the polyphosphate chain in P-DCPD reduces the conversion of hydroxyapatite. Peak broadening and shifting of ACPP accumulate more calcium from TTCP in their polyphosphate chain and improve the stability in P-DCPD. DCPD shows the existence of hydroxyapatite through a high Ca/P ratio but P-DCPD does not indicate the existence of hydroxyapatite. SEM results support the Raman spectroscopy and XRD studies.

A high electronegative zeta potential states initial fast adsorption of calcium ions in DCPD during setting reaction. P-DCPD indicates slower adsorption of calcium ions in polyphosphate chains. DCPD's super hydrophilicity causes faster dissolution of the material than that of P-DCPD in aqueous environment and low cohesion of the matrix upon washout. Thus, the hydrogen ions will be more available in the solution and therefore the pH reduces quickly. Inversely, P-DCPD possesses a polymeric nature, where the chain entanglements enhance the integrity of P-DCPD, thereby the pH remains stable for longer period of time.

CHAPTER 6

Biocompatibility Comparison of the P-DCPD and DCPD Particles in Vitro and in Vivo

6.1 Purpose and Hypothesis

Several factors such as surface charge, microporosity, composition and changes of molecular composition, affect osteoblast cell adhesion and migration process to the surface. Based on the results from physiochemical differences between DCPD and P-DCPD (**Chapter 5**), it is expected that cells behave differently in terms of proliferation and differentiation on each material. Based on unique properties of P-DCPD and DCPD, mouse air pouch tissue represents different inflammatory responses.

6.2 Introduction

Interaction of cell and tissue with a material surface is the subject of this chapter. The surface properties directly influence the cellular response, ultimately affecting the rate and quality of new tissue formation. Initially, molecules from the surrounding fluid start to adsorb and create a conditioned interface to which the cell can attach. The macroscopic morphology, as well as the microscopic features and chemical composition of the surface, determine which molecules can adsorb and how cells will attach and align. In bone and cartilage tissue, osteoblasts are highly sensitive to subtle differences in surface roughness and chemistry. The aforementioned properties on the surface will have direct consequences on cell attachment, proliferation, and differentiation.

Osteoblasts derived from MSCs. Their function is the synthesis of collagen and several additional specialized proteins. Besides MSCs, osteoblasts are also widely used to study the

influence of Ca-P materials on cell response, such as their attachment, proliferation and secreting function. MC3T3-E₁ has been used as classical cell models for detection of osteoblastic differentiation stimulated by biomaterials [153, 154]. Generally, osteoblasts tend to attach more and spread better on osteoinductive Ca-P, and their secretion of ALP, as well as some osteoblastic differentiation markers, are also promoted by these materials. For example, according to the microarray analysis, the phenotype of mouse MC3T3-E₁ osteoblasts was significantly altered by Ca-P with varied phase composition, especially the increased ALP activity and mRNA expression of ALP, COL-I and OPN [155]. Therefore osteoblasts are the best in vitro testing model.

Calcium polyphosphate (CPP) is an inorganic polymeric bioceramic. Due to its low Ca:P ratio, CPP has a long chain-like molecular structure and is easily hydrolyzed into calcium orthophosphate. In contrast to the classical CPC setting formula (reaction of monomeric acid calcium source with alkali calcium source), to prepare injectable and self-setting P-DCPD cement by the reaction of CPP gel with tetracalcium phosphate ($\text{Ca}_4(\text{PO}_4)_2\text{O}$; TTCP), we used CPP gel as the acidic calcium source. In previous studies from our research group, we found that P-DCPD cement formed by CPP gel denotes a new formulation of CPC with some advantages over classical cement such as strong mechanical strength and excellent cohesion to the bones. In the final chapter of this dissertation, my goal is to examine how does biocompatibility of P-DCPD differs from DCPD particles in terms of osteoblast proliferation and differentiation. As such, the question that arises here is that if the differences observed in particle comparison study can effect in Vitro cell biocompatibility and in Vivo tissue absorption?

To determine the inflammatory potential of P-DCPD and compare it with DCPD particles, we are going to subcutaneously inject both materials in the mouse air pouch model developed by Edwards et al. [156]. This model allows us to examine changes in the pouch tissues induced by

the treatment. In addition, the effect of newly developed cement formula; P-DCPD bone graft substitutes; in this pouch model have not been investigated. The host response was evaluated by pouch tissue histology (H&E stains).

In vitro tests provide rapid results for predicting or screening the biocompatibility of materials. They allow a high level of control over the test environments in contrast to in vivo tests in which animal or human subjects may be influenced by variables such as sex, age, activity, diet, etc.

The standard cell biocompatibility testing recommended by the US Food and Drug Administration (FDA), established by ISO 10993 and ASTM F748, which has been designed for testing cured materials. These tests measure the cytotoxicity of material by determining metabolic activity via MTT assay.

Several studies on calcium phosphates have shown that cellular response depends on many factors, such as dissolution, composition, topography, and surface energy.

Depending on the calcium phosphate dissolution–precipitation behavior osteoblast function can be affected, in their proliferation, differentiation, and maturation [157-159]. De Bruijn et al showed that there is a connection between dissolution rate and early bone formation in vivo and the osteogenic differentiation in vitro of osteoprogenitor cells, suggesting, therefore, the influence of free calcium and inorganic phosphates on bone formation [160]. Studies show that calcium and phosphate concentrations of the environment may increase or decrease when calcium phosphate ceramics are immersed. This may be induced by immersing calcium phosphate ceramics can even induce cell death [161]. Changes of calcium or phosphate contents in culture medium also affect directly the osteoblastic activities [162].

From the topographical aspect, grooved calcium phosphate surfaces influence the osteoblastic guidance and the groove profile independently of the nature of the substrate (Lu and Leng 2003). Moreover, osteoblasts can feel the microporosity and macroporosity of calcium phosphate surface and they act accordingly [163]. For osteoblasts differentiation, Chou et al have shown that MC3T3 cells are highly sensitive to the crystal shape: large apatite crystals induced more bone than small apatite crystals after 3 weeks of culture [164].

Considering surface energy as an important feature of surface, it strongly affected the initial osteoblastic activity for proliferation and function, while at a later time the less favorable surface exhibited a comparable osteoblastic activity to the most favorable surface [165].

To assess CPC biocompatibility, in vitro studies using the cement in a bulk form or in a very large particle size form have been performed [166, 167] with different cell types. CPC was well tolerated by the bone cells and could enhance the production of different bone proteins. Regarding osteoblast cells interaction with calcium phosphates, osteoblasts are intimately in contact with calcium phosphate surfaces thanks to the production of extracellular collagen firmly attached perpendicular or parallel to the substrate [168].

Physicochemical dissolution kinetics of the bio-material: calcium phosphate ceramics do not all interact in the same way with osteoclasts. The release of calcium ions from the biomaterial seems to play a critical role in the osteoclastic activity; above a critical range of calcium ions levels, osteoclastic resorption is inhibited [169]. Together with the dissolution behavior, the structure of the calcium phosphate ceramic and the crystallinity influence the osteoclastic activity.

CPP's cellular response has been investigated in several studies from the polymeric point of view as well as physical aspects. A study has been focused on how hydrolytic group percentage affects cellular response as result of degradation [62]. Wang et. al. showed that by increasing

sintering temperature, the proportion of Q^1 groups in polyphosphate chain decreased. Based on their cell viability test results, the porous CPP did not exert cytotoxicity effect on the cells after being cultured for nearly 6 days. Due to the lower degradation rate, CPP sintered at higher temperatures showed better cell attachment and proliferation as well as higher cell density.

Furthermore, from a physical point of view, in previous studies from our group crystalline CPP scaffold has been subjected to in vitro cell studies. In an in vitro study, both homogeneous and gradient CPP scaffolds made by compressing methods from CPP powder [170]. To study cell differentiation and proliferation the samples were soaked in murine preosteoblastic MC3T3-E1 cell suspension. No significant difference in cell proliferation was found between the gradient and the homogenous calcium polyphosphate scaffolds, however a much higher cell differentiation and mineralization were observed in the gradient calcium polyphosphate scaffolds than the homogenous calcium polyphosphate scaffolds, which demonstrated by increased alkaline phosphatase activity. The improved distribution and differentiation of cultured cells within gradient scaffolds were reported. Therefore, gradually increasing pore sizes and interconnectivity provided a favorable microenvironment for the migration, differentiation, and in vitro mineralization of cultured cells.

As previously discussed, based on differences in physicochemical properties of DCPD and P-DCPD, surface chemistry and morphology was altered. As such, there is no doubt that cellular attachment, proliferation, and differentiation will be affected. Ren et. al. [171] have demonstrated the setting mechanism of P-DCPD. They proposed that the setting mechanism of P-DCPD is completely different from the classical calcium phosphate cement (CPC) that achieves crystallization by monophosphates reaction. In previous Aim, a comparative study was done on

how the setting mechanism of P-DCPD is different from DCPD, due to intermolecular interaction between acidic CPP and alkali tetracalcium phosphate (TTCP).

Here, our goal is to examine P-DCPD and DCPD cell differentiation, proliferation and cytotoxicity capacity and drive a conclusion based on physicochemical parameters. As such, the question that arises here is that if the differences observed in previous chapters can effect on in Vitro and in Vivo biocompatibility studies?

Previously, the presence of EM loaded strontium-doped calcium polyphosphate (SCPP) particles in pouch models were tested and they found that particles increase the air pouch membrane thickness, and the number of macrophages in the pouches as well as the cytokine production [172].

However, CPP or P-DCPD, purely, has not been investigated in such an experimental procedure before. Calcium phosphate cement (CPC) has been investigated [173], in vivo experiments on rabbits demonstrated that brushite was resorbed and replaced by newly formed bone within 3 months. During CPC resorption, particle debris was noted around the periphery of the cement. Intracellular accumulations of brushite cement were also apparent in phagocytes. In another study, mineral grains had become detached from the cement and some of them had been phagocytosed by macrophages. These grains were round in shape and did not exceed 12 μm .

As such, in this case, we design and perform a mouse air pouch model to investigate inflammatory response of pouch tissue to the new material and compare it with CPCs.

6.3 Materials and Methods

All chemicals used for preparation and analysis were of analytical grade and obtained from Sigma-Aldrich if not stated otherwise. Murine MC3T3-E1 pre-osteoblast cell line was from ATCC (Manassas, VA), Alpha-modified minimum essential medium (α -MEM) and phosphate-buffered saline (PBS) was purchased from Gibco, Life Technologies. 24-well culture plate was obtained from Falcon™ (3047), and 96 well plates were purchased from Fischer Scientific. MTT and cytotoxicity detection (LDH) kits were purchased from ATCC, Manassas, VA, and Roche Diagnostics, Indianapolis, IN, USA, respectively.

6.3.1 Particle preparation

In order to make P-DCPD particles, CPP gel was prepared by mixing the ACPD powder ($< 75 \mu\text{m}$) with distilled H_2O (0.05 g/mL) and stirring at room temperature for 1.5 h. The CPP slurry mixture was allowed to stand overnight for gel formation. Polymeric DCPD (P-DCPD) cement was prepared by mixing of ACPD hydrogel with tetracalcium phosphate (TTCP) powder (weight ratio 1: 0.87: 0.15, w/w) in the presence of sodium citrate at room temperature. The dried P-DCPD bone cement was ground into the fine powders ($< 75 \mu\text{m}$). Finally, samples were sealed and placed inside the desiccator for further experiments.

Monomeric DCPD cement was prepared by mixing of 10 g β -TCP, 8.127 g calcium phosphate monobasic monohydrate (MCPM), $\text{Ca}(\text{H}_2\text{PO}_4)_2 \cdot \text{H}_2\text{O}$ (Sigma-Aldrich, St. Louis, MO) and 19.1 ml 0.05M citric acid (Sigma, cat# C8532) at room temperature. The mixture was ground into fine powders ($< 75 \mu\text{m}$). Finally, samples were sealed and placed inside the desiccator for further experiments.

6.3.2 Particle sterilization

The prepared particles were sterilized by submerging them into 70 % ethanol for 1 h, the after 1 h residual ethanol was removed by centrifuging the particles and replacing it by phosphate-buffered saline (PBS obtained from Gibco, Life Technologies). The PBS was centrifuged and replaced three times, and finally particles were immersed in cell culture medium (α -MEM obtained from Gibco, Life Technologies) prior to adding to the cells. The process was done right before seeding particles on the cells.

6.3.3 Cell culture

MC3T3-E₁ cells were used to determine the biocompatibility of P-DCPD and DCPD particles. Cells were maintained in cell culture flasks (25 cm²) with α -MEM containing 10% fetal bovine serum (FBS), and 1 % penicillin in an incubator (37 °C, 5% CO₂, and 98% humidity) and were passaged every 5 days. To passage cells, the cell culture flasks were washed with PBS and 1ml trypsin was added to detach cells from the bottom of the flasks. The cell-based assays were run as summarized in **Table 6.1**.

Table 6.1. MC3T3-E₁ cells were treated by P-DCPD and DCPD particles undergone 3 cell-based assays to determine proliferation, differentiation, and toxicity

Experiment Purpose	Assay
Mitochondrial Activity (Proliferation)	MTT
ALP activity (Differentiation)	AKP
Cytotoxicity	LDH

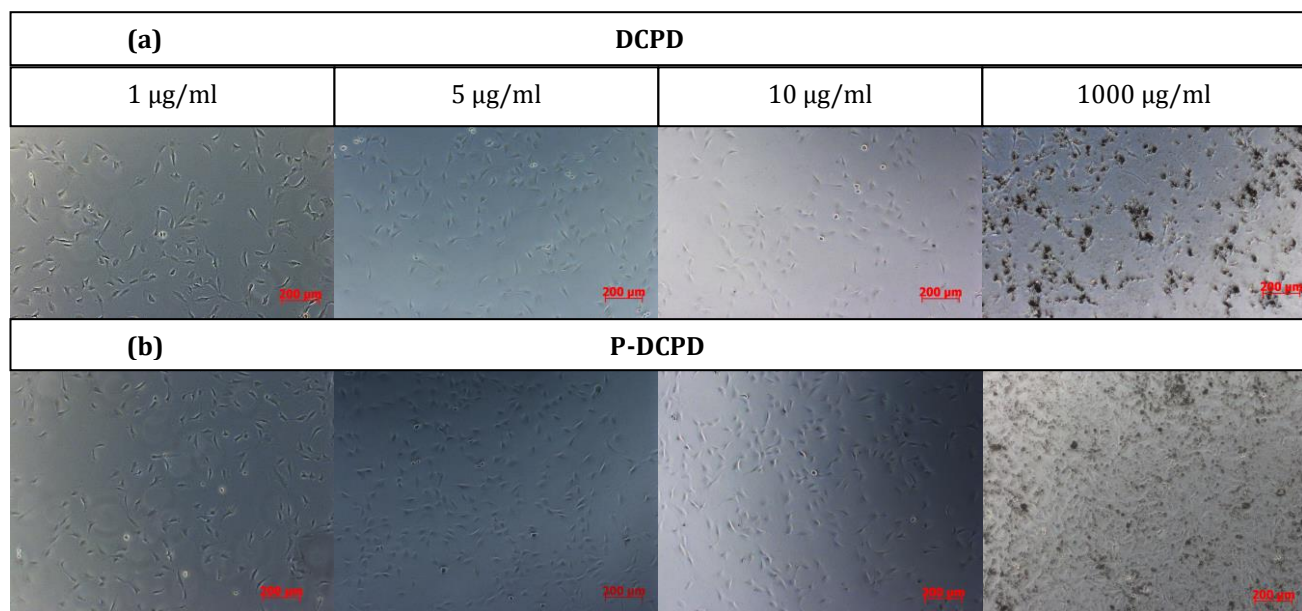


Figure 6.1. MC3T3-E₁ cells treated with particles. (a) DCPD and (b) P-DCPD particles

6.3.4 Cell Proliferation

Cell seeding

To prepare samples for the MTT assay, cells of passage numbers 10–20 were used. About 2×10^5 MC3T3 cells (5-15 passage number) (40 % confluency) in 500 μL of culture medium (α -MEM obtained from Gibco, Life Technologies) were seeded into each well of a 24-well culture plate (Falcon™ Polystyrene Microplates, #3047) and were incubated in a 5% CO₂ atmosphere overnight at 37°C so that the cells could adhere.

Particle seeding

Particles in 1, 5, and 10 $\mu\text{g/ml}$ concentrations were added to cells. 5, 25, 50 μl of stock particle suspension (100 $\mu\text{g/ml}$) were added to the 495, 475, and 450 μl of seeded cells into each well, respectively. Final concentrations to test were 1, 5, 10 $\mu\text{g/ml}$.

MTT (3-(4,5-dimethylthiazol-2-yl)-2,5-diphenyltetrazolium bromide) assay

Cell viability was determined using MTT (3-(4,5-dimethylthiazol-2-yl)-2,5-diphenyltetrazolium bromide) assay (ATCC, Manassas, VA, 30-1010K) in 3 d and 7 d after particle seeding. 20 μ l of MTT reagent was added to each well and plate was incubated at 37 °C for 2 h. After 2 h, all the media was removed and the 100 % DMSO was added to neutralize the effect of reagent (add until the cells become colorless at the bottom of well). Before performing MTT the 300 μ l of culture media was removed from each well and then stored in the freezer for toxicity experiment. The morphology of the cells adhered to the bottom of well was observed with a Zeiss optical microscope (US ZEISS, Brighton, MI) equipped with a Toshiba CCD.

6.3.5 Cell differentiation

Cell seeding

MC3T3-E₁ cells (early passage numbers) were seeded in semi-confluency (20 %) before any treatment. Following 3 d of culture, differentiation was started by culturing cells in differentiation medium (α -MEM supplemented with ascorbic acid, glycerophosphate) 24 h before adding particles. The medium was replaced with fresh medium and in the next d the particles were added. Each time the media were reserved in the freezer for further toxicity experiments. The process was repeated every 3 days until at least 14 days, then cells were analyzed for ALP expression by digesting cells.

Particle seeding

DCPD and PDCPD particles were sterilized by UV and 1, 10,100, 1000 μ g/ml concentrations were added to each well, 24 h after culturing with differentiation medium.

Alkaline phosphatase activity (cell differentiation)

ALP is an important stain to determine cell differentiation. To induce MC3T3-E1 cell differentiation, the differentiation medium was supplemented with 0.2 mM ascorbic acid and β -Glycerphosphate in 10 mM concentration. After culturing 14 days, the cells with particles (ALP assay buffer 50 μ l/well) were harvested to collect lysate for the ALP assay according to the manufacturer's protocol.

6.3.6 Cell toxicity

Lactate dehydrogenase (LDH) assay (cytotoxicity assay)

To prepare samples for the LDH assay, cells of passage numbers 10–20 were used. The previously preserved media before cell proliferation studies (300 μ l) was used to run a cytotoxicity detection kit (Roche Diagnostics, Indianapolis, IN, USA).

6.3.7 In Vivo implantation of injectable particles using animal air pouch model

The animal procedure was done in Providence hospital by Ascension research group. Air pouches were established on 48 mice by subcutaneous injection with 2.5 ml air (**Figure 6.3**). After six days, the animals were divided into 6 groups of 8 mice (**Table 6.2**); they were anesthetized by intraperitoneal injection of pentobarbital (120 mg/kg) and xylazine (10 mg/kg) (Fisher Scientific, Pittsburgh, PA). The particles, with less than 15 μ m of diameter were injected into the air pouch tissue.

Table 6.2. Study Design and Mice Group

Group	n	Harvest	Treatment
I	8	7 days	PBS (saline/control)
		1 month	
II	8	7 days	P-DCPD
		1 month	
III	8	7 days	DCPD
		1 month	

Mice were sacrificed in 7days and 1 month after implantation (**Figure 6.2**). Pouch tissues were collected and washed with 0.5 mL sterile PBS.

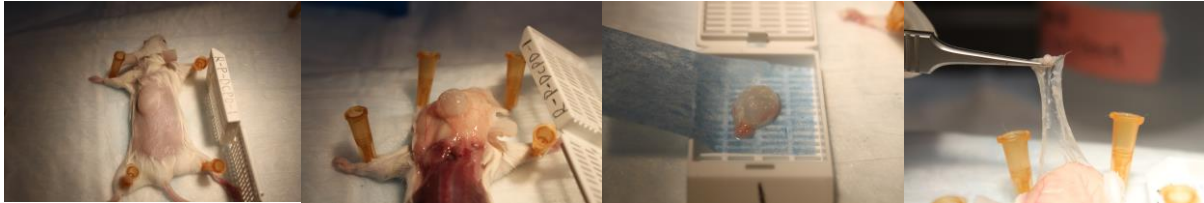


Figure 6.2. Mice were sacrificed and the pouch tissue was collected for histological analysis. The pictures are showing the tissue collection from mice (Mouse air pouch tissue collection and experiments were carried out in Ascension orthopedic research lab at Providence Hospital).

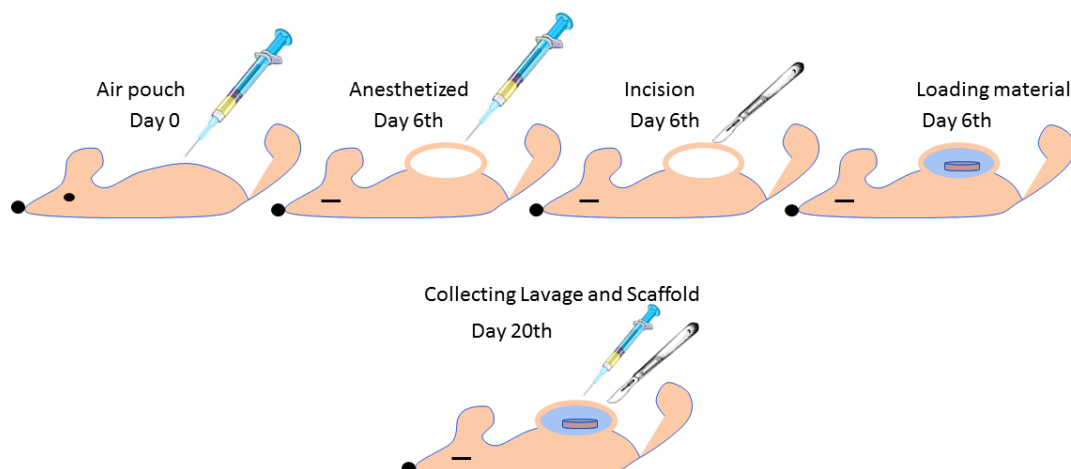


Figure 6.3. Schematic outline of the air pouch model. At the start of the test, 2.5 mL air is injected through a sterile 0.20 μm filter at a dermal site of a mouse to form a pouch.

6.3.8 Histological Analysis of Air Pouch Tissue

Histological evaluations were performed to investigate any presence of inflammation in air pouch tissue resulting from particles in the area. To this goal pouch, tissue samples were fixed in 10% formalin and processed for paraffin embedding. Tissue sections (6 μm) were stained with hematoxylin & eosin (H&E) to evaluate pouch membrane morphology. Four separate sections per specimen were evaluated in a blinded fashion. Digital images were acquired using a light microscope, and these images were analyzed using the Image Pro image analysis software package (Media Cybernetics, Silver Spring, MD). Pouch membrane thickness were determined at six points on each section, with an even distribution of measurement on the proximal side, distal side, and transition curve of the pouch. The total number of cells (based upon nucleus count) were analyzed.

6.4 Data analysis

Data were analyzed with excel. All values were expressed as mean \pm standard deviation.

Statistical significance was set to $p < 0.05$. The experiments were repeated 3 times for 2 groups (DCPD and P-DCPD), so a total of 6 experiments were performed for the MC3T3-E1 cell line. All the variables were summarized and expressed as mean \pm SD. Statistical significance of the results was determined by excel for differences among 2 groups. $p < 0.05$ were considered statistically significant.

For the in vivo part, data were analyzed with excel. All values are expressed as mean \pm SD. Statistical significance was set to $p < 0.05$. The experiment was done for 8 mice for each group (DCPD and P-DCPD), so a total of 8 experiments were performed for mouse air pouch model, and within each experimental procedure such as LDH the samples were triplicated. All the variables were summarized and expressed as mean \pm SD. Statistical significance of the results was determined by excel for differences among 2 groups. $p < 0.05$ were considered statistically significant.

6.5 Results

6.5.1 Cell Proliferation

Cell proliferation in the presence of 3 doses of DCPD and PDCPD particles was determined by MTT assay and shown in **Figure 6.4** at 2-time points. During the time that cells were underexposure of particles in different doses, cell growth was determined by MTT assay. There was a general increase in cell number with time, indicating that both types of cement support cell proliferation (**Figure 6.4**) While the cell growth in presence of 5 $\mu\text{g/ml}$ of DCPD is significantly different than 1 and 10 $\mu\text{g/ml}$ of P-DCPD, there is no significant difference in cell growth between different particle dose of P-DCPD comparing control in 3 days.

In 3rd day of testing cell growth, DCPD and P-DCPD are significantly different for 5 and 10 $\mu\text{g/ml}$, while 7 days after particle seeding, cell growth in presence of DCPD and PDCPD is not significantly different unless for the cells in presence of 5 $\mu\text{g/ml}$ particles.

Overall, cells exposed to P-DCPD grow more in 3 d in compare with DCPD exposed cells regardless of particle dose. Although cell proliferation was significantly inhibited by 5, and 10 $\mu\text{g/ml}$ of P-DCPD particles in 7 d the growth of DCPD exposed cells is normal in comparison with control in 7 d. And in 7d the P-DCPD growth is still higher than DCPD for 1 $\mu\text{g/ml}$ dose.

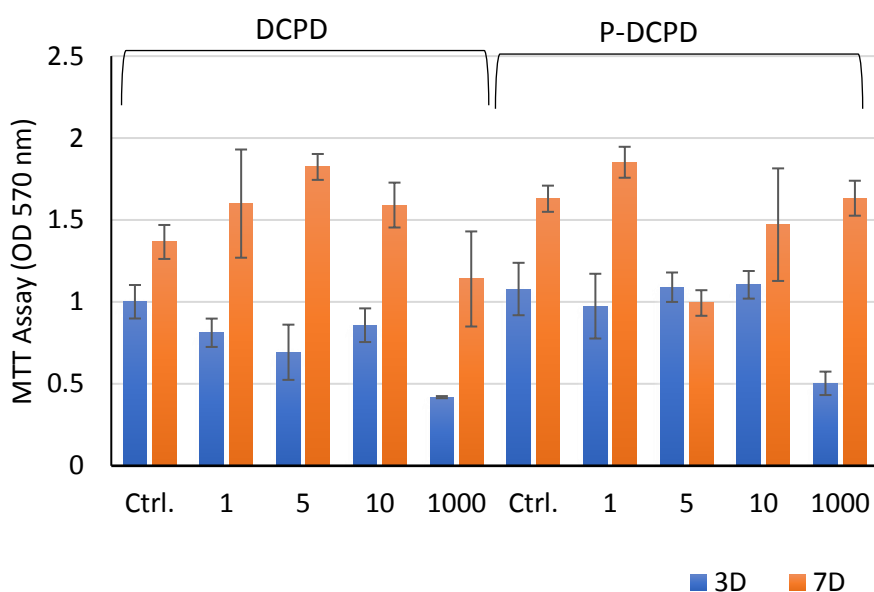


Figure 6.4. MTT assay results of MC3T3-E₁ cells cultured by P-DCPD and DCPD particles with concentrations of 1, 5, 10, and 1000 $\mu\text{g/ml}$ for 3 and 7 days.

6.5.2 Cell Differentiation

To determine the effects of DCPD and P-DCPD particles on MC3T3-E₁ differentiation, intracellular ALP activity was measured. As shown in **Figure 6.5**, the ALP activity of both

particles in each concentration group is significantly lower than control ($P \ll 0.05$). The decrease in ALP activity is highly significant in the cells which were treated by DCPD ($P \ll 0.05$). ALP activity of P-DCPD particles are not statistically significant as compared to untreated cells (control).

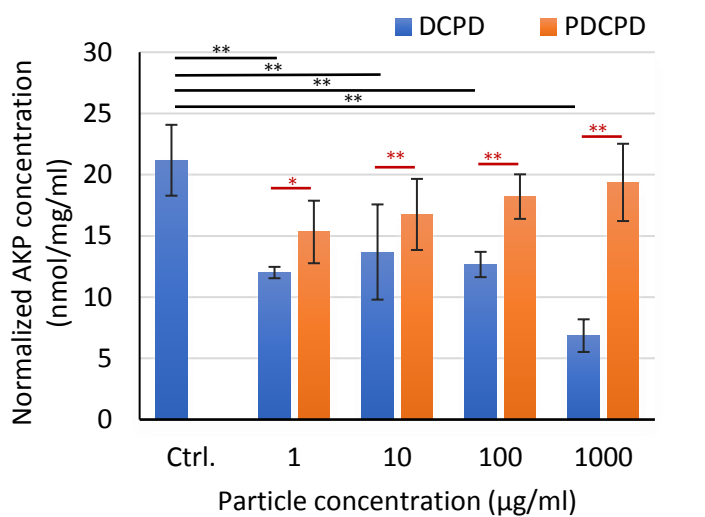


Figure 6.5. Normalized ALP activities of MC3T3 cells cultured with DCPD and P-DCPD particles in 1, 10, 100, and 1000 µg/ml plus Control. Cells were cultured on a well plate. OD of sampled were read on 405 nm, $n = 4$, $*p < 0.05$, $**p < 0.005$.

6.5.3 Cell Toxicity

Toxicity assay of DCPD and PDCPD particles in four concentrations for 3d and 7 d was shown in **Figure 6.6**. The LDH activity of DCPD treated cells is significantly higher when they were treated for a longer period of time (7 days). In 3 days of culturing DCPD treated cells the LDH activity of 10, and 1000 µg/ml groups are significantly higher. Moving forward to P-DCPD treated cells, except 1000 µg/ml P-DCPD treated cells for 7 days of culturing period, none of P-DCPD treated groups show significant LDH activity as compared to untreated cells.

Overall, LDH leakage is significantly higher in 7 d than 3 d for DCPD, however, and it is not the case for PDCPD and LDH amount is lower in 7 d time point.

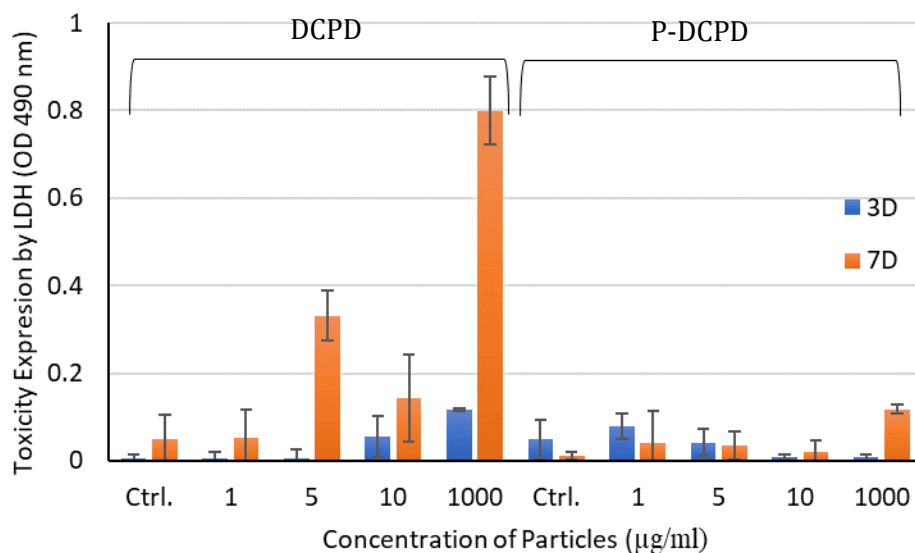


Figure 6.6. LDH activity of MC3T3-E₁ cells in the presence of 1, 5, 10, and 1000 µg/ml DCPD and P-DCPD particles for culturing duration of 3 and 7 days.

6.5.4 Quantitative Analysis of Histological Slides

P-DCPD and DCPD particles induced a similar level of pouch tissue inflammation and membrane thickness in 1 week. In 1 month the inflammatory cells increased significantly for P-DCPD loaded tissue as compared with saline control and DCPD loaded tissues. The inflammation significantly reduced after 1 month for control and DCPD loaded mouse tissue while there is no significant difference between 1 week and 1-month tissue inflammation for P-DCPD loaded air-pouch membrane. H&E staining (**Figure 6.8**) revealed that both particles do not significantly stimulate membrane thickness and the number of infiltrating cells in pouches for 1 week of treatment, as compared to saline controls. However, the quantitative image analysis of histological

sections revealed that in 1 month the membrane thickness reduced significantly for DCPD treated membrane after 1 month, as well as saline controls.

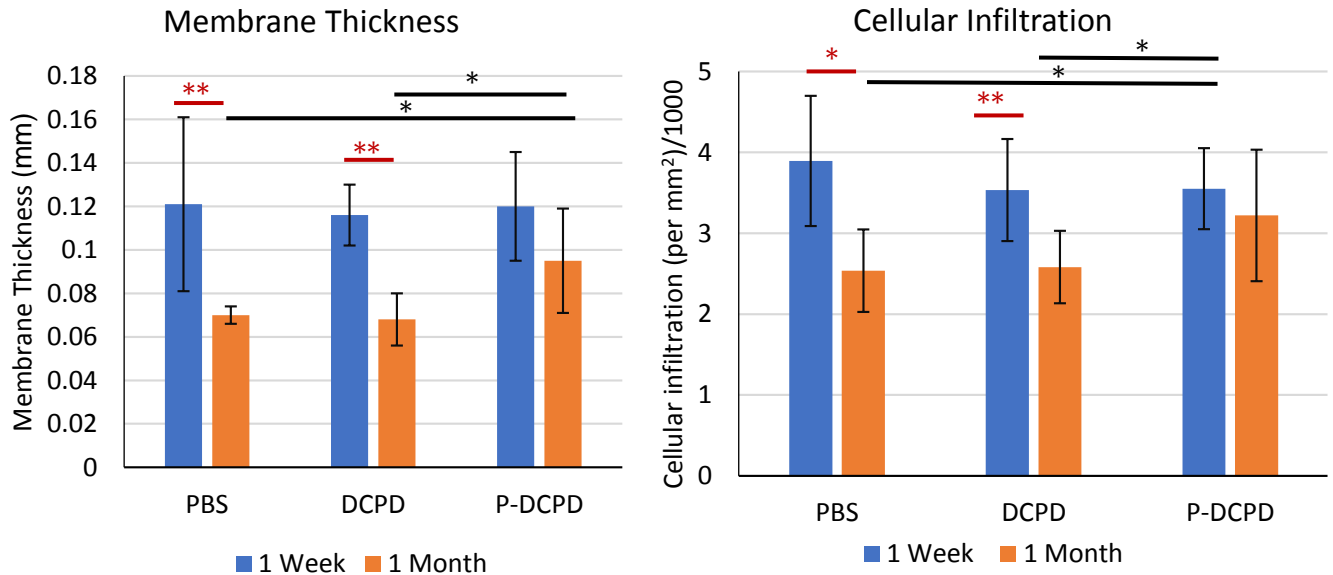


Figure 6.7. Quantitative image analysis of mouse

air-pouch tissue treated by P-DCPD and DCPD particles for 1 week and 1 month. Membrane thickness analysis (a), cellular infiltration analysis (b). The data was compared to control mouse groups which were treated only by injecting sterilized PBS.

The membrane thickness reduced by time in case of DCPD and saline controls tissue but the P-DCPD loaded membrane does not show a significant reduction in membrane thickness by passing time. Membrane thickness is significantly larger than DCPD and control in 1 month of treatment. P-DCPD loaded tissue shows higher integrity upon loading the particles.

Cellular infiltration reduced by the course of time in both control and DCPD cases but for P-DCPD the cellular infiltration didn't change significantly. However, the infiltration increased significantly as compared to control in 1-month time course.

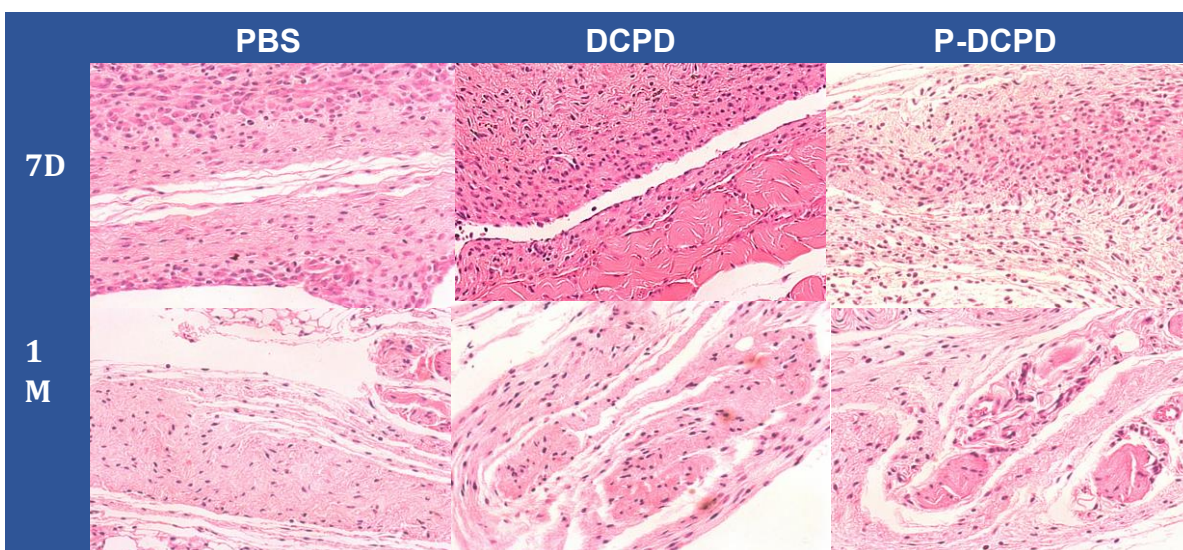


Figure 6.8. Representative pouch tissues histology of microscopic appearance. All the tissue sections stained with hematoxylin and eosin (H&E). (Original magnification, 20x).

6.6 Discussion

P-DCPD and DCPD particles similarly affect cell growth, but growth of P-DCPD treated cells slightly were affected by adhesion of the particles and reduced the growth in some cases for P-DCPD. Moderately hydrophilic P-DCPD with less negative surface charge in compare with DCPD must be more favorable substrate for cells. Thus, P-DCPD shows promising cell differentiation (**Figure 6.5**) as compared to DCPD. Also, P-DCPD induced much lower toxicity, even for higher concentrations up to 1000 μ g/ml. Super hydrophilic nature of DCPD is effecting the cellular adhesion and thus the cell differentiation and growth. In addition, DCPD is highly negative particle, based on Chapter 5, and zeta potential data showed that P-DCPD is less negative.

Cellular proliferation all depends on degree of hydrophilicity and positive charge of the surface [174], thus the higher cellular viability of P-DCPD is due to the impact of moderate

hydrophilicity and lower negative charge of the surface. At the same time P-DCPD's fast adhesion to the surface can be a problematic matter since the cells face some barriers in their path, thus the viability might be affected. Thus far, P-DCPD is a favorable material for cells in terms of toxicity and differentiation. Slight reduce in cell growth in presence of P-DCPD can be due to some material properties such as pH. However, it has been tested that DCPD and P-DCPD maintained at similar pH (~7), it is worthy to note that P-DCPD consists of acidic component such as CPP hydrogel which might be dissolved poorly while making the cement or it might be exposed to the surface of the particles. This acidity can interfere with the results of cell culture.

In Vivo study, the control, P-DCPD and DCPD particles induced similar cellular infiltration in a 1-week time point however for 1-month time point the cellular infiltration reduces as compared to 1-week results but as compared to control the P-DCPD calls more cells to the membrane. From the cellular response one can estimate that P-DCPD and DCPD must have a similar inflammation and membrane thickness profile at least for the shorter time point. The 1-week results fully confirm the idea. For the 1 month as the particles remain inside the pouch membrane, P-DCPD induces more inflammatory response as compared to both control and DCPD which might be due to the interaction of tissue with P-DCPD. On the other hand, P-DCPD is polymeric material that can make a shelter for bacteria to grow [175] and induce inflammatory results in the host tissue therefor as particles remain for the longest time within tissue, it might generate higher cellular infiltration for P-DCPD as oppose to DCPD and control.

6.7 Conclusion and Future Work

In conclusion, based on preliminary results obtained from **Chapter 5**, P-DCPD with moderate hydrophilicity and absorption rate, as opposed to super hydrophilic DCPD showed higher viability for cell proliferation and differentiation.

According to the higher dissolution rate and less cohesion of DCPD matrix, and the increase of Ca and P in material extracts, less favorable differentiation and toxicity results of DCPD-treated materials were observed. Overall, P-DCPD showed more favorable environment for cells to proliferate and remain viable.

Based on in vivo experiments, as it has been noted before an inflammatory response can be caused by several factors. The main factor which is highly distinguishable between P-DCPD and DCPD is matrix adhesion. This can be related to the dissolution rate for both matrices when they are embedded in air pouch tissue. Based on Song et al findings, it is expected that P-DCPD with higher matrix adhesion properties, induced less or no inflammatory response than DCPD embedded sample. In this chapter we showed that P-DCPD and DCPD similarly act in pouch tissue for 1-week and then P-DCPD induce some negligible inflammation as compared to saline control and DCPD-treated mice. Moreover, morphological properties of DCPD and P-DCPD are determinant factors for evaluating tissue response to the embedded particles. P-DCPD as a polymeric bone cement material acts as a shelter for bacteria to grow as it remains for longer time within the tissue.

APPENDIX

10/17/2019

RightsLink Printable License

JOHN WILEY AND SONS LICENSE TERMS AND CONDITIONS

Oct 17, 2019

This Agreement between Wayne State University -- Yasaman Chehreghanianzabi ("You") and John Wiley and Sons ("John Wiley and Sons") consists of your license details and the terms and conditions provided by John Wiley and Sons and Copyright Clearance Center.

License Number	4691550899629
License date	Oct 17, 2019
Licensed Content Publisher	John Wiley and Sons
Licensed Content Publication	JOURNAL OF BIOMEDICAL MATERIALS RESEARCH PART A
Licensed Content Title	Comparing the release of erythromycin and vancomycin from calcium polyphosphate hydrogel using different drug loading methods
Licensed Content Author	Weiping Ren, David C. Markel, Gregory Auner, et al
Licensed Content Date	May 9, 2019
Licensed Content Volume	0
Licensed Content Issue	0
Licensed Content Pages	9
Type of use	Dissertation/Thesis
Requestor type	Author of this Wiley article
Format	Electronic
Portion	Full article
Will you be translating?	No
Title of your thesis / dissertation	INVESTIGATION OF PHYSIOCHEMICAL PROPERTIES, AND BIOCOMPATIBILITY OF AMOURPHOS CALCIUM POLYPHOSPHATE HYDROGEL DOPED WITH ANTIBIOTICS AND INJECTABLE P-DCPD BONE CEMENT
Expected completion date	Dec 2019
Expected size (number of pages)	120
Requestor Location	Wayne State University 675 seward Street

<https://s100.copyright.com/CustomerAdmin/PLF.jsp?ref=bac67732-9cfe-4251-992f-17c07c1e23e1>

DETROIT, MI 48202
United States
Attn: Wayne State University

Publisher Tax ID EU826007151

Total 0.00 USD

[Terms and Conditions](#)

TERMS AND CONDITIONS

This copyrighted material is owned by or exclusively licensed to John Wiley & Sons, Inc. or one of its group companies (each a "Wiley Company") or handled on behalf of a society with which a Wiley Company has exclusive publishing rights in relation to a particular work (collectively "WILEY"). By clicking "accept" in connection with completing this licensing transaction, you agree that the following terms and conditions apply to this transaction (along with the billing and payment terms and conditions established by the Copyright Clearance Center Inc., ("CCC's Billing and Payment terms and conditions"), at the time that you opened your RightsLink account (these are available at any time at <http://myaccount.copyright.com>).

Terms and Conditions

- The materials you have requested permission to reproduce or reuse (the "Wiley Materials") are protected by copyright.
- You are hereby granted a personal, non-exclusive, non-sub licensable (on a stand-alone basis), non-transferable, worldwide, limited license to reproduce the Wiley Materials for the purpose specified in the licensing process. This license, **and any CONTENT (PDF or image file) purchased as part of your order**, is for a one-time use only and limited to any maximum distribution number specified in the license. The first instance of republication or reuse granted by this license must be completed within two years of the date of the grant of this license (although copies prepared before the end date may be distributed thereafter). The Wiley Materials shall not be used in any other manner or for any other purpose, beyond what is granted in the license. Permission is granted subject to an appropriate acknowledgement given to the author, title of the material/book/journal and the publisher. You shall also duplicate the copyright notice that appears in the Wiley publication in your use of the Wiley Material. Permission is also granted on the understanding that nowhere in the text is a previously published source acknowledged for all or part of this Wiley Material. Any third party content is expressly excluded from this permission.

- With respect to the Wiley Materials, all rights are reserved. Except as expressly granted by the terms of the license, no part of the Wiley Materials may be copied, modified, adapted (except for minor reformatting required by the new Publication), translated, reproduced, transferred or distributed, in any form or by any means, and no derivative works may be made based on the Wiley Materials without the prior permission of the respective copyright owner. **For STM Signatory Publishers clearing permission under the terms of the [STM Permissions Guidelines](#) only, the terms of the license are extended to include subsequent editions and for editions in other languages, provided such editions are for the work as a whole in situ and does not involve the separate exploitation of the permitted figures or extracts,** You may not alter, remove or suppress in any manner any copyright, trademark or other notices displayed by the Wiley Materials. You may not license, rent, sell, loan, lease, pledge, offer as security, transfer or assign the Wiley Materials on a stand-alone basis, or any of the rights granted to you hereunder to any other person.
- The Wiley Materials and all of the intellectual property rights therein shall at all times remain the exclusive property of John Wiley & Sons Inc, the Wiley Companies, or their respective licensors, and your interest therein is only that of having possession of and the right to reproduce the Wiley Materials pursuant to Section 2 herein during the continuance of this Agreement. You agree that you own no right, title or interest in or to the Wiley Materials or any of the intellectual property rights therein. You shall have no rights hereunder other than the license as provided for above in Section 2. No right, license or interest to any trademark, trade name, service mark or other branding ("Marks") of WILEY or its licensors is granted hereunder, and you agree that you shall not assert any such right, license or interest with respect thereto
- NEITHER WILEY NOR ITS LICENSORS MAKES ANY WARRANTY OR REPRESENTATION OF ANY KIND TO YOU OR ANY THIRD PARTY, EXPRESS, IMPLIED OR STATUTORY, WITH RESPECT TO THE MATERIALS OR THE ACCURACY OF ANY INFORMATION CONTAINED IN THE MATERIALS, INCLUDING, WITHOUT LIMITATION, ANY IMPLIED WARRANTY OF MERCHANTABILITY, ACCURACY, SATISFACTORY QUALITY, FITNESS FOR A PARTICULAR PURPOSE, USABILITY, INTEGRATION OR NON-INFRINGEMENT AND ALL SUCH WARRANTIES ARE HEREBY EXCLUDED BY WILEY AND ITS LICENSORS AND WAIVED BY YOU.
- WILEY shall have the right to terminate this Agreement immediately upon breach of this Agreement by you.

- You shall indemnify, defend and hold harmless WILEY, its Licensors and their respective directors, officers, agents and employees, from and against any actual or threatened claims, demands, causes of action or proceedings arising from any breach of this Agreement by you.
- IN NO EVENT SHALL WILEY OR ITS LICENSORS BE LIABLE TO YOU OR ANY OTHER PARTY OR ANY OTHER PERSON OR ENTITY FOR ANY SPECIAL, CONSEQUENTIAL, INCIDENTAL, INDIRECT, EXEMPLARY OR PUNITIVE DAMAGES, HOWEVER CAUSED, ARISING OUT OF OR IN CONNECTION WITH THE DOWNLOADING, PROVISIONING, VIEWING OR USE OF THE MATERIALS REGARDLESS OF THE FORM OF ACTION, WHETHER FOR BREACH OF CONTRACT, BREACH OF WARRANTY, TORT, NEGLIGENCE, INFRINGEMENT OR OTHERWISE (INCLUDING, WITHOUT LIMITATION, DAMAGES BASED ON LOSS OF PROFITS, DATA, FILES, USE, BUSINESS OPPORTUNITY OR CLAIMS OF THIRD PARTIES), AND WHETHER OR NOT THE PARTY HAS BEEN ADVISED OF THE POSSIBILITY OF SUCH DAMAGES. THIS LIMITATION SHALL APPLY NOTWITHSTANDING ANY FAILURE OF ESSENTIAL PURPOSE OF ANY LIMITED REMEDY PROVIDED HEREIN.
- Should any provision of this Agreement be held by a court of competent jurisdiction to be illegal, invalid, or unenforceable, that provision shall be deemed amended to achieve as nearly as possible the same economic effect as the original provision, and the legality, validity and enforceability of the remaining provisions of this Agreement shall not be affected or impaired thereby.
- The failure of either party to enforce any term or condition of this Agreement shall not constitute a waiver of either party's right to enforce each and every term and condition of this Agreement. No breach under this agreement shall be deemed waived or excused by either party unless such waiver or consent is in writing signed by the party granting such waiver or consent. The waiver by or consent of a party to a breach of any provision of this Agreement shall not operate or be construed as a waiver of or consent to any other or subsequent breach by such other party.
- This Agreement may not be assigned (including by operation of law or otherwise) by you without WILEY's prior written consent.
- Any fee required for this permission shall be non-refundable after thirty (30) days from receipt by the CCC.

- These terms and conditions together with CCC's Billing and Payment terms and conditions (which are incorporated herein) form the entire agreement between you and WILEY concerning this licensing transaction and (in the absence of fraud) supersedes all prior agreements and representations of the parties, oral or written. This Agreement may not be amended except in writing signed by both parties. This Agreement shall be binding upon and inure to the benefit of the parties' successors, legal representatives, and authorized assigns.
- In the event of any conflict between your obligations established by these terms and conditions and those established by CCC's Billing and Payment terms and conditions, these terms and conditions shall prevail.
- WILEY expressly reserves all rights not specifically granted in the combination of (i) the license details provided by you and accepted in the course of this licensing transaction, (ii) these terms and conditions and (iii) CCC's Billing and Payment terms and conditions.
- This Agreement will be void if the Type of Use, Format, Circulation, or Requestor Type was misrepresented during the licensing process.
- This Agreement shall be governed by and construed in accordance with the laws of the State of New York, USA, without regards to such state's conflict of law rules. Any legal action, suit or proceeding arising out of or relating to these Terms and Conditions or the breach thereof shall be instituted in a court of competent jurisdiction in New York County in the State of New York in the United States of America and each party hereby consents and submits to the personal jurisdiction of such court, waives any objection to venue in such court and consents to service of process by registered or certified mail, return receipt requested, at the last known address of such party.

WILEY OPEN ACCESS TERMS AND CONDITIONS

Wiley Publishes Open Access Articles in fully Open Access Journals and in Subscription journals offering Online Open. Although most of the fully Open Access journals publish open access articles under the terms of the Creative Commons Attribution (CC BY) License only, the subscription journals and a few of the Open Access Journals offer a choice of Creative Commons Licenses. The license type is clearly identified on the article.

The Creative Commons Attribution License

The [Creative Commons Attribution License \(CC-BY\)](#) allows users to copy, distribute and transmit an article, adapt the article and make commercial use of the article. The CC-BY license permits commercial and non-

Creative Commons Attribution Non-Commercial License

The [Creative Commons Attribution Non-Commercial \(CC-BY-NC\) License](#) permits use, distribution and reproduction in any medium, provided the original work is properly cited and is not used for commercial purposes.(see below)

Creative Commons Attribution-Non-Commercial-NoDerivs License

The [Creative Commons Attribution Non-Commercial-NoDerivs License](#) (CC-BY-NC-ND) permits use, distribution and reproduction in any medium, provided the original work is properly cited, is not used for commercial purposes and no modifications or adaptations are made. (see below)

Use by commercial "for-profit" organizations

Use of Wiley Open Access articles for commercial, promotional, or marketing purposes requires further explicit permission from Wiley and will be subject to a fee.

Further details can be found on Wiley Online Library

<http://olabout.wiley.com/WileyCDA/Section/id-410895.html>

Other Terms and Conditions:

v1.10 Last updated September 2015

Questions? customercare@copyright.com or +1-855-239-3415 (toll free in the US) or +1-978-646-2777.

BIBLIOGRAPHY

1. Taichman, R.S., *Blood and bone: two tissues whose fates are intertwined to create the hematopoietic stem-cell niche*. Blood, 2005. **105**(7): p. 2631-2639.
2. Brodsky, B. and A.V. Persikov, *Molecular structure of the collagen triple helix*, in *Advances in protein chemistry*. 2005, Elsevier. p. 301-339.
3. Whyte, M.P., *Hypophosphatasia and the role of alkaline phosphatase in skeletal mineralization*. Endocrine reviews, 1994. **15**(4): p. 439-461.
4. Clarke, B., *Normal bone anatomy and physiology*. Clinical journal of the American Society of Nephrology, 2008. **3**(Supplement 3): p. S131-S139.
5. Soontornvipart, K., A. Nečas, and M. Dvořák, *Effect of Metallic Implant on the Risk of Bacterial Osteomyelitis in Small Animals*. Acta Veterinaria Brno, 2003. **72**(2): p. 235-247.
6. Larsen, R.M., *Intramedullary pressure with particular reference to massive diaphyseal bone necrosis: experimental observations*. Annals of surgery, 1938. **108**(1): p. 127.
7. Lew, D.P. and F.A. Waldvogel, *Osteomyelitis*. New England Journal of Medicine, 1997. **336**(14): p. 999-1007.
8. Parsons, B. and E. Strauss, *Surgical management of chronic osteomyelitis*. The American journal of surgery, 2004. **188**(1): p. 57-66.
9. Mast, N.H. and D. Horwitz, *Osteomyelitis: a review of current literature and concepts*. Operative Techniques in Orthopaedics, 2002. **12**(4): p. 232-241.
10. Bamberger, D.M., *Diagnosis and treatment of osteomyelitis*. Comprehensive therapy, 2000. **26**(2): p. 89-95.
11. Lew, D.P. and F.A. Waldvogel, *Osteomyelitis*. The Lancet, 2004. **364**(9431): p. 369-379.
12. Gentry, L.O., *Management of osteomyelitis*. International journal of antimicrobial agents, 1997. **9**(1): p. 37-42.
13. Haas, D.W. and M.P. McAndrew, *Bacterial osteomyelitis in adults: evolving considerations in diagnosis and treatment*. The American journal of medicine, 1996. **101**(5): p. 550-561.

14. García-Lechuz, J. and E. Bouza, *Treatment recommendations and strategies for the management of bone and joint infections*. Expert opinion on pharmacotherapy, 2009. **10**(1): p. 35-55.
15. Lucke, M., et al., *Gentamicin coating of metallic implants reduces implant-related osteomyelitis in rats*. Bone, 2003. **32**(5): p. 521-531.
16. Gautier, H., G. Daculsi, and C. Merle, *Association of vancomycin and calcium phosphate by dynamic compaction: in vitro characterization and microbiological activity*. Biomaterials, 2001. **22**(18): p. 2481-2487.
17. Reynolds, P.E., *Structure, biochemistry and mechanism of action of glycopeptide antibiotics*. European Journal of Clinical Microbiology and Infectious Diseases, 1989. **8**(11): p. 943-950.
18. Edin, M.L., et al., *Effect of cefazolin and vancomycin on osteoblasts in vitro*. Clinical orthopaedics and related research, 1996(333): p. 245-251.
19. Antoci Jr, V., et al., *Antibiotics for local delivery systems cause skeletal cell toxicity in vitro*. Clinical orthopaedics and related research, 2007. **462**: p. 200-206.
20. Li, B., et al., *Sustained release of vancomycin from polyurethane scaffolds inhibits infection of bone wounds in a rat femoral segmental defect model*. Journal of Controlled Release, 2010. **145**(3): p. 221-230.
21. Jelić, D. and R. Antolović, *From erythromycin to azithromycin and new potential ribosome-binding antimicrobials*. Antibiotics, 2016. **5**(3): p. 29.
22. Cervin, A., *The anti-inflammatory effect of erythromycin and its derivatives, with special reference to nasal polyposis and chronic sinusitis*. Acta oto-laryngologica, 2001. **121**(1): p. 83-92.
23. Amsden, G., *Anti-inflammatory effects of macrolides—an underappreciated benefit in the treatment of community-acquired respiratory tract infections and chronic inflammatory pulmonary conditions?* Journal of Antimicrobial Chemotherapy, 2005. **55**(1): p. 10-21.
24. Ren, W., et al., *Erythromycin inhibits wear debris - induced inflammatory osteolysis in a murine model*. Journal of orthopaedic research, 2006. **24**(2): p. 280-290.

25. Ren, W., R. Blasier, and D. C Markel, *Serendipity of Erythromycin in the Management of Periprosthetic Inflammation*. Current Drug Therapy, 2011. **6**(2): p. 113-120.
26. Bezerra dos Santos, A.T., et al., *Organic extracts from Indigofera suffruticosa leaves have antimicrobial and synergic actions with Erythromycin against Staphylococcus aureus*. Frontiers in microbiology, 2015. **6**: p. 13.
27. Domanska, U., et al., *p K_a and Solubility of Drugs in Water, Ethanol, and 1-Octanol*. The Journal of Physical Chemistry B, 2009. **113**(26): p. 8941-8947.
28. Gerzon, K., et al., *ERYTHROMYCIN. IX. 1 DEGRADATIVE STUDIES OF ERYTHROMYCIN B*. Journal of the American Chemical Society, 1956. **78**(24): p. 6412-6413.
29. Vijan, L.E., *The interaction of vancomycin with DNA*. Rev Roum Chim, 2009. **54**(807): p. e13.
30. Stigter, M., et al., *Incorporation of different antibiotics into carbonated hydroxyapatite coatings on titanium implants, release and antibiotic efficacy*. Journal of controlled release, 2004. **99**(1): p. 127-137.
31. Pacheco, H., et al., *Tissue engineering scaffold for sequential release of vancomycin and rhBMP2 to treat bone infections*. Journal of Biomedical Materials Research Part A, 2014. **102**(12): p. 4213-4223.
32. Ooya, T., et al., *Carboxyethylester-polyrotaxanes as a new calcium chelating polymer: synthesis, calcium binding and mechanism of trypsin inhibition*. International journal of pharmaceutics, 2002. **242**(1-2): p. 47-54.
33. Kriwet, B. and T. Kissel, *Interactions between bioadhesive poly (acrylic acid) and calciumions*. International journal of pharmaceutics, 1996. **127**(2): p. 135-145.
34. Del Valle, H.B., et al., *Dietary reference intakes for calcium and vitamin D*. 2011: National Academies Press.
35. Verron, E., J. Bouler, and J. Guicheux, *Controlling the biological function of calcium phosphate bone substitutes with drugs*. Acta biomaterialia, 2012. **8**(10): p. 3541-3551.
36. Loll, P.J., et al., *Simultaneous recognition of a carboxylate-containing ligand and an intramolecular surrogate ligand in the crystal structure of an asymmetric vancomycin dimer*. Journal of the American Chemical Society, 1997. **119**(7): p. 1516-1522.

37. Izquierdo-Barba, I., et al., *Release evaluation of drugs from ordered three-dimensional silica structures*. European Journal of Pharmaceutical Sciences, 2005. **26**(5): p. 365-373.
38. Nandi, S.K., et al., *Local antibiotic delivery systems for the treatment of osteomyelitis—A review*. Materials Science and Engineering: C, 2009. **29**(8): p. 2478-2485.
39. Lucke, M., et al., *Systemic versus local application of gentamicin in prophylaxis of implant-related osteomyelitis in a rat model*. Bone, 2005. **36**(5): p. 770-778.
40. Gitelis, S. and G.T. Brebach, *The treatment of chronic osteomyelitis with a biodegradable antibiotic-impregnated implant*. Journal of Orthopaedic Surgery, 2002. **10**(1): p. 53-60.
41. Wang, C.-W., et al., *Degradation behavior of porous calcium phosphates*. Journal of Medical and Biological Engineering, 2003. **23**(3): p. 159-163.
42. Jarcho, M., *Calcium phosphate ceramics as hard tissue prosthetics*. Clinical Orthopaedics and Related Research®, 1981. **157**: p. 259-278.
43. Dion, A., et al., *Vancomycin release behaviour from amorphous calcium polyphosphate matrices intended for osteomyelitis treatment*. Biomaterials, 2005. **26**(35): p. 7276-7285.
44. Wang, Q., et al., *Degradation kinetics of calcium polyphosphate bioceramic: an experimental and theoretical study*. Materials Research, 2009. **12**(4): p. 495-501.
45. Ziran, B.H., W.R. Smith, and S.J. Morgan, *Use of calcium-based demineralized bone matrix/allograft for nonunions and posttraumatic reconstruction of the appendicular skeleton: preliminary results and complications*. Journal of Trauma and Acute Care Surgery, 2007. **63**(6): p. 1324-1328.
46. Lee, C.H., A. Singla, and Y. Lee, *Biomedical applications of collagen*. International journal of pharmaceutics, 2001. **221**(1-2): p. 1-22.
47. Schlickewei, C.W., S. Yarar, and J.M. Rueger, *Eluting antibiotic bone graft substitutes for the treatment of osteomyelitis in long bones. A review: Evidence for their use*. Orthop Res Rev, 2014. **6**: p. 71-79.
48. Kluin, O.S., et al., *Biodegradable vs non-biodegradable antibiotic delivery devices in the treatment of osteomyelitis*. Expert opinion on drug delivery, 2013. **10**(3): p. 341-351.

49. Jones, J.R., *Reprint of: Review of bioactive glass: From Hench to hybrids*. Acta biomaterialia, 2015. **23**: p. S53-S82.
50. Chevalier, J. and L. Gremillard, *Ceramics for medical applications: A picture for the next 20 years*. Journal of the European Ceramic Society, 2009. **29**(7): p. 1245-1255.
51. Kandel, R., et al., *Repair of osteochondral defects with biphasic cartilage-calcium polyphosphate constructs in a sheep model*. Biomaterials, 2006. **27**(22): p. 4120-4131.
52. Wang, F.M., et al., *Biodegradable porous calcium polyphosphate scaffolds for the three - dimensional culture of dental pulp cells*. International endodontic journal, 2006. **39**(6): p. 477-483.
53. Comeau, P. and M. Filiaggi, *Calcium polyphosphate precipitation—A strategy to tune the chain length of the glass and control the subsequent release of vancomycin*. Materials Chemistry and Physics, 2015. **159**: p. 56-63.
54. Baksh, D., J. Davies, and S. Kim, *Three-dimensional matrices of calcium polyphosphates support bone growth in vitro and in vivo*. Journal of materials science: Materials in medicine, 1998. **9**(12): p. 743-748.
55. Chen, Y., et al., *Interaction of endothelial cells with biodegradable strontium-doped calcium polyphosphate for bone tissue engineering*. Applied Surface Science, 2008. **255**(2): p. 331-335.
56. Lee, Y.M., et al., *Tissue engineered bone formation using chitosan/tricalcium phosphate sponges*. Journal of periodontology, 2000. **71**(3): p. 410-417.
57. Park, E.K., et al., *Cellular biocompatibility and stimulatory effects of calcium metaphosphate on osteoblastic differentiation of human bone marrow-derived stromal cells*. Biomaterials, 2004. **25**(17): p. 3403-3411.
58. Dion, A., et al., *The effect of processing on the structural characteristics of vancomycin-loaded amorphous calcium phosphate matrices*. Biomaterials, 2005. **26**(21): p. 4486-4494.
59. Petrone, C., et al., *Compaction strategies for modifying the drug delivery capabilities of gelled calcium polyphosphate matrices*. Acta biomaterialia, 2008. **4**(2): p. 403-413.
60. Brow, R.K., *the structure of simple phosphate glasses*. Journal of Non-Crystalline Solids, 2000. **263**: p. 1-28.

61. Van Wazer, J.R., *Phosphorus and its Compounds*. 1958.
62. Wang, K., et al., *The effect of polymeric chain-like structure on the degradation and cellular biocompatibility of calcium polyphosphate*. *Materials Science and Engineering: C*, 2008. **28**(8): p. 1572-1578.
63. Kasuga, T., et al., *Hydrogelation of calcium metaphosphate glass*. *Chemistry letters*, 2001. **30**(8): p. 820-821.
64. Porter, N., R. Pilliar, and M. Grynepas, *Fabrication of porous calcium polyphosphate implants by solid freeform fabrication: a study of processing parameters and in vitro degradation characteristics*. *Journal of Biomedical Materials Research Part A*, 2001. **56**(4): p. 504-515.
65. Omelon, S., et al., *Polymeric crystallization and condensation of calcium polyphosphate glass*. *Materials Research Bulletin*, 2008. **43**(1): p. 68-80.
66. Cle, J., et al., *Analysis of the structural changes of a phosphate glass during its dissolution in simulated body fluid*. *Journal of Materials Science: Materials in Medicine*, 1999. **10**(12): p. 729-732.
67. Balamurugan, A., et al., *Melt - Derived Condensed Polymorphic Calcium Phosphate as Bone Substitute Material: An In Vitro Study*. *Journal of the American Ceramic Society*, 2011. **94**(9): p. 3023-3029.
68. Delahaye, F., et al., *Dissolution of (50-x) Na₂O-xCaO-50P₂O₅ metaphosphate glasses in different saline solutions: mechanism and kinetic control*. *Glass science and technology*, 1999. **72**(5): p. 161-166.
69. Huffman, E. and J. Fleming, *Calcium polyphosphate—rate and mechanism of its hydrolytic degradation*. *The Journal of Physical Chemistry*, 1960. **64**(2): p. 240-244.
70. Umegaki, T. and T. Kanazawa, *Degradation of magnesium and calcium highpolyphosphate coacervates*. *Bulletin of the chemical society of Japan*, 1979. **52**(7): p. 2124-2126.
71. Pilliar, R., et al., *Porous calcium polyphosphate scaffolds for bone substitute applications—in vitro characterization*. *Biomaterials*, 2001. **22**(9): p. 963-972.

72. Song, W., et al., *Influence of particle size and soaking conditions on rheology and microstructure of amorphous calcium polyphosphate hydrogel*. Journal of the American Ceramic Society, 2015. **98**(12): p. 3758-3769.
73. Tadic, D. and M. Epple, *A thorough physicochemical characterisation of 14 calcium phosphate-based bone substitution materials in comparison to natural bone*. Biomaterials, 2004. **25**(6): p. 987-994.
74. Yu, D., et al., *Self - setting hydroxyapatite cement: a novel skeletal drug - delivery system for antibiotics*. Journal of pharmaceutical sciences, 1992. **81**(6): p. 529-531.
75. Hamanishi, C., et al., *A self - setting TTCP - DCPD apatite cement for release of vancomycin*. Journal of Biomedical Materials Research: An Official Journal of The Society for Biomaterials and The Japanese Society for Biomaterials, 1996. **33**(3): p. 139-143.
76. Gautier, H., et al., *Isostatic compression, a new process for incorporating vancomycin into biphasic calcium phosphate: comparison with a classical method*. Biomaterials, 2000. **21**(3): p. 243-249.
77. Brown, W., *A new calcium phosphate setting cement*. J Dent Res, 1983. **63**: p. 672.
78. Zhang, J., et al., *Calcium phosphate cements for bone substitution: chemistry, handling and mechanical properties*. Acta biomaterialia, 2014. **10**(3): p. 1035-1049.
79. Dorozhkin, S.V., *Biphasic, triphasic and multiphasic calcium orthophosphates*. Acta biomaterialia, 2012. **8**(3): p. 963-977.
80. Sheikh, Z., et al., *In vitro degradation and in vivo resorption of dicalcium phosphate cement based grafts*. Acta biomaterialia, 2015. **26**: p. 338-346.
81. Von Rechenberg, B., et al., *Evaluation of four biodegradable, injectable bone cements in an experimental drill hole model in sheep*. European Journal of Pharmaceutics and Biopharmaceutics, 2013. **85**(1): p. 130-138.
82. Kuemmerle, J.M., et al., *Assessment of the suitability of a new brushite calcium phosphate cement for cranioplasty—an experimental study in sheep*. Journal of cranio-maxillo-facial surgery, 2005. **33**(1): p. 37-44.

83. Shadanbaz, S., et al., *Monetite and brushite coated magnesium: in vivo and in vitro models for degradation analysis*. Journal of Materials Science: Materials in Medicine, 2014. **25**(1): p. 173-183.
84. Tamimi, F., Z. Sheikh, and J. Barralet, *Dicalcium phosphate cements: Brushite and monetite*. Acta biomaterialia, 2012. **8**(2): p. 474-487.
85. Geffers, M., J. Groll, and U. Gbureck, *Reinforcement strategies for load-bearing calcium phosphate biocements*. Materials, 2015. **8**(5): p. 2700-2717.
86. Khairoun, I., et al., *Addition of cohesion promoters to calcium phosphate cements*. Biomaterials, 1999. **20**(4): p. 393-398.
87. Ataol, S., et al., *Synthesis and characterization of nanosized calcium phosphates by flame spray pyrolysis, and their effect on osteogenic differentiation of stem cells*. Journal of Nanoparticle Research, 2015. **17**(2): p. 95.
88. Lin, K., C. Wu, and J. Chang, *Advances in synthesis of calcium phosphate crystals with controlled size and shape*. Acta biomaterialia, 2014. **10**(10): p. 4071-4102.
89. Moreau, J.L., M.D. Weir, and H.H. Xu, *Self - setting collagen - calcium phosphate bone cement: Mechanical and cellular properties*. Journal of Biomedical Materials Research Part A, 2009. **91**(2): p. 605-613.
90. Palmer, I., et al., *Biocompatibility of calcium phosphate bone cement with optimized mechanical properties*. Journal of Biomedical Materials Research Part B: Applied Biomaterials, 2016. **104**(2): p. 308-315.
91. Cui, G., et al., *The mechanical and biological properties of an injectable calcium phosphate cement - fibrin glue composite for bone regeneration*. Journal of Biomedical Materials Research Part B: Applied Biomaterials, 2010. **92**(2): p. 377-385.
92. Omelon, S. and M. Grynypas, *Polyphosphates affect biological apatite nucleation*. Cells Tissues Organs, 2011. **194**(2-4): p. 171-175.
93. Cini, N. and V. Ball, *Polyphosphates as inorganic polyelectrolytes interacting with oppositely charged ions, polymers and deposited on surfaces: fundamentals and applications*. Advances in colloid and interface science, 2014. **209**: p. 84-97.
94. Grynypas, M., et al., *Porous calcium polyphosphate scaffolds for bone substitute applications in vivo studies*. Biomaterials, 2002. **23**(9): p. 2063-2070.

95. Jackson, L.E., et al., *Synthesis and structure of a calcium polyphosphate with a unique criss-cross arrangement of helical phosphate chains*. Chemistry of materials, 2005. **17**(18): p. 4642-4646.
96. Laurencin, C., et al., *Bioerodible polyanhydrides for antibiotic drug delivery: in vivo osteomyelitis treatment in a rat model system*. Journal of orthopaedic research, 1993. **11**(2): p. 256-262.
97. Norden, C.W., et al., *Chronic staphylococcal osteomyelitis: treatment with regimens containing rifampin*. Reviews of infectious diseases, 1983. **5**(Supplement_3): p. S495-S501.
98. Shirliff, M.E., J.H. Calhoun, and J.T. Mader, *Experimental osteomyelitis treatment with antibiotic-impregnated hydroxyapatite*. Clinical orthopaedics and related research, 2002. **401**: p. 239-247.
99. Girschick, H.J., et al., *Chronic recurrent multifocal osteomyelitis: what is it and how should it be treated?* Nature Reviews Rheumatology, 2007. **3**(12): p. 733.
100. Riediger, D., *Restoration of masticatory function by microsurgically revascularized iliac crest bone grafts using enosseous implants*. Plastic and reconstructive surgery, 1988. **81**(6): p. 861-877.
101. Van de Belt, H., et al., *Surface roughness, porosity and wettability of gentamicin-loaded bone cements and their antibiotic release*. Biomaterials, 2000. **21**(19): p. 1981-1987.
102. Bohner, M., et al., *Gentamicin - loaded hydraulic calcium phosphate bone cement as antibiotic delivery system*. Journal of pharmaceutical sciences, 1997. **86**(5): p. 565-572.
103. Niikura, T., et al., *Vancomycin-impregnated calcium phosphate cement for methicillin-resistant Staphylococcus aureus femoral osteomyelitis*. Orthopedics, 2007. **30**(4).
104. Parent, M., et al., *Design of calcium phosphate ceramics for drug delivery applications in bone diseases: a review of the parameters affecting the loading and release of the therapeutic substance*. Journal of Controlled Release, 2017. **252**: p. 1-17.
105. Solberg, B.D., A.P. Gutow, and M.R. Baumgaertner, *Efficacy of gentamycin-impregnated resorbable hydroxyapatite cement in treating osteomyelitis in a rat model*. Journal of orthopaedic trauma, 1999. **13**(2): p. 102-106.

106. Shinto, Y., et al., *Calcium hydroxyapatite ceramic used as a delivery system for antibiotics*. The Journal of bone and joint surgery. British volume, 1992. **74**(4): p. 600-604.
107. Miyai, T., et al., *Antibiotic-loaded poly- ϵ -caprolactone and porous β -tricalcium phosphate composite for treating osteomyelitis*. Biomaterials, 2008. **29**(3): p. 350-358.
108. Dingeldein, E., et al., *Tricalcium phosphate for implant materials wherein the pores of the tricalciumphosphate are filled with antibiotic and amino acid*. 1989, Google Patents.
109. Lambotte, J., et al., *Tricalcium phosphate, an antibiotic carrier: a study focused on experimental osteomyelitis in rabbits*. Chirurgie; memoires de l'Academie de chirurgie, 1998. **123**(6): p. 572-579.
110. Queiroz, A., et al., *Adsorption and release studies of sodium ampicillin from hydroxyapatite and glass-reinforced hydroxyapatite composites*. Biomaterials, 2001. **22**(11): p. 1393-1400.
111. Fang, T., et al., *Poly (ϵ - caprolactone) coating delays vancomycin delivery from porous chitosan/ β - tricalcium phosphate composites*. Journal of Biomedical Materials Research Part B: Applied Biomaterials, 2012. **100**(7): p. 1803-1811.
112. Amjadi, I., et al., *Synthesis and characterization of doxorubicin-loaded poly (lactide-co-glycolide) nanoparticles as a sustained-release anticancer drug delivery system*. Applied biochemistry and biotechnology, 2012. **168**(6): p. 1434-1447.
113. Amjadi, I., et al., *Nanoencapsulation of Hypericum perforatum and doxorubicin anticancer agents in PLGA nanoparticles through double emulsion technique*. Micro & Nano Letters, 2013. **8**(5): p. 243-247.
114. Ginebra, M.-P., T. Traykova, and J.A. Planell, *Calcium phosphate cements as bone drug delivery systems: a review*. Journal of Controlled Release, 2006. **113**(2): p. 102-110.
115. Schnieders, J., et al., *Controlled release of gentamicin from calcium phosphate—poly (lactic acid-co-glycolic acid) composite bone cement*. Biomaterials, 2006. **27**(23): p. 4239-4249.

116. Habraken, W., J. Wolke, and J. Jansen, *Ceramic composites as matrices and scaffolds for drug delivery in tissue engineering*. *Advanced drug delivery reviews*, 2007. **59**(4-5): p. 234-248.
117. Roy, A., et al., *Porous calcium phosphate-poly (lactic-co-glycolic) acid composite bone cement: A viable tunable drug delivery system*. *Materials Science and Engineering: C*, 2016. **59**: p. 92-101.
118. Macha, I.J., et al., *Marine structure derived calcium phosphate-polymer biocomposites for local antibiotic delivery*. *Marine drugs*, 2015. **13**(1): p. 666-680.
119. Lagow, R., P. Capano, and S. Hoffman, *Calcium bioceramic implants in canine mandibular block defects*. *J Dent Res*, 1991. **70**: p. 41A.
120. Nelson, S.R., et al., *Evaluation of new high-performance calcium polyphosphate bioceramics as bone graft materials*. *Journal of oral and maxillofacial surgery*, 1993. **51**(12): p. 1363-1371.
121. Fukui, H., Y. Taki, and Y. Abe, *Implantation of new calcium phosphate glass-ceramics*. *Journal of dental research*, 1977. **56**(10): p. 1260-1260.
122. Schofield, S., et al., *Gelled calcium polyphosphate matrices delay antibiotic release*. *Journal of dental research*, 2006. **85**(7): p. 643-647.
123. Shahabooei, M., et al., *A histomorphometric study of the effect of doxycycline and erythromycin on bone formation in dental alveolar socket of rat*. *Advanced biomedical research*, 2015. **4**.
124. Song, W., et al., *Cyclodextrin-erythromycin complexes as a drug delivery device for orthopedic application*. *International journal of nanomedicine*, 2011. **6**: p. 3173.
125. Campoccia, D., et al., *Antibiotic resistance in Staphylococcus aureus and Staphylococcus epidermidis clinical isolates from implant orthopedic infections*. *The International journal of artificial organs*, 2005. **28**(11): p. 1186-1191.
126. Campoccia, D., L. Montanaro, and C.R. Arciola, *The significance of infection related to orthopedic devices and issues of antibiotic resistance*. *Biomaterials*, 2006. **27**(11): p. 2331-2339.
127. Bishop, A.R., et al., *Vancomycin elution, activity and impact on mechanical properties when added to orthopedic bone cement*. *Journal of the mechanical behavior of biomedical materials*, 2018. **87**: p. 80-86.

128. Arayne, M.S., N. Sultana, and S. Begum, *A New Colorimetric Method for the Assay of Erythromycin*. JPMA. The Journal of the Pakistan Medical Association, 1983. **33**(10): p. 256-259.
129. Koya, S.K., et al., *Rapid detection of Clostridium difficile toxins in serum by Raman spectroscopy*. Journal of Surgical Research, 2018. **232**: p. 195-201.
130. Lora, R.C., et al., *Dispersive Raman spectroscopy for the in vitro identification and quantification of injected vancomycin intra-vitreous*. Spectroscopy, 2011. **25**(2): p. 103-112.
131. Schlünzen, F., et al., *Structural basis for the interaction of antibiotics with the peptidyl transferase centre in eubacteria*. Nature, 2001. **413**(6858): p. 814.
132. Miroshnyk, I., et al., *Insight into thermally induced phase transformations of erythromycin A dihydrate*. Crystal growth & design, 2006. **6**(2): p. 369-374.
133. Diéguez, A., et al., *The complete Raman spectrum of nanometric SnO₂ particles*. Journal of applied physics, 2001. **90**(3): p. 1550-1557.
134. Pfeiffer, R.R., *Structural features of vancomycin*. Reviews of infectious diseases, 1981. **3**(Supplement): p. S205-S209.
135. Ren, W., et al., *Setting mechanism of a new injectable Dicalcium Phosphate Dihydrate (DCPD) forming cement*. Journal of the mechanical behavior of biomedical materials, 2018. **79**: p. 226-234.
136. Campana, V., et al., *Bone substitutes in orthopaedic surgery: from basic science to clinical practice*. Journal of Materials Science: Materials in Medicine, 2014. **25**(10): p. 2445-2461.
137. Winkler, H. and P. Haiden, *Treatment of chronic bone infection*. Operative Techniques in Orthopaedics, 2016. **26**(1): p. 2-11.
138. Klemm, K., *[Gentamicin-PMMA-beads in treating bone and soft tissue infections (author's transl)]*. Zentralbl Chir, 1979. **104**(14): p. 934-42.
139. Buchholz, H.W. and H. Engelbrecht, *[Depot effects of various antibiotics mixed with Palacos resins]*. Chirurg, 1970. **41**(11): p. 511-5.
140. Nelson, C.L., et al., *Sonication of antibiotic spacers predicts failure during two-stage revision for prosthetic knee and hip infections*. Clin Orthop Relat Res, 2014. **472**(7): p. 2208-14.

141. Neut, D., et al., *Biomaterial-associated infection of gentamicin-loaded PMMA beads in orthopaedic revision surgery*. J Antimicrob Chemother, 2001. **47**(6): p. 885-91.
142. Akashi, A., et al., *Release profile of antimicrobial agents from α -tricalcium phosphate cement*. Biomaterials, 2001. **22**(20): p. 2713-2717.
143. Gautier, H., et al., *Influence of isostatic compression on the stability of vancomycin loaded with a calcium phosphate-implantable drug delivery device*. Journal of Biomedical Materials Research: An Official Journal of The Society for Biomaterials, The Japanese Society for Biomaterials, and The Australian Society for Biomaterials and the Korean Society for Biomaterials, 2000. **52**(2): p. 308-314.
144. Lazarettos, J., et al., *A bioresorbable calcium phosphate delivery system with teicoplanin for treating MRSA osteomyelitis*. Clinical Orthopaedics and Related Research®, 2004. **423**: p. 253-258.
145. Luo, J., et al., *Compressive, diametral tensile and biaxial flexural strength of cutting-edge calcium phosphate cements*. journal of the mechanical behavior of biomedical materials, 2016. **60**: p. 617-627.
146. Chehreghanianzabi, Y., et al., *Comparing the release of erythromycin and vancomycin from calcium polyphosphate hydrogel using different drug loading methods*. Journal of Biomedical Materials Research Part B: Applied Biomaterials, 2019.
147. Information, N.C.f.B. *Erythromycin*. Available from: <https://pubchem.ncbi.nlm.nih.gov/compound/erythromycin>.
148. Information., N.C.f.B. *Vancomycin*. Available from: National Center for Biotechnology Information. PubChem Database. Vancomycin, CID=14969, <https://pubchem.ncbi.nlm.nih.gov/compound/14969> (accessed on Apr. 18, 2019).
149. Fiese, E. and S. Steffen, *Comparison of the acid stability of azithromycin and erythromycin A*. Journal of Antimicrobial Chemotherapy, 1990. **25**(suppl_A): p. 39-47.
150. Lorian, V. and L. Sabath, *Effect of pH on the activity of erythromycin against 500 isolates of gram-negative bacilli*. Appl. Environ. Microbiol., 1970. **20**(5): p. 754-756.
151. Wiegand, C., et al., *pH influence on antibacterial efficacy of common antiseptic substances*. Skin pharmacology and physiology, 2015. **28**(3): p. 147-158.

152. Zhou, Z., et al., *Release of vancomycin and tobramycin from polymethylmethacrylate cements impregnated with calcium polyphosphate hydrogel*. Journal of Biomedical Materials Research Part B: Applied Biomaterials, 2018. **106**(8): p. 2827-2840.
153. Specchia, N., et al., *Effect of hydroxyapatite porosity on growth and differentiation of human osteoblast-like cells*. Journal of materials science, 2002. **37**(3): p. 577-584.
154. Huang, L., et al., *Effect of apatite formation of biphasic calcium phosphate ceramic (BCP) on osteoblastogenesis using simulated body fluid (SBF) with or without bovine serum albumin (BSA)*. Materials Science and Engineering: C, 2017. **70**: p. 955-961.
155. Zhang, L., et al., *Porous hydroxyapatite and biphasic calcium phosphate ceramics promote ectopic osteoblast differentiation from mesenchymal stem cells*. Science and technology of advanced materials, 2009. **10**(2): p. 025003.
156. Edwards, J., A. Sedgwick, and D. Willoughby, *The formation of a structure with the features of synovial lining by subcutaneous injection of air: an in vivo tissue culture system*. The Journal of pathology, 1981. **134**(2): p. 147-156.
157. Midy, V., M. Dard, and E. Hollande, *Evaluation of the effect of three calcium phosphate powders on osteoblast cells*. Journal of Materials Science: Materials in Medicine, 2001. **12**(3): p. 259-265.
158. Berube, P., et al., *The effect of sputtered calcium phosphate coatings of different crystallinity on osteoblast differentiation*. Journal of periodontology, 2005. **76**(10): p. 1697-1709.
159. Wang, C., et al., *Phenotypic expression of bone-related genes in osteoblasts grown on calcium phosphate ceramics with different phase compositions*. Biomaterials, 2004. **25**(13): p. 2507-2514.
160. de Bruijn, J.D., Y. Bovell, and C. Van Blitterswijk, *Structural arrangements at the interface between plasma sprayed calcium phosphates and bone*. Biomaterials, 1994. **15**(7): p. 543-550.
161. Hyakuna, K., et al., *The influence of calcium phosphate ceramics and glass - ceramics on cultured cells and their surrounding media*. Journal of Biomedical Materials Research Part A, 1989. **23**(9): p. 1049-1066.

162. Dvorak, M.M., et al., *Physiological changes in extracellular calcium concentration directly control osteoblast function in the absence of calciotropic hormones*. Proceedings of the National Academy of Sciences of the United States of America, 2004. **101**(14): p. 5140-5145.
163. Annaz, B., et al., *Porosity variation in hydroxyapatite and osteoblast morphology: a scanning electron microscopy study*. Journal of Microscopy, 2004. **215**(1): p. 100-110.
164. Chou, Y.-F., et al., *The effect of biomimetic apatite structure on osteoblast viability, proliferation, and gene expression*. Biomaterials, 2005. **26**(3): p. 285-295.
165. Redey, S.A., et al., *Behavior of human osteoblastic cells on stoichiometric hydroxyapatite and type A carbonate apatite: role of surface energy*. Journal of Biomedical Materials Research: An Official Journal of The Society for Biomaterials, The Japanese Society for Biomaterials, and The Australian Society for Biomaterials and the Korean Society for Biomaterials, 2000. **50**(3): p. 353-364.
166. HIGASHI, S., et al., *Evaluation of cytotoxicity of calcium phosphate cement consisting of α -tricalcium phosphate and dicalcium phosphate dihydrate*. Dental materials journal, 1998. **17**(3): p. 186-194.
167. Oreffo, R.O., et al., *Growth and differentiation of human bone marrow osteoprogenitors on novel calcium phosphate cements*. Biomaterials, 1998. **19**(20): p. 1845-1854.
168. Annaz, B., et al., *An ultrastructural study of cellular response to variation in porosity in phase - pure hydroxyapatite*. Journal of microscopy, 2004. **216**(2): p. 97-109.
169. De Bruijn, J., et al., *Osteoclastic resorption of calcium phosphates is potentiated in postosteogenic culture conditions*. Journal of biomedical materials research, 1994. **28**(1): p. 105-112.
170. Chen, L., et al., *Flow perfusion culture of MC3T3-E1 osteogenic cells on gradient calcium polyphosphate scaffolds with different pore sizes*. Journal of biomaterials applications, 2016. **30**(7): p. 908-918.
171. Ren, W., et al., *Setting Mechanism of a New Injectable Dicalcium Phosphate Dihydrate (DCPD) Forming Cement*. Journal of the mechanical behavior of biomedical materials, 2018.

172. Ren, W., et al., *Blockade of vascular endothelial growth factor activity suppresses wear debris-induced inflammatory osteolysis*. The Journal of rheumatology, 2007. **34**(1): p. 27-35.
173. Palmer, I., et al., *Biocompatibility of calcium phosphate bone cement with optimised mechanical properties: an in vivo study*. Journal of Materials Science: Materials in Medicine, 2016. **27**(12): p. 191.
174. Hallab, N.J., et al., *Cell adhesion to biomaterials: correlations between surface charge, surface roughness, adsorbed protein, and cell morphology*. Journal of long-term effects of medical implants, 1995. **5**(3): p. 209-231.
175. Ren, W.P., et al., *Effect of erythromycin - doped calcium polyphosphate scaffold composite in a mouse pouch infection model*. Journal of Biomedical Materials Research Part B: Applied Biomaterials, 2014. **102**(6): p. 1140-1147.

ABSTRACT**INVESTIGATION OF PHYSIOCHEMICAL PROPERTIES AND BIOCOMPATIBILITY OF AMORPHOUS CALCIUM POLYPHOSPHATE HYDROGEL DOPED WITH ANTIBIOTICS AND INJECTABLE P-DCPD BONE CEMENT**

by

YASAMAN CHEHREGHANIANZABI**MAY 2020****Advisor:** Dr. Weiping Ren**Major:** Biomedical Engineering (Tissue Engineering)**Degree:** Doctor of Philosophy

Amorphous calcium polyphosphate (ACPP) is an inorganic polymer ceramic. Here we use a simple method of preparing ACPP hydrogel in the presence of excess volume of water. Essentially, water availability to polyphosphate chains accelerates water molecule ingress and microstructural transformation of ACPP hydrogels. Antibiotic delivery capacity of ACPP hydrogel increases by the specific mixing and molding method, where the vancomycin (VCM) and erythromycin (EM) have higher antibiotic encapsulation efficiency with the small burst release for the compressed discs as compared to VCM and EM release from manually molded discs. Also VCM demonstrates higher efficacy upon encapsulation and interaction with acidic ACPP hydrogel, where EM's sensitivity was disrupted.

In part of this study, we investigate impact of ACPP hydrogel replacement by monomeric calcium phosphate on the quality of final product (dicalcium phosphate dihydrates (DCPD) cement). The physiochemical properties of polymeric bone cement as compared to classical bone cement were determined. Moreover, antibacterial activity of Polymeric Dicalcium Phosphate Dihydrate (P-DCPD) cement is one crucial step toward insuring material viability for avoiding the

bacterial growth. Thus in vitro bactericidal experiment shows the potency of P-DCPD material and selected antibiotics to invade bacteria and the correlation of the results with the antibiotic activity results from ACPH hydrogel discs. For further advancement of P-DCPD material, an in vitro and in vivo biocompatibility study of the cement particles reveals the effect of physicochemical properties of the cement on cellular and tissue viability.

We believe that the formation of ACPH hydrogel is through the mechanisms of intermolecular ionic interaction and entanglement of polyphosphate chains affect drug retention within the matrix in a favorable way. As such, some of the surface physiochemical properties such as cement cohesion may affect cellular and tissue response. P-DCPD shows similar or even superior biocompatibility than classical/monomeric DCPD. In the future, the drug-eluting capacity of polymeric DCPD will be investigated to correlate it with the obtained results from ACPH hydrogel.

VITA AUCTORIS

Yasaman Chehreghanianzabi was born in Tehran, Iran on June 23, 1987. She attended Azad University of Tehran for her undergraduate education from 2005 – 2010. She studied Physics and received her bachelor's degree in February 2010 and graduated as ranked 3rd among 50 classmates. Despite having the opportunity of pursuing a Master's degree in Iran, she decided to continue her studies in the USA. She started her education as temporary research assistant in Prof. Cui Lab at the Biomedical Engineering Department of Washington University in Saint Louis from 2013-2014. Starting August 2014, she attended graduate school at Saint Louis University studying Biomedical Engineering and focusing on diffusion in polymer solutions and networks. She is received her Master's degree in May 2016. The results of her Master's thesis was published as three papers, one conference proceedings paper, and four conference presentations.

In August 2016, she started her Ph.D. in Biomedical Engineering Department and focusing on physiochemical characterization of bone cement material, at Wayne State University. She is anticipating her Ph.D. degree in May 2020. She anticipates the results completed in this dissertation to be submitted for publication in December 2019. Her dedication to the project has already resulted in one paper. She is going to submit at least two first authored papers and several co-authored papers from her Ph.D. research, as mentioned in this dissertation.